

---

Electronic Thesis and Dissertation Repository

---

11-28-2018 2:30 PM

## Robust Earthquake Site Classification Assessment at Ontario Bridge Sites.

Alex Bilson Darko  
*The University of Western Ontario*

Supervisor  
Molnar, Sheri  
*The University of Western Ontario*  
Sadrekarimi, Abouzar  
*The University of Western Ontario*

Graduate Program in Geophysics

A thesis submitted in partial fulfillment of the requirements for the degree in Master of Science

© Alex Bilson Darko 2018

Follow this and additional works at: <https://ir.lib.uwo.ca/etd>



Part of the [Geophysics and Seismology Commons](#), and the [Geotechnical Engineering Commons](#)

---

### Recommended Citation

Bilson Darko, Alex, "Robust Earthquake Site Classification Assessment at Ontario Bridge Sites." (2018).  
*Electronic Thesis and Dissertation Repository*. 5903.  
<https://ir.lib.uwo.ca/etd/5903>

This Dissertation/Thesis is brought to you for free and open access by Scholarship@Western. It has been accepted for inclusion in Electronic Thesis and Dissertation Repository by an authorized administrator of Scholarship@Western. For more information, please contact [wlsadmin@uwo.ca](mailto:wlsadmin@uwo.ca).

## Abstract

Canadian seismic design guidelines classify subsurface ground conditions based on the average shear-wave velocity ( $V_S$ ) of the upper 30 meters ( $V_{S30}$ ). We seek to optimize a robust earthquake site classification procedure for Ontario bridge sites, assessed primarily from blind comparison of non-invasive  $V_S$  depth profiling techniques. Non-invasive seismic testing is performed at 10 bridge sites in southern Ontario co-located with invasive penetration and/or borehole  $V_S$  measurements. Non-invasive surface wave dispersion and site amplification functions are jointly inverted to retrieve  $V_S$  profiles at each site. A general correlation between corrected  $V_S$  and cone tip resistance ( $q_{c1}$ ) is developed for all soils encountered in Windsor, Ontario. We determine an overall average relative difference in  $V_S$  between methodologies of 17% for soil layers at all bridge sites. Earthquake site classification based on  $V_S$  is consistent at all sites regardless of methodology. Non-invasive techniques offer an efficient but lower-resolution  $V_S$  profiling alternative to invasive earthquake site classification techniques with the advantages of measuring site period and  $V_S$  of the impenetrable substratum.

## Keywords

Shear wave velocity, seismic hazard, site classification, ambient vibrations, cone penetration, cone tip resistance, surface wave dispersion, microtremors, site response, earthquake site assessment

## Co-Authorship Statement

This thesis is prepared in integrated article format and includes the following papers written by Alex Bilson Darko and the co-authors. Alex is the first author and performed the analyses described in this thesis with guidance, assistance and revisions from the co-authors.

Chapter 2: Bilson Darko, A., Molnar, S., Sadrekarimi, A., Blind comparison of non-invasive shear wave velocity profiling with invasive methods at bridge sites in Windsor, Ontario. This manuscript is prepared for submission to the Canadian Geotechnical Journal.

Sections 2.1 to 2.6 appear in: Bilson Darko, A., Molnar, S., Sadrekarimi, A., (2018). Robust earthquake site characterization at Ontario bridge sites, Geotechnical Earthquake Engineering and Soil Dynamics V, Austin, Texas, June 10-13 2018, doi: 10.1061/9780784481486.051.

Chapter 3: Bilson Darko, A., Molnar, S., Sadrekarimi, A., Assessment of earthquake site classification methodologies at Ontario bridge sites. This manuscript is prepared for submission to the ASTM Geotechnical Testing Journal.

The thesis and corresponding papers were completed under the supervision of Dr. Sheri Molnar and Dr. Abouzar Sadrekarimi.

## Acknowledgments

I would like to express my profound gratitude to my supervisors Dr. Sheri Molnar and Dr. Abouzar Sadrekarimi for the opportunity to study my masters here at Western. The success and final outcome of this research required a lot of guidance and assistance and I am extremely privileged to have had this from my supervisors all through to the completion of my degree.

Thank you to the Ministry of Transportation Ontario (MTO) for providing the necessary funding for this research.

Finally, I would like to thank my family and friends for their support especially to everyone in Good Vibrations and Excitations research group. Your love and constant support made this very much possible.

# Table of Contents

Abstract.....	i
Co-Authorship Statement.....	ii
Acknowledgments.....	iii
Table of Contents.....	iv
List of Tables.....	vii
List of Figures.....	viii
List of Abbreviations, Symbols and Nomenclature.....	xi
Chapter 1.....	1
1 Introduction and Literature Review.....	1
1.1 Aim of Research.....	7
1.2 Organization of work.....	7
1.3 References.....	8
Chapter 2.....	12
2 Blind comparison of non-invasive and invasive shear wave velocity profiling at bridge sites in Windsor, Ontario.....	12
2.1 Introduction.....	12
2.2 Location and geological setting.....	14
2.3 Non-invasive methodology.....	15
2.4 Survey geometry and data acquisition.....	17
2.5 Data processing and analysis.....	19
2.5.1 MHVSR.....	19
2.5.2 Dispersion curves.....	21
2.6 Preliminary $V_{S30}$ assessment.....	23
2.7 Inversion methodology.....	24

2.8	Inversion results .....	27
2.9	Geotechnical data.....	30
2.9.1	Invasive $V_S$ profiles .....	31
2.10	Blind comparison of non-invasive and invasive $V_S$ profiles.....	34
2.11	Inter-method variability of $V_S$ .....	39
2.12	$V_{S30}$ -based earthquake site classification .....	40
2.13	Statistical correlation of $V_S$ and cone tip resistance.....	41
2.13.1	Proposed empirical correlation for $V_{s1}$ and $qc1$ .....	43
2.14	Discussion and conclusions.....	45
2.15	Data and resources.....	47
2.16	Acknowledgements .....	47
2.17	References .....	47
Chapter 3	.....	55
3	Shear-wave Velocity Profiling at Ontario Bridge Sites in Ottawa and Oshawa.....	55
3.1	Introduction.....	55
3.2	Location and geological setting .....	56
3.3	Data collection .....	58
3.4	Data processing and analysis .....	60
3.4.1	MHVSR .....	60
3.4.2	Dispersion curves.....	62
3.5	Preliminary $V_{S30}$ assessment.....	64
3.6	Inversion results .....	65
3.7	Invasive methods .....	67
3.7.1	Ottawa.....	67
3.7.2	Oshawa.....	68
3.8	Invasive $V_S$ profiles .....	69

3.9 Laboratory tests.....	71
3.9.1 Specimen preparation and consolidation .....	71
3.9.2 Laboratory bender element $V_s$ measurements .....	71
3.9.3 Direct simple shear test.....	73
3.10 Comparison of $V_s$ from different methodologies.....	74
3.11 $V_{S30}$ -based earthquake site classification .....	75
3.12 $S_u$ -based site classification .....	77
3.13 Conclusions .....	78
3.14 Data and resources.....	79
3.15 Acknowledgements .....	79
3.16 References .....	79
Chapter 4.....	82
4 Conclusions and recommendations.....	82
4.1 Robust earthquake site classification procedure.....	83
4.2 Future Work .....	87
4.3 References.....	87
Appendices.....	88
Appendix A. HRFK and MSPAC dispersion comparison.....	88
Appendix B. Alternate inversion attempts considering higher modes.....	89
Appendix C. CPT logs .....	93
Appendix D. Other $q_c$ to $V_s$ relations. ....	95
Appendix E. $q_c$ to $V_s$ relations for Ottawa and Oshawa sites.....	96
Curriculum Vitae .....	99

## List of Tables

Table 1.1: Site categories in CHBDC (CSA Group 2014). .....	3
Table 2.1: Correlations used for converting $N$ to $V_S$ for sand, silt and clay.....	32
Table 2.2: Correlations investigated for converting $q_c$ to $V_S$ .....	32
Table 2.3 Assessment of the difference in $V_S$ between mean invasive and inverted $V_S$ profiles. ....	39
Table 2.4 Site classification for both invasive and non-invasive methodologies. ....	41
Table 2.5: Some correlations between $V_S$ and $qc$ in literature. ....	43
Table 3.1: Summary of subsurface geology at Ottawa sites (Thurber 2015). ....	68
Table 3.2: RMSE obtained for each correlation used at the Ottawa site (OT-15).....	69
Table 3.3: Site classification for both invasive and non-invasive methodologies.....	77
Table 3.4: Soil parameters for $S_u$ -based site classification. ....	78



## List of Figures

Figure 1.1: Nishinomiya-ko Bridge collapse in the 1995 Kobe earthquake in Japan (Moehle and Eberhard 2000).....	1
Figure 2.1: Surface geological map of Windsor. Black triangles show locations of the test sites (modified from Hudec 1998). .....	15
Figure 2.2: Location of test sites and previous invasive tests. ....	18
Figure 2.3: (a) Schematic diagram of 3-sensor triangular array. Each color represents different array aperture. (b) Photo of a 5 m array set up on a baseball playing field at Site-4. Tromino sensors appear as small red boxes surrounded by orange traffic cones. ....	19
Figure 2.4: Array-averaged MHVSR calculated from all sensors in each array aperture. Red, blue, magenta and green lines represents 5, 10, 15 and 30 m array spacings respectively. Upper left to lower right panels are sites from northwest to southeast along the Parkway....	21
Figure 2.5: Picked dispersion estimates (open circles) for each site; blue circles represent potential higher mode dispersion estimates, grey circles represent transitional picks between fundamental and first higher modes. Background shading is MSPAC dispersion estimates; darker shades indicate higher count. Minimum resolution and aliasing limits are shown as solid and dashed lines respectively. ....	22
Figure 2.6: Fundamental mode dispersion curves for each site. Black triangles indicate $V_{S30}$ boundaries (converted to $V_{R40}$ ) between site classes E, D, and C. ....	24
Figure 2.7: Inversion results for bridge sites in Windsor. The left panel show the dispersion data (black dots), the middle panels show the MHVSR data (black dots) and the right panels show the retrieved $V_S$ profiles for each site. The colored region represents the first 1,000 lowest misfit models and the solid brown line shows the minimum misfit model. Grey dots represents portions of datasets excluded from the inversion. ....	29
Figure 2.8: Comparison between predicted $V_S$ from empirical $q_c$ -to- $V_S$ relations in literature and measured $V_S$ from crosshole and downhole surveys. ....	33

Figure 2.9: Invasive $V_s$ measurements at the six study locations: converted CPT (red circles), converted SPT (green squares), crosshole $V_s$ (crosses), downhole (black triangles) $V_s$ measurements and refusal depth (stars). .....	34
Figure 2.10: Comparison of invasive and non-invasive $V_s$ profiles. ....	36
Figure 2.11: Measured dispersion from microtremor array data (black dots) compared to fundamental (solid line) and first higher mode (dashed line) theoretical dispersion estimates based on invasive 1D models. Black lines represent dispersion estimates from invasive data and blue lines represents continuation into a 1000 m/s half-space $V_s$ . ....	38
Figure 2.12: Correlation between $V_{s1}$ and $qc_1$ . ....	45
Figure 3.1: Location of three test sites in Ottawa; blue squares represent bridges, green circles represent structural culverts and red triangles represent non-invasive test sites (modified from Thurber 2015). ....	57
Figure 3.2: Location of test sites in Oshawa. ....	58
Figure 3.3: (a) MASW array setup for 1 m (white symbols) and 3 m (grey symbols) spacings. Upward triangles represent geophone locations and downward triangles represent shot locations. (b) Three array apertures of the 5-sensor cross-shaped array geometry at the BS150. (c) Four apertures of the 3-sensor triangular array geometry at sites OT-8, 11 and 15. ....	60
Figure 3.4: Time-averaged MHVSR curves (red lines) representative of each site with one standard deviation (black dash lines). ....	61
Figure 3.5: Fundamental mode dispersion estimates (open circles). MSPAC dispersion estimates for (A) OT-15, (B) BS150, (C) OT-11 and (D) OT-8; background shading is MSPAC dispersion histogram; darker shades indicate higher count. FK dispersion estimates obtained from MASW processing for (E) OT-11 and (F) OT-8. ....	64
Figure 3.6: Fundamental mode dispersion curves for each site. Black triangles indicate boundaries between site classes E, D, and C. ....	65

Figure 3.7: Inversion results from bridge sites. Left panels show dispersion data (black dots), middle panels show MHVSR data (black line) and right panels show the retrieved  $V_S$  profiles for each site. The colored region represents the first 1,000 lowest misfit models and the solid brown line shows the minimum misfit model. Grey dots represents portions of MHVSR not included in the inversion. .... 66

Figure 3.8: Invasive  $V_S$  measurements at the tested borehole locations: converted CPT (circles), converted SPT (squares), SCPT  $V_S$  (upward triangle), bender element  $V_S$  measurement (downward triangle) and refusal depth (stars). .... 70

Figure 3.9: Incipient and transmitted waveforms from the bender element test. .... 72

Figure 3.10: Stress paths obtained from DSS test. .... 73

Figure 3.11: Comparison of invasive and non-invasive  $V_S$  profiles. .... 75

Figure 3.12: Average invasive  $V_S$  profiles for  $V_{S30}$  estimation at sites OT-8 and OT-11 calculated using the subsurface description from Table 3.1. .... 76

Figure 4.1: Flow chart summarizing proposed robust earthquake site classification procedure. Dashed line indicates  $V_S$  proxy method, solid line indicates  $V_S$  method; the thicker the solid lines, the more preferred the method. .... 86

## List of Abbreviations, Symbols and Nomenclature

1D	One dimensional
2D	Two dimensional
AVA	Ambient Vibration Array
CHBDC	Canadian Highway and Bridge Design Code
CPT	Cone Penetration Test
DSS	Direct Simple Shear
F-K	Frequency Wavenumber
$f_0$	Fundamental frequency
$f_{\text{peak}}$	Frequency of maximum amplification from MHVSR
HRFK	High-Resolution Frequency Wavenumber
HVSR	Horizontal-to-Vertical Spectral Ratio
MASW	Multi-channel Analysis of Surface Waves
MHVSR	Microtremor Horizontal-to-Vertical Spectral Ratio
MSPAC	Modified Spatial Auto-Correlation
MTO	Ministry of Transportation Ontario
N	SPT Blowcount number
NBCC	National Building Code of Canada
$q_{c1}$	Normalized cone tip resistance
RMSE	Root-Mean-Square Error

SCPT	Seismic Cone Penetration Test
SPAC	SPatial Auto Correlation
SPT	Standard Penetration Test
$S_u$	Undrained shear strength
$V_{R40}$	Phase velocity of a Rayleigh-wave with a 40-m wavelength
$V_S$	Shear wave velocity
$V_{S1}$	Normalized shear-wave velocity
$V_{S30}$	Time-weighted average $V_S$ in the upper 30 meters

## Chapter 1

### 1 Introduction and Literature Review

Earthquakes are one of the natural hazards which can result in excessive harm because of the vibrations caused by the rapid release of energy stored in the earth's crust. Observations made in previous earthquakes show that the damage caused by an earthquake can be significantly higher on unconsolidated soils than on rock (e.g., 1985 magnitude (M) 8.0 Mexico City, 1989 M 6.9 Loma Prieta, 1994 M 6.7 Northridge, and 1995 M 6.9 Kobe earthquakes). The M 6.9 Kobe earthquake caused major damage to bridges and elevated road structures (Figure 1.1). This was mainly because several of the bridges were built on sand-gravel terraces overlying gravel-sand-mud deposits which resulted in the amplification of ground motion (Moehle and Eberhard 2000). Earthquake shaking varies depending on the type of material present. Therefore, understanding specific ground properties beneath a site is important when constructing high-risk infrastructure like bridges. Near surface geotechnical site evaluation is essential in studying a site's response to earthquake shaking.



**Figure 1.1: Nishinomiya-ko Bridge collapse in the 1995 Kobe earthquake in Japan  
(Moehle and Eberhard 2000)**

When an earthquake occurs, the frequency amplitude and duration of ground motion changes as the seismic wave travels through the soil to the ground surface (Kramer 1996). Thus, the soil layer acts as a filter and amplifier and alters the characteristics of the ground motion. How these waves are altered by subsurface geology is largely dependent on seismic impedance(s), material damping, and nonlinear behavior of the soil. The linear amplification of ground motion is mainly controlled by impedance contrast, and thickness and shear wave velocity ( $V_S$ ) of the soil layer.  $V_S$  is important in defining the small-strain shear modulus primarily expressed as

$$G_0 = \rho \cdot V_S^2 \quad (1.1)$$

where  $G_0$  is the shear modulus, and  $\rho$  is the mass density of the material. Shear waves are of major importance to engineers as they impart lateral load to structures due to its mode of propagation (Crow and Hunter, 2012). Geological conditions may differ from site to site and it is important to understand how earthquake shaking will be altered within a soil deposit, particularly in soft unconsolidated sediments which may have a sharp near-surface impedance contrast with underlying bedrock. A strong impedance contrast will result in higher ground motion amplification and due to the presence of the unconsolidated soil, an earthquake shaking will be significantly stronger at the ground surface. The presence of thick, soft (or loose), fluvial and lacustrine sediments combined with aging infrastructure built to out-dated seismic design standards (or none) leads to a higher seismic risk in eastern Canada (Hunter and Atukorala 2015), particularly in Ottawa and surrounding cities. Therefore, it is important to understand site characteristics and seismic response of these sites

Various geotechnical parameters are essential for the safe seismic design of structures, however, this research is focused on the methods involved in determining the time-averaged shear wave velocity in the upper 30 meters ( $V_{S30}$ ). The ability to capture general impedance-based amplification led to the proposal of  $V_{S30}$  for earthquake site classification (Borcherdt 1994).  $V_{S30}$  is widely used in building codes and seismic hazard analysis such as ground-motion prediction equations (GMPEs) because it is a simplified quantitative parameter to estimate earthquake site amplification. Various research is

ongoing to incorporate the use of predominant site period in site classification schemes (e.g., Zhao et al., 2006; di Alessandro et al., 2012). In 2005, the National Building Code of Canada (NBCC) adopted the use of  $V_{S30}$  for earthquake site classification (Humar 2015), which was recently adopted in the 2015 Canadian Highway Bridge Design Code (CHBDC; CSA Group 2014). Table 1.1 summarizes the six earthquake site classes in CHBDC, their defined  $V_{S30}$ , standard penetration resistance ( $N_{60}$ ) and soil undrained shear strength ( $S_u$ ) limits. Nevertheless, these Canadian seismic design codes do not provide any recommendation for using a specific method to measure  $V_{S30}$ , and thus, geotechnical engineers are often challenged with determining the appropriate technique to measure this important parameter.

**Table 1.1: Site categories in CHBDC (CSA Group 2014).**

Site Class	Site Description	Average properties in top 30 m		
		$V_{S30}$ (m/s)	Standard penetration resistance, $N_{60}$	Soil undrained shear strength, $S_u$ (kPa)
A	Hard rock	$1500 < V_{S30}$	Not applicable	Not applicable
B	Rock	$760 < V_{S30} \leq 1500$	Not applicable	Not applicable
C	Very dense soil and soft rock	$360 < V_{S30} \leq 760$	$50 < N_{60}$	$100 < S_u$
D	Stiff soil	$180 < V_{S30} \leq 360$	$15 < N_{60} < 50$	$50 < S_u < 100$
E	Soft soil	$V_{S30} < 180$	$N_{60} < 15$	$S_u < 50$
F	Very soft soils (e.g., peat, organic soils, etc)	Site-specific measurements are required		

There are several  $V_s$  profiling methods broadly grouped into invasive and non-invasive techniques. Understanding the accuracy and limitations of these methods plays a significant role in selecting the appropriate method for site characterization. Invasive techniques sample small volumes of subsurface material at a high resolution, providing discrete  $V_s$  measurements with depth. Examples of invasive methods include Standard Penetration Testing (SPT; Skempton 1986), Cone Penetration Testing (CPT; Robertson et al., 1995), and downhole and crosshole velocity measurements. In a SPT (ASTM D1586), a thick walled sample tube is advanced by a heavy slide hammer up to 18 inches into the ground. The number of hammer strikes (blow counts) required to advance the sample tube to the second and third 6-inch depth intervals is known as the standard penetration resistance,  $N$ . It is a popular *in situ* test of material stiffness with depth. A



CPT test (ASTM D3441) involves pushing an ASTM standard hardened cone shape into the ground. The cone is advanced using steel rods and a hydraulic ram. A CPT provides measurements of sleeve friction ( $f_s$ ) and tip resistance ( $q_c$ ) which are related to the strength characteristics of the soil. In general, coarse grained sediments will produce relatively higher tip resistance compared to fine grained sediments. CPT is widely used because of its speed of data acquisition and ability to provide precise data (Schmertmann 1977). A seismic CPT (SCPT; Campanella et al., 1986) provides interval shear-wave velocity measurements each meter as the cone is advanced; a geophone located near the cone tip records interval shear-wave travel times generated by hammer blows to a well-coupled steel beam on the ground surface immediately beside the CPT.

Invasive methods are not free of challenges. Cone or rod penetration methods do not penetrate through very stiff material and therefore fail to measure the stiffness of the substratum. Single or multiple borehole techniques require drilling which increases costs. Non-invasive surface seismic techniques for  $V_s$  profiling are attractive because they are quick, relatively cheap, and cause little or no destruction to the ground compared to invasive methods. Examples of non-invasive seismic techniques include Multichannel Analysis of Surface Waves (MASW; Park et al., 1999), Spectral Analysis of Surface Waves (SASW; Stokoe et al., 1988) and Ambient Vibration Array (AVA; Aki, 1957; Asten and Henstridge, 1985) methods.

Surface waves propagate parallel to the surface of the earth and are generated in the presence of a free boundary. The two main types of surface waves are Rayleigh waves which involve elliptical particle motion and Love waves which involve transverse motion. The dispersion of surface waves at a site depends on the underlying elastic material properties. Surface waves propagate at different modes in a horizontally layered heterogeneous medium. Different modes, which are governed by their own propagation velocities exists at each given frequency with the lowest propagation velocity being the fundamental mode and higher propagating velocities being higher modes. Inversion of surface wave dispersion data from active- or passive-source array measurements provides  $V_s$  profiles for site characterization.

Active-source surface wave dispersion techniques require the generation of seismic energy with explosives, weight drops or sledgehammers. A sledgehammer source is most commonly used due to its low cost and portability. A 5 to 8 kg sledgehammer provides a limited energy source within frequencies  $> 8$  to 10 Hz which makes it suitable only for short array lengths and an investigation depth of tens of meters below the ground surface (Foti et al., 2018). In instances when a wider frequency band is required, multiple seismic source types may be used, where a sledgehammer source is used to acquire higher frequency (near surface) data and a weight drop or an explosive source is used to acquire lower frequency (deeper depth) data.

Alternatively, passive-source surface wave dispersion techniques use the natural vibrations of the earth as a seismic energy source. These vibrations (ambient vibrations or microtremor) originate from the constant vibration of the earth's surface produced by low frequency ( $\leq 1$  Hz) natural processes (such as tides, earthquakes and wind) and high frequency ( $\geq 1$  Hz) human activities. The ability of passive source methods to rapidly sample a wide frequency band and produce a greater depth of investigation at a relatively cheaper cost makes them advantageous compared to active source methods. It is assumed that the ambient wave field is mainly composed of surface waves (Arai & Tokimatsu, 2004), and hence passive-source methods are heavily dependent and restricted to the penetration depth of surface waves which goes from tens to a few hundreds of meters. The passive seismic array techniques, first developed by Aki (1957) have been widely used to assess dynamic properties of the earth's subsurface. Methods based on surface-wave analysis have become more popular because they are quick and require less labor for data acquisition. Surface-wave methods such as AVA use the natural vibrations of the earth (microtremors). From microtremor recordings, the Horizontal to Vertical (Fourier) Spectral Ratio (HVSr) is calculated. The maximum of the HVSr generally occurs at the fundamental resonance frequency of the site (equation provided in Chapter 2), if there is a significant impedance contrast at depth. Surface-wave dispersion data are also extracted from array-based microtremor recordings. Both HVSr and dispersion data are jointly or individually inverted to obtain  $V_s$  profiles.

Surface wave methods have gained popularity over the last two decades to obtain  $V_S$  profiles. However, complex data processing coupled with the non-uniqueness of surface wave inversion problem and non-expert usage have contributed to the lack of confidence in the use of non-invasive surface wave analysis in the engineering community (Foti et al., 2018). Several comparisons between invasive and non-invasive  $V_S$  profiling methods have been performed to assess their intra- and inter-variability. Through the InterPACIFIC project, Garofalo et al. (2015a, b) analyzed the variability of  $V_S$  profiling methods for three sites in Italy and France with different subsurface conditions (soft soil, stiff soil or sedimentary rock) and found comparable  $V_{S30}$  estimates between invasive and non-invasive methods. They concluded that, since the variability in  $V_{S30}$  estimates was small, the non-uniqueness of  $V_S$  profiles obtained from non-invasive surface wave techniques plays a limited role in the overall  $V_{S30}$  estimates. Similarly, Molnar et al. (2015) performed blind test comparisons at 11 strong-motion stations in central and southern Chile, and found an average relative difference in  $V_S$  between both methods to be ~10% for soil layers and ~30% for bedrock.

In cases where  $V_S$  cannot be directly measured in the field due to economic constraints or site-specific challenges, empirical relationships between  $V_S$  and available penetration testings can be useful. For this reason, a number of penetration-to- $V_S$  correlations have been developed in literature for different soil types (Baldai et al. 1989; Mayne and Rix 1993; Karray et al. 2011; Tonni and Simonini 2013). This is particularly useful for small scale or low risk projects where direct  $V_S$  measurements are not available.

With the adoption of  $V_{S30}$  as the earthquake site classification criterion in the 2015 bridge design code (CSA Group 2014), the Ministry of Transportation Ontario (MTO) seeks a wider range of applicable geophysical techniques towards optimizing a robust site classification procedure(s) for Ontario bridge sites. For this reason, we performed a true blind test comparison of non-invasive with invasive  $V_S$  profiles at ten bridge sites in southwestern, Ontario. To objectively assess the difference between invasive and non-invasive  $V_S$  profiling methodologies and subsequent site classification, detailed geotechnical information from MTO online reports was only examined by the authors after the joint inversions of the non-invasive data had been completed. Only the locations

and type of invasive testing was known prior to our non-invasive testing. This blind comparison protocol was employed such that, the velocity profiles determined from the non-invasive surface wave analysis are truly independent of the any influence from the borehole velocity measurements (considered here as ground truth).

## 1.1 Aim of Research

Our goal is to aid geotechnical engineers in determining the most appropriate field-based method(s) to determine  $V_{S30}$  and therefore earthquake site classification. We primarily perform blind comparisons of non-invasive shear-wave velocity depth profiling with invasive penetration and/or borehole methods at 10 bridge sites in southern Ontario. Overall, we seek to optimize a robust earthquake site classification procedure(s) for bridge sites in Ontario.

## 1.2 Organization of work

This thesis is comprised of two main chapters which assess  $V_S$  profiling methods and earthquake site classification methodologies at bridge sites within three different geological settings in Ontario.

In Chapter 2, we apply non-invasive AVA testing to obtain  $V_S$  profiles at six bridge sites along the Rt. Hon. Herb Gray Parkway in Windsor, Ontario. Our non-invasive testing is co-located with previous invasive testing, including SPT, CPT and downhole and crosshole  $V_S$  data. We perform a blind comparison of non-invasive  $V_S$  profiling with invasive techniques to assess the variability between methodologies. This chapter also includes regression analysis to develop a correlation between CPT tip resistance and measured  $V_S$ . We use our non-invasive  $V_S$  profiles obtained from the surface wave inversion together with the previous invasive  $V_S$  data to develop this relation. We also find that our relation compares well with other relations for similar soils in literature.

Chapter 3 describes the use of both active and passive source non-invasive surface seismic measurements conducted at Ontario bridge sites in different geological settings,

including a bridge site in Oshawa and three bridge sites in Ottawa. Laboratory bender element  $V_S$  measurements of a borehole sample for the Oshawa site are presented. We find that the active-source surface wave array technique provides additional constraints on near surface velocity structure and is useful at sites with shallow depth to significant impedance. We highlight the effectiveness of non-invasive seismic techniques which offer a rapid and cost effective  $V_S$  profiling method and alternative for earthquake site classification at bridge sites in Ontario.

Chapter 4 presents overall thesis findings and conclusions. A robust earthquake site classification procedure (reliable  $V_{S30}$  estimates) for bridge sites across Ontario is evaluated and proposed from the available combinations of invasive and non-invasive  $V_S$  profiling methods.

### 1.3 References

- Aki, K. (1957). Space and time spectra of stationary stochastic waves, with special reference to microtremors. *Bulletin of the Earthquake Research Institute, University of Toronto*, 35, 415–456.
- Arai, H., and Tokimatsu, K. (2004). S-Wave Velocity Profiling by Inversion of Microtremor H/V Spectrum. *Bulletin of the Seismological Society of America*, 94(1), 53–63. <http://doi.org/10.1785/0120030028>
- Asten, M. W., and Henstridge, J. (1984). Array estimators and the use of microseisms for reconnaissance of sedimentary basins. *Geophysics*, 49(11), 1828–1837.
- Baldi, G., Bellotti, R., Ghionna, V., Jamiolkowski, M., and Pasqualini, E. (1986). Interpretation of CPT's and CPTU's. 2: Drained penetration in sands. *Proc., 4th Int. Geotechnical Seminar Field Instrumentation and In Situ Measurements*, Nanyang Technological Institute, Singapore, 143–156.

- Borcherdt, R. D. (1994). Estimates of site-dependent response spectra for design (methodology and justification). *Earthquake spectra*, 10(4), 617-653.
- Campanella, R. G., Robertson, P. K., and Gillespie, D. (1986). Seismic cone penetration test. In *Use of in situ tests in geotechnical engineering*, ASCE, 116-130.
- CSA Group (2014). S6-14 Canadian Highway Bridge Design Code, Section 4 – Seismic design, Mississauga, Ontario, 171-226.
- Crow, H.L. and Hunter, J.A., (2012). Chapter 5.0: Shear Wave Guidelines for Non-technical Users; in *Shear Wave Velocity Measurement Guidelines for Canadian Seismic Site Characterization in Soil and Rock*, (ed.) J.A. Hunter and H.L. Crow; Geological Survey of Canada, Open File 7078, 211-223.
- di Alessandro, C., L. F. Bonilla, D. M. Boore, A. Rovelli, and O. Scotti (2012). Predominant-Period Site Classification for Response Spectra Prediction Equations in Italy, *Bull. Seismol. Soc. Am.* 102, 680-695.
- Foti, S., Hollender, F., Garofalo, F., Albarello, D., Asten, M., Bard, P. Y., and Forbriger, T. (2018). Guidelines for the good practice of surface wave analysis: a product of the InterPACIFIC project. *Bulletin of Earthquake Engineering*, 16(6), 2367-2420.
- Garofalo, F., Foti, S., Hollender, F., Bard, P.Y., Cornou, C., Cox, B.R., Ohrnberger, M., Sicilia, D., Asten, M., Di Giulio, G. and Forbriger, T. (2016a). InterPACIFIC project: Comparison of invasive and non-invasive methods for seismic site characterization. Part I: Intra-comparison of surface wave methods. *Soil Dynamics and Earthquake Engineering*, 82, 222-240.
- Garofalo, F., Foti, S., Hollender, F., Bard, P.Y., Cornou, C., Cox, B.R., Ohrnberger, M., Sicilia, D., Asten, M., Di Giulio, G. and Forbriger, T. (2016b). InterPACIFIC project: Comparison of invasive and non-invasive methods for seismic site characterization. Part I: Inter-comparison of surface wave methods. *Soil Dynamics and Earthquake Engineering*, 82, 241-254

- Humar, J. (2015). Background to some of the seismic design provisions of the 2015 National Building Code of Canada. *Can. J. Civil Eng.*, 42, 940-952.
- Hunter, J.A. and Atukorala, U. (2015). Chapter 1.0: Introduction; in Shear Wave Velocity Measurement Guidelines for Canadian Seismic Site Characterization in Soil and Rock, (ed.) J.A. Hunter and H.L. Crow; Geological Survey of Canada, Earth Science Sector, General Information Product 110 e:8- 17.
- Karray, M., Lefebvre, G., Ethier, Y., and Bigras, A. (2011). Influence of particle size on the correlation between shear wave velocity and cone tip resistance. *Canadian Geotechnical Journal*, 48(4), 599-615
- Kramer, S. L. (1996). Geotechnical earthquake engineering. Upper Saddle River, NJ: Prentice Hall.
- Mayne, P. W., and Rix, G. J. (1993).  $G_{max}$ -qc relationships for clays. *Geotechnical Testing Journal*, 16(1), 54-60.
- Moehle, J. P., and Eberhard, M. O. (2000). Earthquake damage to bridges. Bridge engineering handbook, 1-34.
- Molnar, S., Ventura, C. E., Boroschek, R., and Archila, M. (2015). Site characterization at Chilean strong-motion stations: Comparison of downhole and microtremor shear-wave velocity methods. *Soil Dynamics and Earthquake Engineering*, 79, 22-35.
- Park, C. B., Miller, R. D., and Xia, J. (1999). Multichannel analysis of surface waves." *Geophysics*, 64(3), 800-808.
- Robertson, P. K., Sasitharan, S., Cunning, J. C., and Segoo, D. C. (1995). Shear-wave velocity to evaluate in-situ state of Ottawa sand. *Journal of Geotechnical Engineering*, 121(3), 262-273
- Schmertmann, J. H. (1977). Guidelines for CPT performance and Desing. *Federal Highway Administration HDV*, 22.

- Skempton, A. W. (1986). Standard penetration test procedures and the effects in sands of overburden pressure, relative density, particle size, ageing and overconsolidation. *Geotechnique*, 36(3), 425-447.
- Stokoe, K. H., Nazarian, S., Rix, G. J., Sanchez-Salinero, I., Sheu, J.-C., and Mok, Y.-J. (1988). In situ seismic testing of hard-to-sample soils by surface wave method. *in Geotechnical Special Publication. Recent advances in ground-motion evaluation* 264-278. ASCE.
- Tonni, L., and Simonini, P. (2013). Shear wave velocity as function of cone penetration test measurements in sand and silt mixtures. *Engineering Geology*, 163, 55-67.
- Zhao, J. X., K. Irikura, J. Zhang, Y. Fukushima, P. G. Somerville, A. Asano, Y. Ohno, T. Oouchi, T. Takahashi, and H. Ogawa (2006). An empirical site-classification method for strong-motion stations in Japan using H/V response spectral ratio, *Bull. Seismol. Soc. Am.* 96, 914–925.



## Chapter 2

# 2 Blind comparison of non-invasive and invasive shear wave velocity profiling at bridge sites in Windsor, Ontario

## 2.1 Introduction

Understanding a site's response to earthquake shaking plays a key role in near surface geotechnical site evaluation. The presence of soft unconsolidated sediments results in higher ground motion amplification when there is a significant impedance contrast between the soil and underlying bedrock. These conditions are site dependent and therefore it is important to evaluate the near-surface ground properties for effective site classification in constructing high risk infrastructure such as bridges. The effects of site conditions can be assessed through the determination of the impedance contrast between soil and bedrock and measurement of shear wave velocity ( $V_s$ ) of soil layers which is directly related to material stiffness. Site classification for seismic site response is primarily based on the time-averaged  $V_s$  of the upper 30 meters ( $V_{s30}$ ) of a site. This was first introduced by Borchardt (1994) and then adopted by many building codes around the world including the National Building Code of Canada (NBCC) in 2005 and the Canadian Highway Bridge Design Code (CHBDC; CSA Group 2014) in 2015. These building codes also allow site classification based on the undrained shear strength ( $S_u$ ) of soil layers, and standard penetration resistance (SPT) blowcount ( $N_{60}$ ; where 60 is the percentage of the theoretical free-fall hammer energy) of the upper 30 m. In most cases, site classification is based on  $V_{s30}$  rather than  $S_u$  or  $N_{60}$ .

Different field techniques are used for  $V_s$  depth profiling and can be broadly categorized into invasive and non-invasive methods. Invasive methods, including SPT, CPT (Schmertmann 1977) or crosshole  $V_s$  profiling (Butler and Curro 1981), provides discrete  $V_s$  measurements, typically in 1-2 m depth increments. SPT is designed to measure the penetration blow count,  $N$  which indicates soil stiffness. It is a popular *in situ* test which is used in correlations with density, unit weight, stiffness, and shear strength. CPT is widely used because of its speed of data acquisition and ability to provide precise data

(Schmertmann 1977). A typical CPT test provides sleeve friction ( $f_s$ ) and tip resistance ( $q_c$ ) which are related to the strength characteristics of the soil. In general, coarse grained sediments will produce relatively higher tip resistance compared to fine grained sediments. However, their costly borehole drilling requirement or inability to penetrate through stiff sublayers (SPT and CPT) and disruptive nature to the ground presents major disadvantages. Conversely, non-invasive methods, including AVA and MASW are less expensive and less disruptive.

Several blind test comparisons between invasive and non-invasive  $V_s$  profiling methods have been performed to assess their intra- and inter-variability. Through the InterPACIFIC project, Garofalo et al. (2015a, b) analyzed the variability of  $V_s$  profiling methods for three sites in Italy and France with different subsurface conditions (soft soil, stiff soil or sedimentary rock) and found comparable  $V_{S30}$  estimates between invasive and non-invasive methods. They concluded that, since the variability in  $V_{S30}$  estimates was small, the non-uniqueness of  $V_s$  profiles obtained from non-invasive surface wave techniques plays a limited role in the overall  $V_{S30}$  estimates. Similarly, Molnar et al. (2015) performed blind test comparisons at 11 strong-motion stations in central and southern Chile, and found an average relative difference in  $V_s$  between both methods to be ~10% for soil layers and ~30% for bedrock.

With the adoption of  $V_{S30}$  as the earthquake site classification criterion in the 2015 bridge design code (CSA Group 2014), the Ministry of Transportation Ontario (MTO) seeks a wider range of applicable geophysical techniques towards optimizing a robust site classification procedure(s) for Ontario bridge sites. For this reason, we performed a true blind test comparison of non-invasive with invasive  $V_s$  profiles at six bridge sites in Windsor, Ontario. To objectively assess the difference between invasive and non-invasive  $V_s$  profiling methodologies and subsequent site classification, detailed geotechnical information from MTO online reports was only examined by the authors after the joint inversions of the non-invasive data had been completed. Only the locations and type of invasive testing was known prior to our non-invasive testing. Additionally, we propose a general correlation between corrected tip resistance and  $V_s$  from the analysis of both invasive and non-invasive data for all soils encountered in the study area.

## 2.2 Location and geological setting

The Rt. Hon Herb Gray Parkway (the Parkway; <http://www.hgparkway.ca/>) is a \$1.4 billion (Canadian dollars) four-to-six lane 11-km highway extension for the proposed Gordie Howe International bridge linking Windsor to Detroit, Michigan. The Parkway is located in the Essex Clay Plain which is part of the larger St. Clair Plain deposited in the late Pleistocene Era (Hudec 1998). The bedrock within this region comprises of bioclastic limestone of the Detroit River Group (Morris 1994). The St. Clair Plain is comprised of glaciolacustrine clay, clayey silt till and silty clay till with successive overburden strata of desiccated lacustrine clay, normally consolidated lacustrine clay, silty Travistock till, glaciolacustrine clay and coarse Catfish Creek till. Hudec (1998) describes a clear change in the overburden strata of Windsor, east and west of Huron Church Road. There is a thin silt, sand and gravel cover in the sites west of Huron Church Road which is generally missing to the east. The east sites are underlain by stiff glaciolacustrine silts and clays with deposits of sandy to silty weathered clay crusts on top. Figure 2.1 shows the locations of the six bridge sites. From north to south, Sites-5 and 6 are located to the northwest, Sites-3 and 4 are located southward along Huron Church Road and Sites-1 and 2 to the southeast.

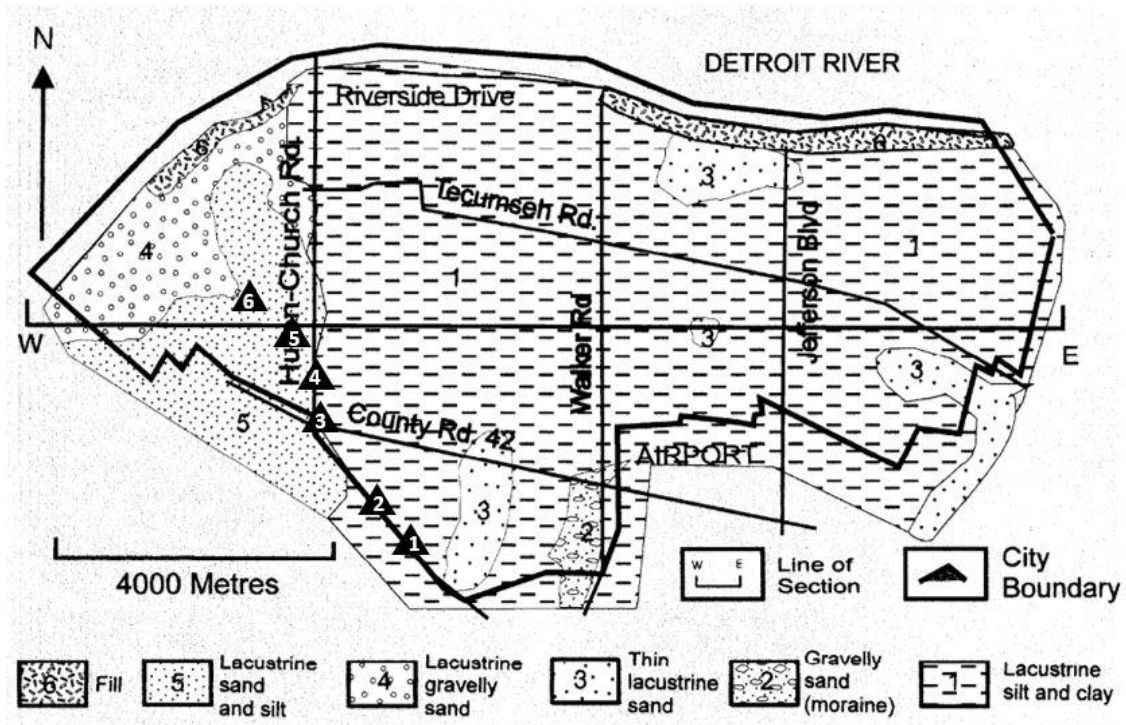


**Figure 2.1: Surface geological map of Windsor. Black triangles show locations of the test sites (modified from Hudec 1998).**

## 2.3 Non-invasive methodology

Ambient vibration techniques are passive-source seismic methods and include single sensor or multi-sensor array methods. The single sensor method involves calculation of a microtremor horizontal to vertical spectral ratio (MHVSR) which provides the site's resonance frequencies. Microtremors are ambient vibrations from natural and human activities. Multi-sensor array methods measure surface wave dispersion using either active or passive seismic sources. Either MHVSR or dispersion curves, or both, is inverted to obtain  $V_s$  profiles to characterize or classify the site.

The single station method first developed by Nogoshi and Igarashi (1971) in Japan and distributed around the world by Nakamura (1989), involves calculating the Fourier HVSR of the ambient vibration record (Molnar et al. 2018). Only a single three component seismometer is required to measure a MHVSR. Various studies have demonstrated that the MHVSR peak frequency corresponds to the fundamental shear-

wave resonance frequency ( $f_0$ ) of the site, which is dependent on  $V_s$  and thickness of the resonating layer. This can be represented by:

$$f_0 = \frac{V_{s\_ave}}{4h} \quad (2.1)$$

where  $V_{s\_ave}$  and  $h$  are the average  $V_s$  and thickness of the soil layer respectively.

It is assumed that ambient vibrations are predominantly made up of surface waves. Thus in a 1D layered medium with a strong impedance contrast at depth, the MHVSR can be assumed to be an approximation of the ellipticity of Rayleigh waves (Scherbaum et al., 2003). For this reason, MHVSR's can be used, through inversion, to determine  $V_s$  profiles.

In instances where there are multiple peaks in the MHVSR record, the peak at the lowest frequency represents the fundamental mode and the other peaks at higher frequencies represent near surface geologic interfaces with sufficient impedance contrast. It is typically assumed that fundamental peak frequency is correlated with bedrock depth, but it is technically a measure of the most significant impedance contrast at the site or the resonator depth. In southwestern Ontario, soft sediments typically overlie very stiff (overconsolidated) glacial till or seismic bedrock. Hence, resonator depth determined from the MHVSR's fundamental peak frequency may indicate the depth of either glacial till or seismic bedrock.

Ambient vibration array (AVA) methods involve recording ambient vibrations simultaneously with multiple sensors in a 2D array. It is typically assumed that vertical component ambient vibrations are mainly composed of Rayleigh surface waves and are dispersive. That is, waves of longer wavelengths (low frequency) penetrate deeper into typically higher velocity layers and arrive earlier than shorter wavelength (higher frequency) waves which travel slower in the near surface. Thus, the phase velocity of Rayleigh waves at particular frequencies is a dispersion curve, which is nonlinear and specific to the site's underlying velocity structure. Array measurements are repeated with increasing radii to penetrate deeper into the subsurface (increasing wavelengths). The goal is to obtain dispersion estimates over a wide frequency range and produce a "full"

dispersion curve of the site for subsequent inversion. Through inversion of extracted surface wave dispersion data from array recordings, it is possible to obtain  $V_s$  depth profile(s) of the subsurface.

Dispersion estimates are extracted from AVA recordings using the spatial auto-correlation (SPAC) technique (Aki 1957). This technique operates on the assumption that the ambient vibration signal is stochastic and stationary in both time and space. Circular or triangular arrays provide ideal azimuthal sampling of the vibration wavefield, but can be difficult to deploy in urban environments. The modified SPAC technique (MSPAC; Bettig et al. 2001) accounts for non-symmetric arrays. Station pair recordings at various azimuths of each array are analyzed for different narrow radii intervals or distance rings. The azimuthal-averaged spatial auto-correlation ratio is a summation of the auto-correlation ratios of each station pair within each ring. Phase velocities at select frequencies can then be calculated by inverting the azimuthal averaged spatial auto-correlation ratio:

$$\overline{\rho_{r_1, r_2}}(\omega) = \frac{2}{r_2^2 - r_1^2} \frac{c(\omega)}{\omega} [r \cdot J_1\left(\frac{\omega r}{c(\omega)}\right)]_{r_1}^{r_2} \quad (2.2)$$

where  $J_1$  is the Bessel function of the first order,  $\omega$  is the angular frequency,  $r$  is the interstation distance,  $c$  is the Rayleigh wave velocity, and  $r_1$  and  $r_2$  are the radii of the inner and outer rings, respectively.

## 2.4 Survey geometry and data acquisition

We conducted non-invasive seismic testing along the Windsor-Essex Parkway from May 23<sup>rd</sup> to 26<sup>th</sup>, 2017. The non-invasive tests were conducted within 300 m from existing invasive tests (Figure 2.2). Ambient vibrations were collected using Trominos<sup>®</sup> which are ultra-compact and ultra-lightweight instruments with three component high-sensitivity velocimetric channels and a low frequency limit of 0.1 Hz. These tri-axial seismic sensors operating at a 128 Hz sampling frequency were placed on the ground surface to record ambient vibrations near 6 bridge sites along the Parkway. Example measurement locations are shown in Figure 2.3. Arrays of sensors were set up on the baseball playing field at two locations (Site-1 and 4) and in open park spaces with grass removed for the

other sites. Each array was composed of 3 sensors in an equilateral triangular configuration. The distance between the sensors was varied 4 times from 5, 10, 15 to 30 m. At Site-5, the site environment did not allow for 30 m sensor spacing. Ambient vibrations were recorded simultaneously for approximately 15 minutes at 5 and 10 m array spacings, and for approximately 20 minutes at 15 and 30 m array spacings.

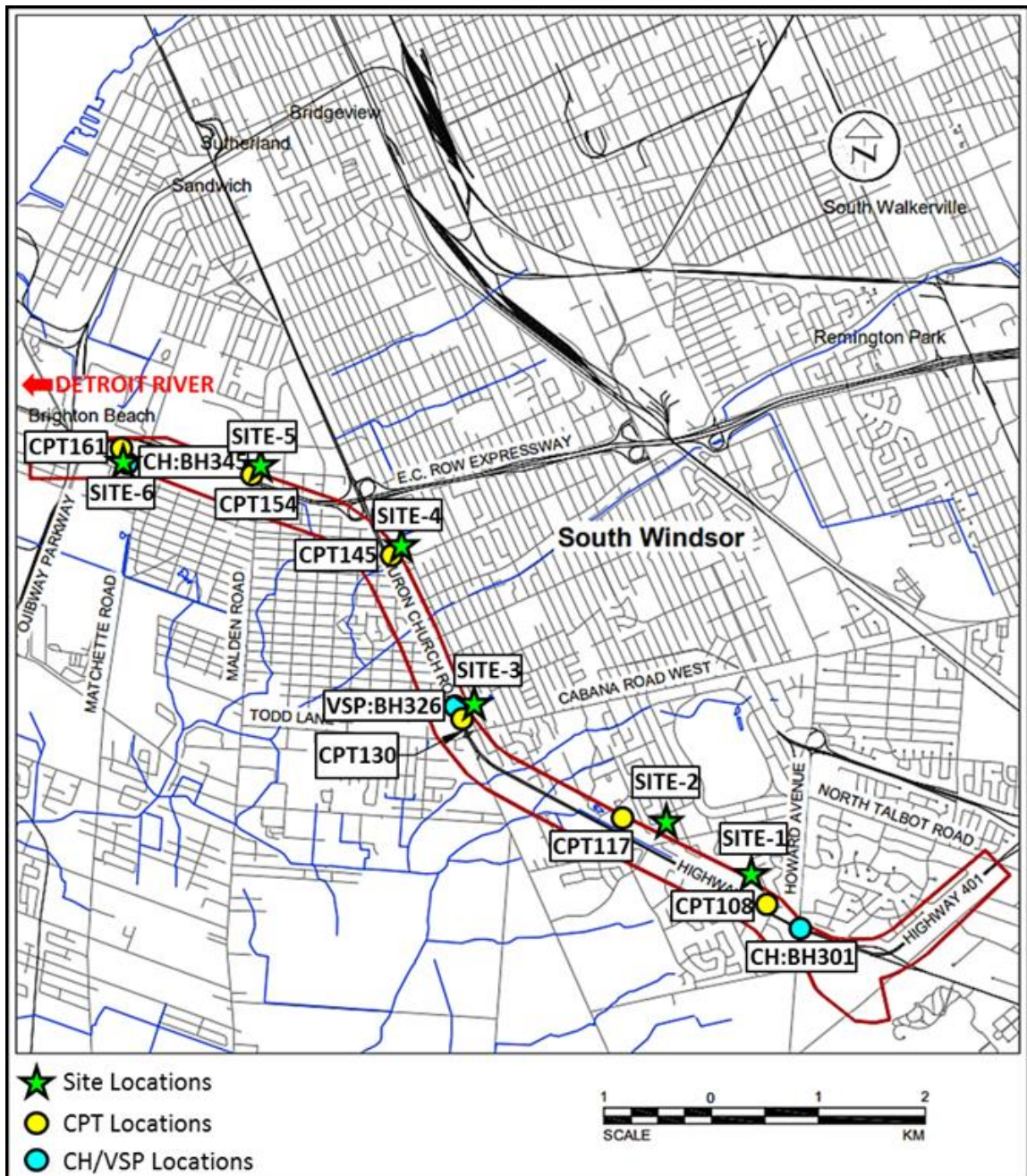
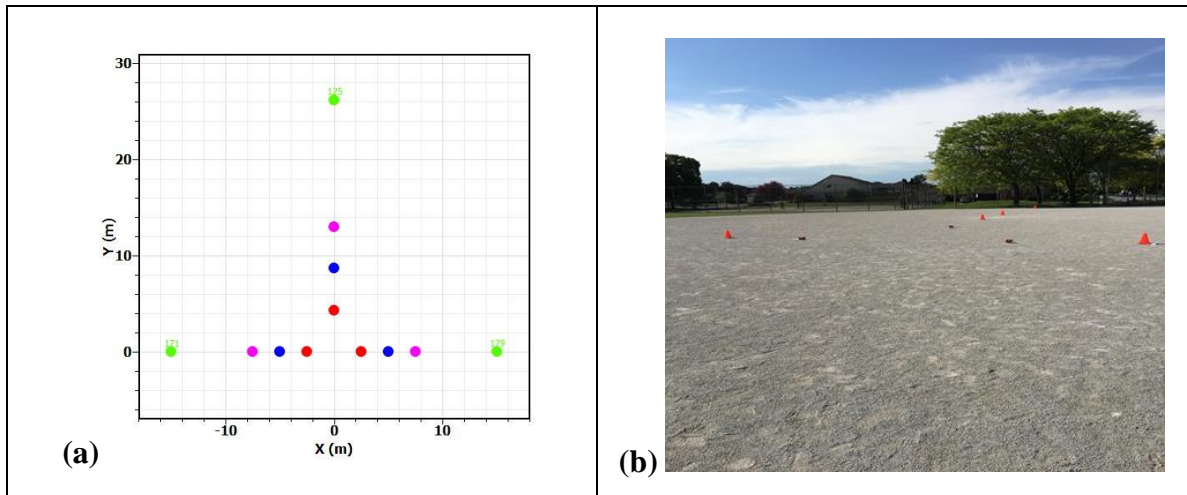


Figure 2.2: Location of test sites and previous invasive tests.



**Figure 2.3: (a) Schematic diagram of 3-sensor triangular array. Each color represents different array aperture. (b) Photo of a 5 m array set up on a baseball playing field at Site-4. Tromino sensors appear as small red boxes surrounded by orange traffic cones.**

## 2.5 Data processing and analysis

For both dispersion and MHVSR processing, we used the Geopsy open source software (Wathelet, 2008; v. 2.9.1). When required, spurious noise signals resulting from personnel walking to and from sensors at the beginning and end of each array set up are removed from the analysis.

### 2.5.1 MHVSR

Each three-component recording is divided into 60-second-time windows and a 5% cosine taper is applied to each trace. The traces are then transformed to the frequency domain and smoothed by the Konno Ohmachi filter with a bandwidth of 40 (Konno and Ohmachi 1998). By dividing the squared average horizontal spectra by the vertical spectrum, the time-averaged MHVSR is calculated between 0.5 and 15 Hz. The time-averaged MHVSRs are averaged for all sensor recordings in the array to obtain an array-averaged MHVSR. Consistency of the array-averaged MHVSRs confirms lateral uniformity of the subsurface ground conditions. The array-averaged MHVSRs are presented in Figure 2.4. The array-averaged MHVSRs for most sites show a clearly



defined sharp peak at ~2 Hz with a fairly consistent amplification of ~10. For two sites (Site-6, Site-2), large amplification is observed at frequencies  $\leq 1$  Hz, likely due to bad sensor coupling. The ~2 Hz peak is still present at these sites with reduced amplification to ~6. Generally, we did not observe peaks at higher frequencies except at Site-5.

The single high-amplification peak observed at Sites-1, 3, 4 and 5 is due to a near surface strong impedance contrast and likely represents a simple profile with a single soil layer till or over bedrock. These sites also show similar depth to the resonator due to their consistent peak frequency. Subtle changes in the shapes of MHVSRs may indicate subtle changes in subsurface conditions amongst sites; where a subtle peak at ~6.5 Hz at Site-5 may be indicative of the thin lacustrine silt and sand cover in the western part of Windsor which is absent in the east (see Figure 2.1). The reduction in peak amplification at Sites-2 and 6 could be attributed to changes in wavefield conditions and/or poor sensor coupling (Sharma et al. 2018).

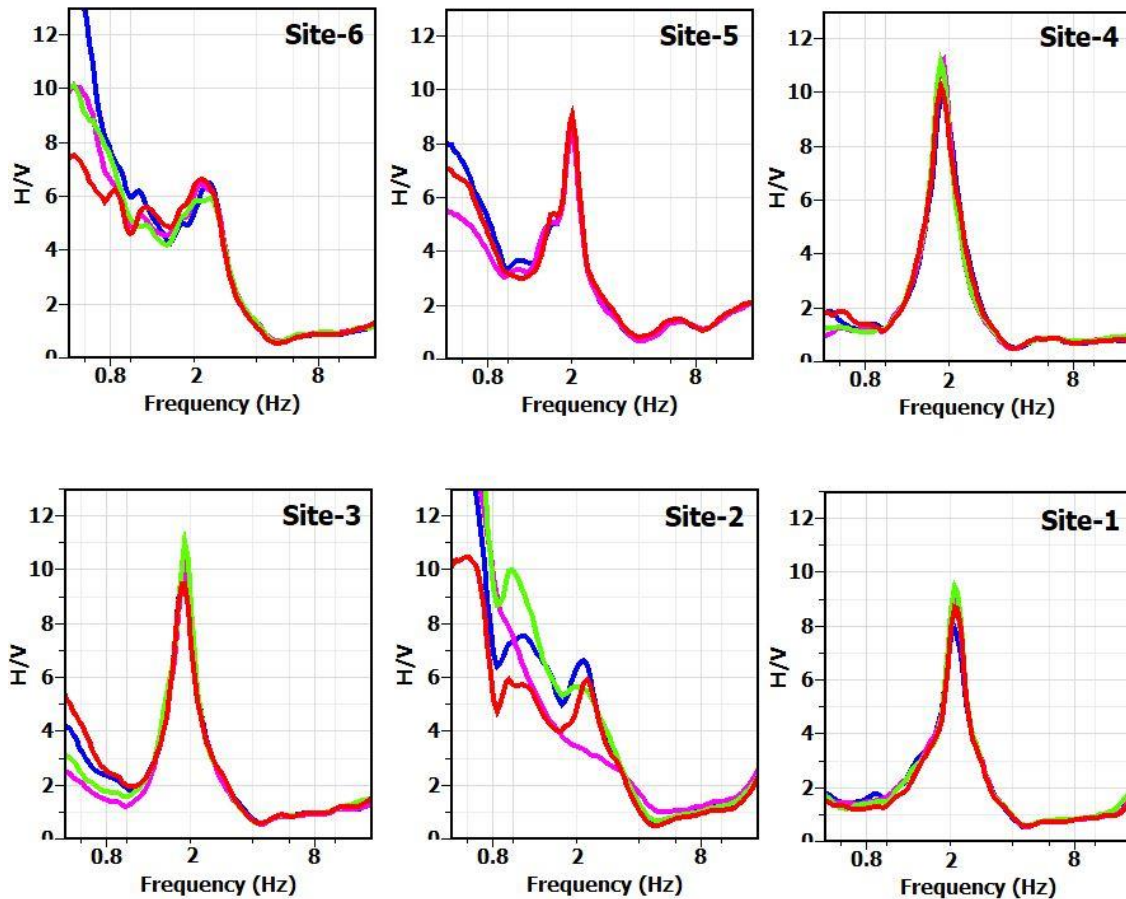


**Figure 2.4: Array-averaged MHVSR calculated from all sensors in each array aperture. Red, blue, magenta and green lines represents 5, 10, 15 and 30 m array spacings respectively. Upper left to lower right panels are sites from northwest to southeast along the Parkway.**

### 2.5.2 Dispersion curves

Ambient vibration vertical-component recordings for each array are analyzed using MSPAC to extract dispersion estimates. A stacked histogram of dispersion estimates from all azimuthally averaged spatial autocorrelation ratios calculated at narrow distance intervals (rings) at select frequencies is generated (Figure 2.5). The resolution and aliasing limits shown here are set based on the maximum peak of the spatially-averaged autocorrelation curve calculated from the largest ring and the minimum peak (trough) of the spatially-averaged autocorrelation curve calculated from the smallest ring of all

arrays, respectively. These minimum resolution and aliasing limits of all arrays define the boundaries within which dispersion estimates are reliable. For quality control, we also performed high resolution frequency wavenumber dispersion analysis to generate dispersion curves for each site (see Appendix A) and confirmed that dispersion estimates were consistent with the MSPAC results.

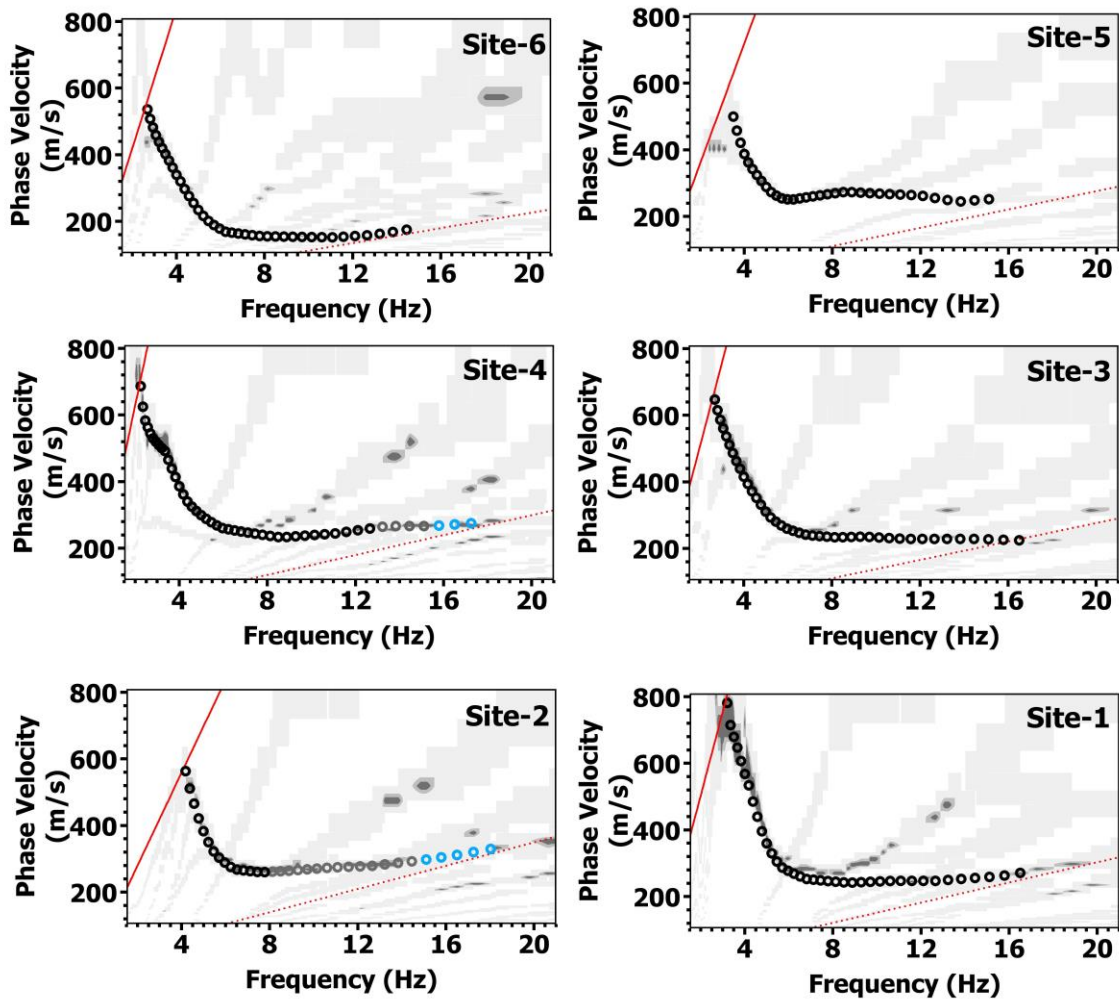


**Figure 2.5: Picked dispersion estimates (open circles) for each site; blue circles represent potential higher mode dispersion estimates, grey circles represent transitional picks between fundamental and first higher modes. Background shading is MSPAC dispersion estimates; darker shades indicate higher count. Minimum resolution and aliasing limits are shown as solid and dashed lines respectively.**

Figure 2.5 shows that, phase velocities range between 150 to 800 m/s for these Windsor sites, with a rapid increase in phase velocities at frequencies below  $\sim 4$  Hz (approaching the  $\sim 2$  Hz peak frequency). The fundamental mode Rayleigh wave dispersion curve is manually picked within the resolution and spatial aliasing limits of each array. The lowest phase velocities occur at the northernmost Site-6. At Site-5 the variation in phase velocities at higher frequencies (between 6 to 15 Hz) may be an indication of the varying shallow subsurface conditions as mentioned in earlier sections and are therefore selected as the fundamental mode. At almost all sites, an increase in phase velocity is also observed at the high frequency ‘end’ of the dispersion curve. This is an “apparent” dispersion trend generated by mode mixing typically due to a near-surface stiffer layer over a softer layer, i.e., velocity inversion. Consequently, the measured fundamental mode dispersion data progressively increase to higher modes at Sites-2 and 4. This phenomenon has been explored by Foti et al (2017). They propose different strategies to account for higher modes however there is yet to be a standardized procedure to fully account for the influence of higher modes. Alternate Rayleigh wave dispersion curve picks identifying potential higher modes for Sites-2 and 4 are presented in Appendix B.

## 2.6 Preliminary $V_{S30}$ assessment

Preliminary  $V_{S30}$  was estimated for each site from the experimentally determined dispersion curve based on relations between phase velocity and  $V_{S30}$  (e.g., Brown et al 2000; Martin and Diehl 2004). Martin and Diehl (2004) suggest that  $V_{S30}$  can be estimated from the phase velocity of a 40-45 m wavelength Rayleigh wave, given by:

$$V_{S30} = 1.045 V_{R[40-45]} \quad (2.3)$$

where  $V_{R[40-45]}$  is the phase velocity of the Rayleigh wave corresponding to the fundamental mode, at wavelengths from 40 to 45 m. As shown in Figure 2.6, we determine  $V_{S30}$  for each site from the phase velocity value that intersects with the  $V_{R40}$  line. The data indicate  $V_{S30}$  values between 220 and 275 m/s corresponding to a CHBDC site Class D ( $V_{S30}$  of 180-360 m/s) for the six bridge sites in Windsor, Ontario studied in this paper.

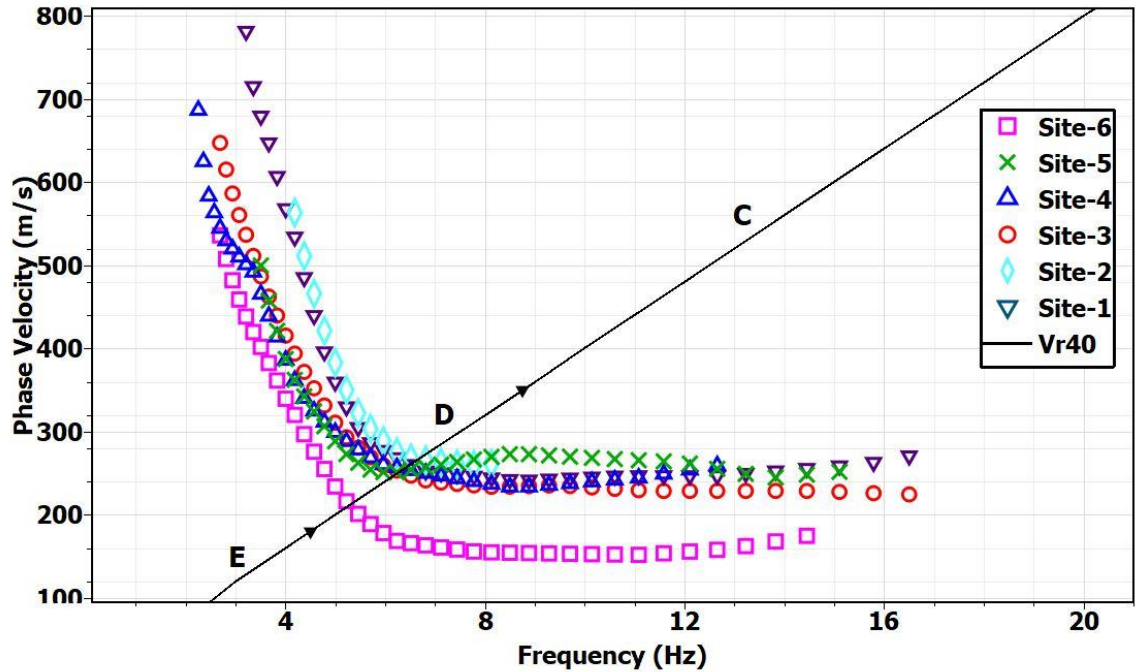


**Figure 2.6: Fundamental mode dispersion curves for each site. Black triangles indicate  $V_{S30}$  boundaries (converted to  $V_{R40}$ ) between site classes E, D, and C.**

## 2.7 Inversion methodology

The inversion of Rayleigh wave dispersion and/or ellipticity data to obtain shear-wave velocity profiles is a non-linear and non-unique problem for which there is no single unique earth model that fits the experimentally measured dataset(s). Solving this problem requires the use of an iterative inversion algorithm which searches for a range of possible solutions that fit the observed data based on the misfit function (difference between generated models and measured data). Inversion methods can be broadly grouped into local search methods and global search methods based on their principle of inversion. The inversions in this study are performed using the Dinver inversion tool which is part of the Geopsy software package. This tool uses a modified conditional neighborhood algorithm (Wathelet 2008) which is a stochastic direct search method. The neighborhood algorithm (Sambridge et al., 1999) searches for the minima of the misfit function by investigating the multi-dimensional parameter space. The neighborhood algorithm is

unique because of the use of previously generated samples to guide the search for improved models by interpolating the misfit neighborhood of samples using Voronoi cells. The misfit between a theoretical and measured dispersion curve is defined by (Wathelet 2005):

$$misfit = \sqrt{\sum_{i=0}^{n_F} \frac{(x_{di} - x_{ci})^2}{\sigma_i^2 n_F}} \quad (2.4)$$

where  $x_{di}$  is the velocity of the measured dispersion curve at frequency  $f_i$ ,  $x_{ci}$  is the velocity of the calculated dispersion curve at the same frequency  $f_i$ ,  $\sigma_i$  is the standard deviation of the frequency samples considered and  $n_F$  is the number of frequency samples considered. If no uncertainty is provided, then  $\sigma_i$  is replaced by  $x_{di}$  in the equation above.

The misfit between a theoretical and measured ellipticity curve is defined by (Wathelet 2005):

$$misfit_{ellipticity} = \frac{(f_{peak})_{measured} - (f_{peak})_{theoretical}}{(df_{peak})_{measured}} \quad (2.5)$$

where  $(df_{peak})_{measured}$  is the standard deviation of the experimentally measured peak frequency.

For the forward problem, which involves computation of the theoretical dispersion curves and/or Rayleigh wave ellipticity, the neighborhood algorithm generates a pseudo-random seed number used to draw starting models from the provided (default or user-modified) model parameterization. The computation results are then compared to the measured dispersion curve and/or Rayleigh wave ellipticity to obtain the misfit value using the two equations above. The neighborhood algorithm does this by generating models in parameter space and constructs Voronoi cells around the recently generated set of models based on their misfit with the measured data. The models with lowest misfits are then identified using a Gibbs sampler by performing a uniform random walk from each cell selected previously to a location in the parameter space but restricted to the chosen cell. This way the inversion is driven forward using the misfit obtained from the previous

sample. In cases where both dispersion and ellipticity data are jointly inverted, separate misfit values are calculated for each individual dataset then a final misfit value, which is a weighted average of both values, is computed.

We perform a joint inversion of the MHVSR and dispersion curve to minimize the non-uniqueness of the model solution. An inversion of the higher-frequency dispersion curve alone constrains the near-surface sedimentary velocity profile, however the inclusion of MHVSR peaks provides additional constraints on bedrock depth and velocity. The MHVSR inversion alone yields ambiguous  $V_s$  profiles (Hobiger et al., 2012); either soil layer thickness (resonator depth) or its average  $V_s$  is required to provide non-ambiguous MHVSR inversions. Joint inversion of dispersion (near surface velocities) and MHVSR (impedance contrasts) therefore helps to constrain the inversion and reduces non-uniqueness. These two unique datasets do not overlap in frequency and also serve to widen the frequency band in the inversion leading to improved resolution in  $V_s$  with depth. Joint dispersion curve and MHVSR inversion thereby provides a robust  $V_s$  profile with depth.

The model parameterization is made up of four elastic parameters for each layer: thickness, compressional wave velocity ( $V_p$ ),  $V_s$  and density. Parameterizations vary in the number of layers with model parameter values drawn from uniform distributions for each layer. Poisson's ratio is used to link  $V_p$  to  $V_s$  and the default search range of 0.2 to 0.5 is used. The thickness of each layer is drawn from a uniform distribution set between 1 to 100 m. Based on the measured dispersion data,  $V_s$  of the layers are set to either increase or decrease with depth. Soil density is the least influential parameter and a fixed value of  $2000 \text{ kg/m}^3$  was used for all layers. DiGiulio et al. (2012) show that misfit decreases with increasing number of sublayers within the model space parametrization. As in, the more complex a model, the more model parameters involved in the inversion, and the lower the misfit. We started with a single uniform layer over a homogeneous half-space and progressively added layers to obtain an adequate fit to the complexity of our data. Adding more layers simply to reduce the misfit would introduce unjustified model complexity. The total number of layers in our final models were therefore site dependent and ranged between 2 to 3 layers including an elastic half-space. Several

inversion trials for the selected model parameterization were run using different random seeds to find an inverted model with the least misfit.

It is important to consider that joint inversion provides a reduced fit of each dataset than their individual inversions. We first performed a sole inversion of the dispersion curve to establish appropriate velocity distributions of the uppermost layers. These velocity distributions informed from the dispersion only inversion were used in the joint inversion with the MHVSR. In this way, we provided adequate fitness of both the dispersion and MHVSR datasets. No standard deviations of the dispersion and MHVSR estimates are included in the inversion.

## 2.8 Inversion results

The inversion results shown in Figure 2.7 for each site include the minimum misfit model along with the next 1000 models with the lowest misfit. These 1001 lowest misfit models do not fully represent uncertainty in the  $V_S$  profile, but are a measure of variability around the minimum misfit model. They help to convey how well the inversion (and hence the non-invasive data) has determined the velocity and depths of each model layer but the true uncertainties are greater (Molnar et al. 2010). For sites that did not show a clearly defined peak in the MHVSR curve (Sites-2 and 6),  $V_S$  profiles were generated based on inversion of the dispersion curve only. This was done to avoid biases and/or wrong velocity estimates in the final  $V_S$  model since the reason for the absence of a well-defined peak and variations at lower frequencies in the MHVSR curve could be attributed to changes in wavefield conditions and/or poor sensor coupling (Sharma et al. 2018).

Figure 2.7 presents the inverted  $V_S$  profiles for all bridge sites tested in this study. Adequate fitness of the fundamental peak frequency is obtained at all sites for which joint inversion was performed. The measured peak amplification tends to be over predicted by theoretical Rayleigh wave ellipticity functions which are asymptotic at frequencies related to changes in polarization. An appropriate impedance contrast was determined since both sides (width) of the peak amplification is fit well. Additionally, fitness of the MHVSR curve degrades at lower and higher frequency segments (below 1 Hz and above 4 Hz) which deviate from “pure” Rayleigh ellipticity response or are “contaminated” by



other wave types, e.g. body, surface (Love waves), diffuse wave types and combinations thereof. We seek to fit primarily the MHVSR peaks (black circles in Figure 2.7) and not the entire MHVSR curve (grey circles).

Overall, the inversion is able to fit measured dispersion estimates but less so at each end of the dispersion curve. For three sites, 2, 4 and 6, dispersion estimates increase at frequencies higher than 11 Hz in the dispersion curve's 'tail', indicating stiffer geology near or at the ground surface. At Site-2, the strong phase velocity increase in the dispersion tail at frequencies higher than 8 Hz was not included in the inversion. Alternative inversions based on identification of higher modes at Sites-2 and 4 are provided in Appendix B. Dispersion curves typically occur above  $f_{peak}$  (in this case at frequencies  $> 2.5$  Hz), thus the sedimentary  $V_S$  was resolved well in our models by obtaining a good fit of the dispersion data within the high frequency bandwidth.

The  $V_S$  profiles obtained from our inversions are characterized by soil layers with  $V_S$  between 160 to 313 m/s. The stiffness of these sediments generally increase towards southeast along the Windsor-Essex Parkway with the softest sediments occurring at Site - 6 (160 m/s) towards the Detroit river. We determine depths to major impedance contrast at depths ranging from 16.5 to 35 m with the deepest site occurring at Site -4.

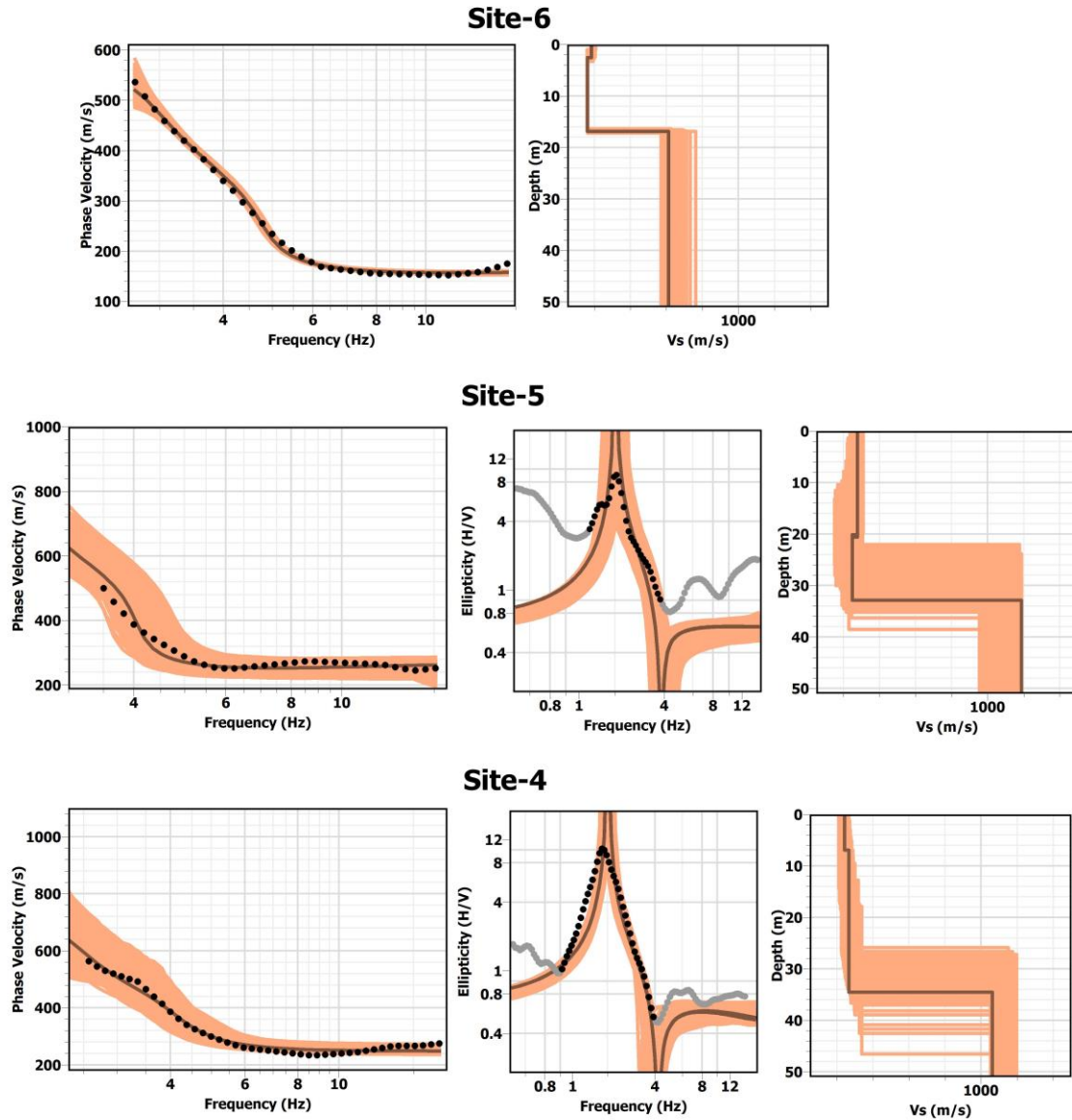


**Figure 2.7: Inversion results for bridge sites in Windsor. The left panel show the dispersion data (black dots), the middle panels show the MHVSR data (black dots) and the right panels show the retrieved  $V_s$  profiles for each site. The colored region represents the first 1,000 lowest misfit models and the solid brown line shows the minimum misfit model. Grey dots represents portions of datasets excluded from the inversion.**

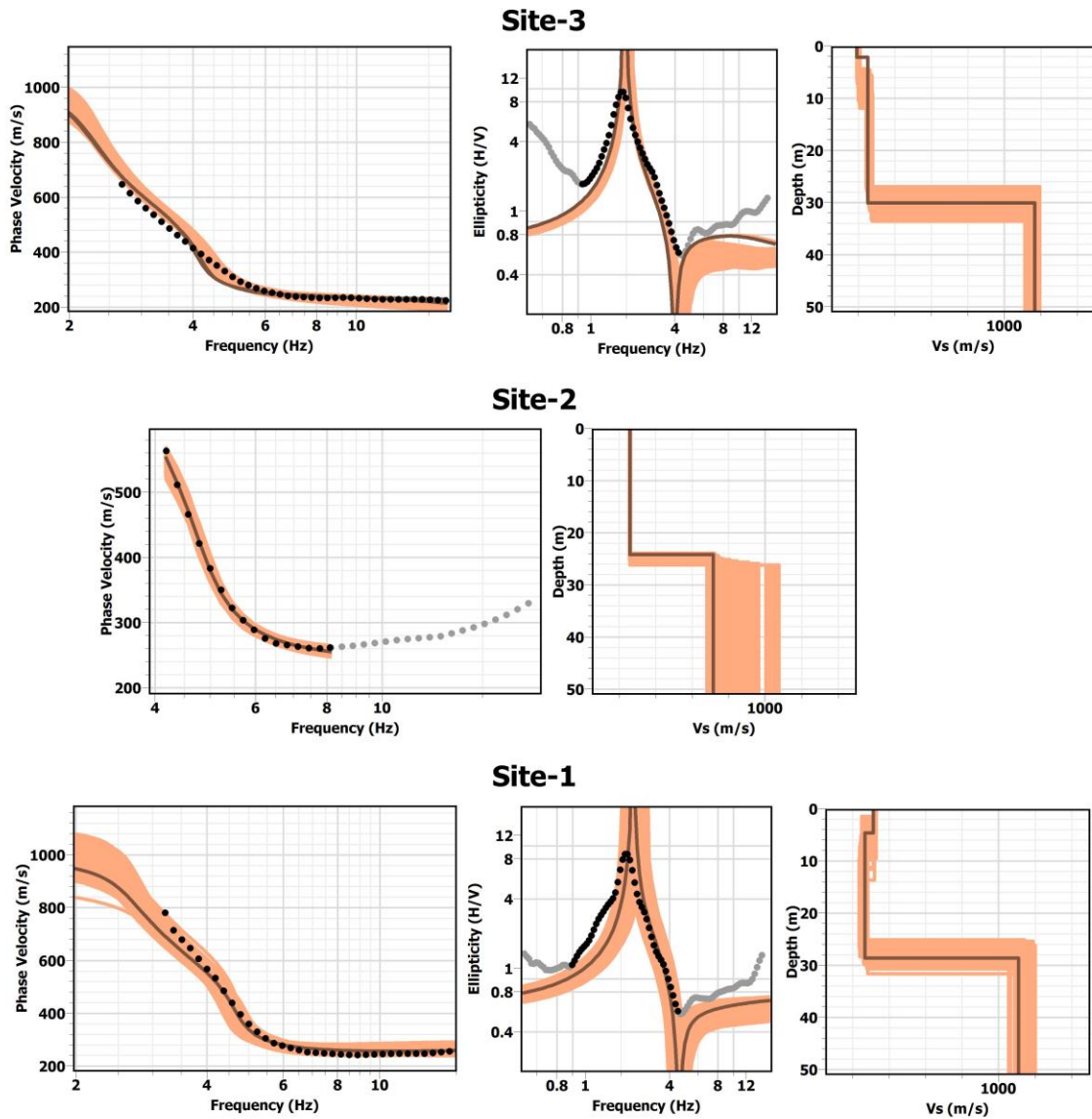


Figure 2.7 (Continued)

## 2.9 Geotechnical data

The MTO geotechnical database was used to select representative bridge sites located in different geological settings across Ontario (<http://www.mto.gov.on.ca/FoundationLibrary/index.shtml>). Six bridge sites with CPT and SPT measurements, and borehole velocity measurements at three of these six sites,

were selected along the Herb Grey Parkway in Windsor. Crosshole  $V_S$  measurements were performed at two sites (BH345, BH301) and downhole  $V_S$  measurements at one site (BH326). These invasive tests were performed between June 2009 and March 2010, prior to construction of the Parkway infrastructure. The invasive testing is described briefly below. Additional details are available in the geotechnical reports (Golder 2009, 2010).

The CPT probe was advanced using a hydraulic ram system on the drill rigs. All CPTs were advanced to refusal, which was encountered at depths ranging from 12.4 to 31.4 m below ground surface. Measurements of raw tip resistance, porewater pressure during pushing and sleeve-friction were obtained. CPT logs are shown in Appendix C.

$V_S$  measurements were obtained from downhole and crosshole seismic techniques. Measurements for the crosshole seismic testing were conducted between two boreholes with the source and receiver at the same depth and a depth increment of interval  $V_S$  measurements performed every 1 m. The three recorded components (vertical, longitudinal and transverse) were split into wave trains. Shear and compression wave arrivals were picked and the velocities were then calculated based on the distance between the boreholes. For the downhole seismic testing, geophones were placed at different depths (at 1 m intervals) in the borehole and an active source energy was generated at the ground surface. The average shear and compression velocities were calculated from the travel time of the wave energy from the source to the receivers.

### 2.9.1 Invasive $V_S$ profiles

SPT blow-count (N-values) and CPT tip resistance ( $q_c$ ) must first be converted to  $V_S$  for comparison with downhole and crosshole  $V_S$  measurements. SPT blowcounts were converted to  $V_S$  using the average of several empirical correlations for the given 'soil type' determined from nearby boreholes at each depth. Table 2.1 summarizes the empirical correlations used for the average N to  $V_S$  conversions in this study. Values reported as refusal were assigned a  $V_S$  value of 465 m/s, which is the average  $V_S$  of surficial tills found in southern Ontario (Crow et al. 2017).

A suite of  $q_c$  to  $V_S$  relations developed by various researchers in literature were investigated (Table 2.2). Figure 2.8 shows the comparison between  $V_S$  values predicted by empirical correlations from tip resistance averaged over 1 m depth interval with the cross- and down-hole  $V_S$  values measured near the CPT profiles. For brevity, four comparisons are shown here and the rest with their corresponding root-mean-square error (RMSE) reported in Appendix D. The following  $q_c$ -to- $V_S$  relation developed by Madiai and Simoni (2004) for lacustrine Pleistocene sediments was subsequently found to provide the best agreement (with the least RMSE of 49 m/s) between predicted and measured  $V_S$ :

$$V_S = 230q_c^{0.25} \quad (q_c \text{ in MPa, } V_S \text{ in m/s}). \quad (2.6)$$

**Table 2.1: Correlations used for converting N to  $V_S$  for sand, silt and clay**

Sand	Silt	Clay	Reference
$87.2N^{0.36}$			Ohta et al. (1972)
	$91N^{0.337}$		Imai et al. (1975)
$100.5N^{0.29}$			Sykora and Stokoe (1983)
$57N^{0.49}$	$105.64N^{0.32}$	$114.43N^{0.31}$	Lee (1990)
		$76.55N^{0.445}$	Athanasopoulos (1995)
$90.82N^{0.319}$		$97.89N^{0.269}$	Hasancebi and Ulusay (2006)
	$60N^{0.36}$		Dikmen (2009)

**Table 2.2: Correlations investigated for converting  $q_c$  to  $V_S$**

Reference	Correlation	Comment
Hegazy and Mayne (1995)	$V_S = 12.02q_c^{0.319}f_s^{-0.0466}$	$q_c$ in kPa
Baldai et al. (1989)	$V_S = 227q_c^{0.13}$	$q_c$ in MPa
Mayne and Rix (1995)	$V_S = 1.75q_c^{0.627}$	$q_c$ in kPa
Madiai and Simoni (2004)	$V_S = 230q_c^{0.25}$	Pleistocene coarse grained soils $q_c$ in MPa
Samui and Sitharam (2010)	$V_S = 1.93q_c^{0.58}$	$q_c$ in kPa
Piratheepan (2002)	$V_S = 25.3q_c^{0.163}f_s^{0.029}z^{0.155}$	For Holocene age soils
McGann et al. (2015)	$V_S = 18.4q_c^{0.144}f_s^{0.0832}z^{0.278}$	For Holocene-age sands
Perrett et al. (2016)	$V_S = 39q_t^{0.164}z^{0.137}$	For marine deltaic sands

\*z is depth below ground surface (m);  $f_s$  is sleeve friction (kPa).

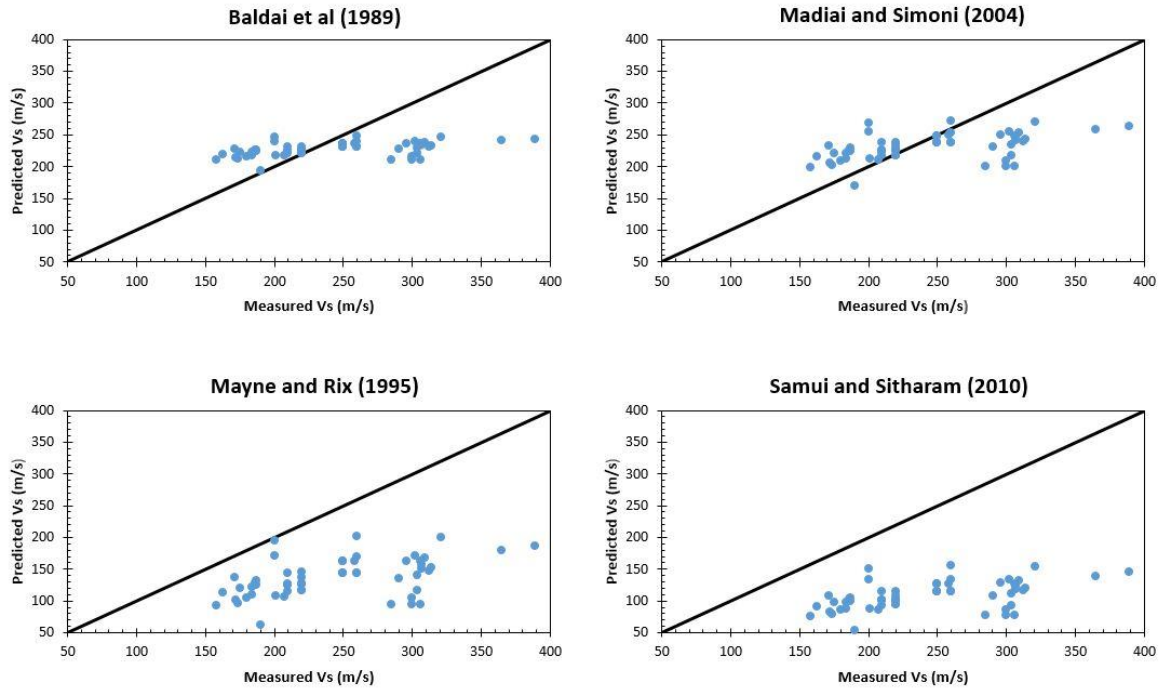


**Figure 2.8: Comparison between predicted  $V_s$  from empirical  $q_c$ -to- $V_s$  relations in literature and measured  $V_s$  from crosshole and downhole surveys.**

Figure 2.9 presents  $V_s$  profiles from the converted SPT and CPT data, as well as the crosshole and downhole  $V_s$  measurements for all sites. SPT measurements are performed near surface or at depth in sand-to-gravel sediments, CPT measurements are performed in finer-grained sand and clay sediments and borehole velocity measurements are conducted over the entire borehole depth. All measurements end at refusal (very stiff ground) in the tested hole. Despite some variation, the converted and measured  $V_s$  profiles from the invasive techniques indicate comparable  $V_s$  values with an increasing trend of  $V_s$  with depth. At Site-1, the SPT and CPT profiles were farther away (~500 m) from the crosshole testing.

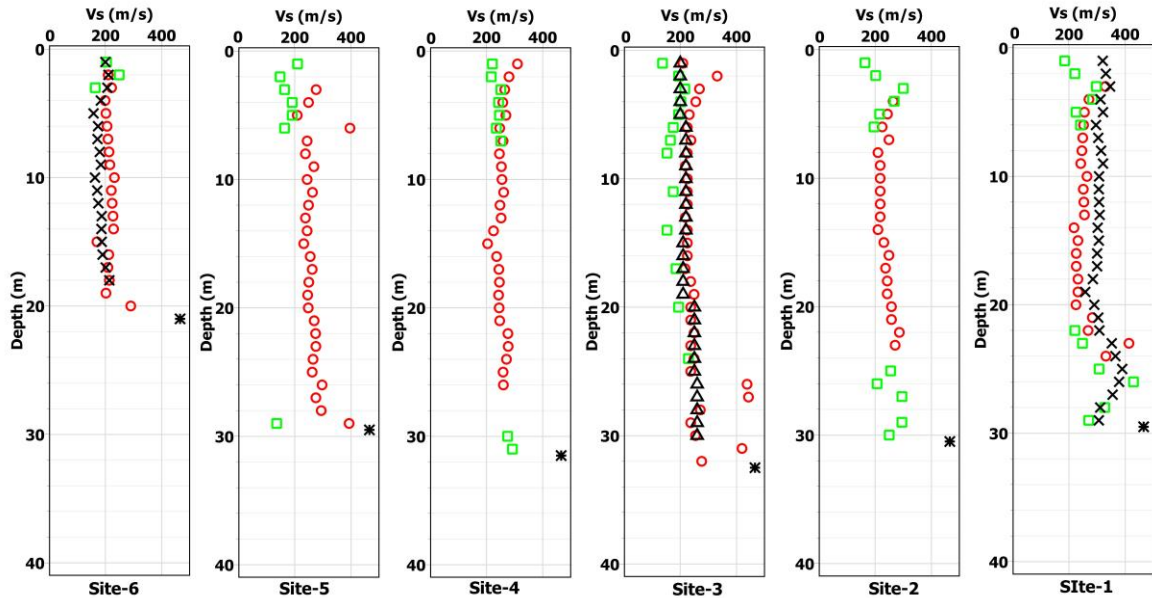


**Figure 2.9: Invasive  $V_s$  measurements at the six study locations: converted CPT (red circles), converted SPT (green squares), crosshole  $V_s$  (crosses), downhole (black triangles)  $V_s$  measurements and refusal depth (stars).**

## 2.10 Blind comparison of non-invasive and invasive $V_s$ profiles

The inverted  $V_s$  profiles from the non-invasive surface wave data compared with the co-located invasive data in Figure 2.10. At Site-6, the inversion resolves a thin ( $\sim 4$  m) layer with  $V_s \sim 180$  m/s overlying a  $V_s \sim 160$  m/s layer to 17 m depth. This is consistent with the layering in both crosshole and converted CPT  $V_s$  profiles, although the inverted velocities are slightly underestimated. The near surface stiffer material measured by both invasive and non-invasive methods can be attributed to the thin silt, sand and gravel cover found to the west of Huron Church road as described in earlier sections. For Site-5, which is also located in the western part, the expected stiff material ( $V_s \sim 280$  m/s) near surface extends to  $\sim 20$  m, over a slightly lower velocity layer ( $V_s \sim 250$  m/s) to  $\sim 33$  m depth. We identify the depth to significant impedance contrast from the inverted models to be around  $\sim 17$  m and  $\sim 33$  m at Site-6 and 5 respectively. This is in close agreement with the invasive profiles.

At Site-4 and 3 the  $V_S$  determined by the inverted models are in good agreement with the invasive profiles with some overestimation within the upper 20 m at both sites. The downhole  $V_S$  profile at Site-3 shows three distinct stratigraphic layers (Figure 2.10), with velocities increasing with depth. This layering is not resolved by the inverted profile which only required two uniform layers over a half space to adequately fit the joint datasets. As in, the dispersion data are sensitive to the impedance contrast at 2-4 m of similar  $V_S$  at 18-30 m depth; the dispersion data are insensitive to lower velocities between 4-18 m depth. Additionally, thin high velocity layers (at ~4, 26 and 31 m) is identified in the converted CPT profile (Figure 2.10) but not by the inverted  $V_S$  profile due to the lack of high resolution layers associated with surface wave data inversion. Despite the fact that the depths to major impedance at Site-3 and Site-4 are underestimated and overestimated respectively by the inverted profiles, they are consistent with the SPT and CPT profiles.

Sites-1 and 2 are located to the east of Huron Church Road where an absence of sand and gravel layers at surface is expected. This is observed (Figure 2.10) in the near surface (< 5 m) crosshole  $V_S$  values (~320 m/s) at Site-1, which is also well resolved by the inverted  $V_S$  profile. The thin stiff material agrees with the presence of stiff glaciolacustrine silts and clays at surface on the east side of Huron Church Road (Hudec 1998). This stiff layer is not resolved by the inverted model at Site-2 which required only a single layer over half-space to adequately fit the dispersion estimates. At Site-2 the inverted profile overestimates  $V_S$  to a depth of about 20 m. The depth to a significant impedance is in good agreement between methods although the converted SPT values extend deeper than the inverted model at Site-2. In addition, the resolution capabilities of the inversion do not allow the retrieval of the high velocity zone (between 22 and 27 m depth) measured by the invasive methods at Site-1 (Figure 2.10). However, the inverted  $V_S$  model resolves the depth to bedrock at ~28 m depth which is in excellent agreement with all invasive  $V_S$  profiles at Site -1.



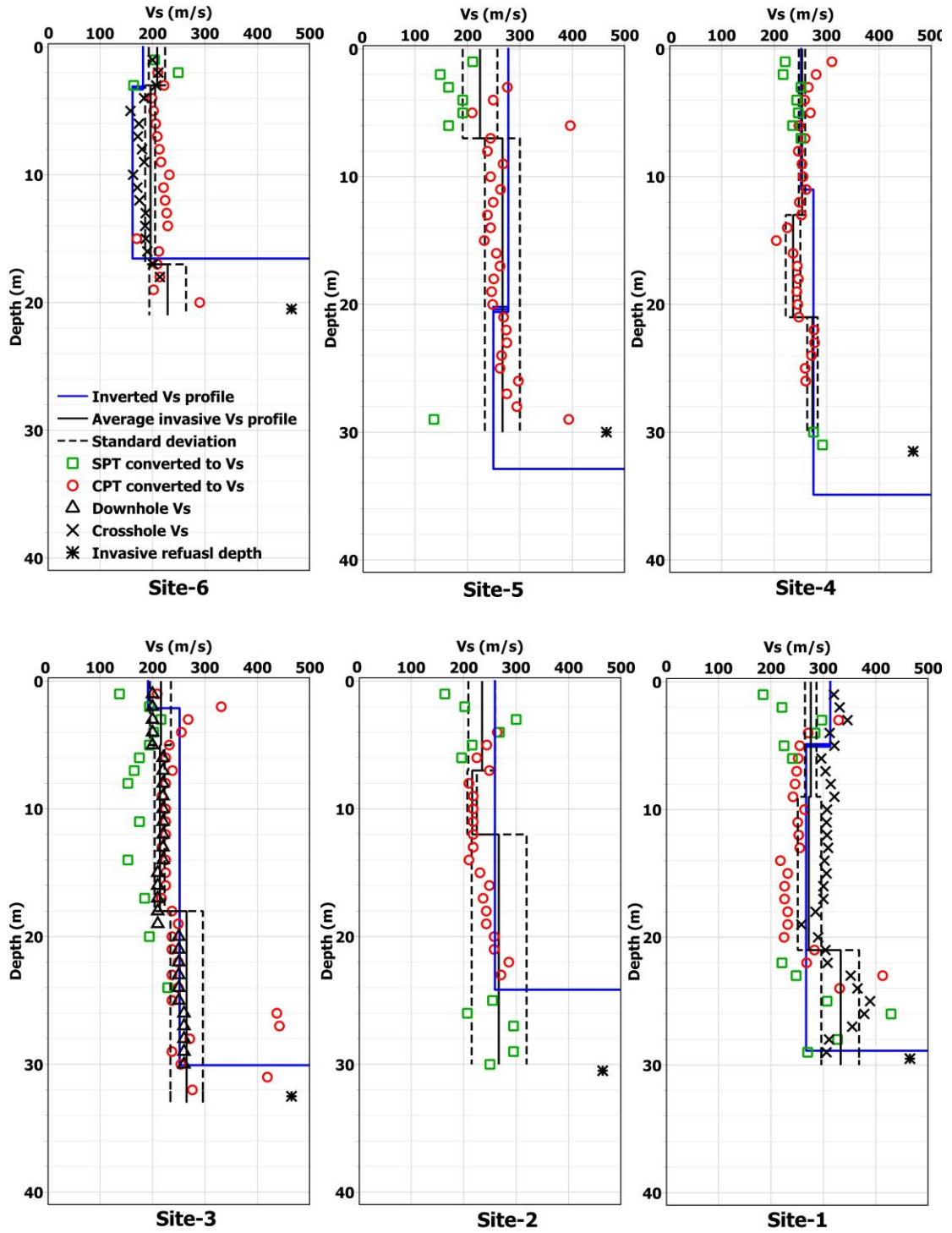
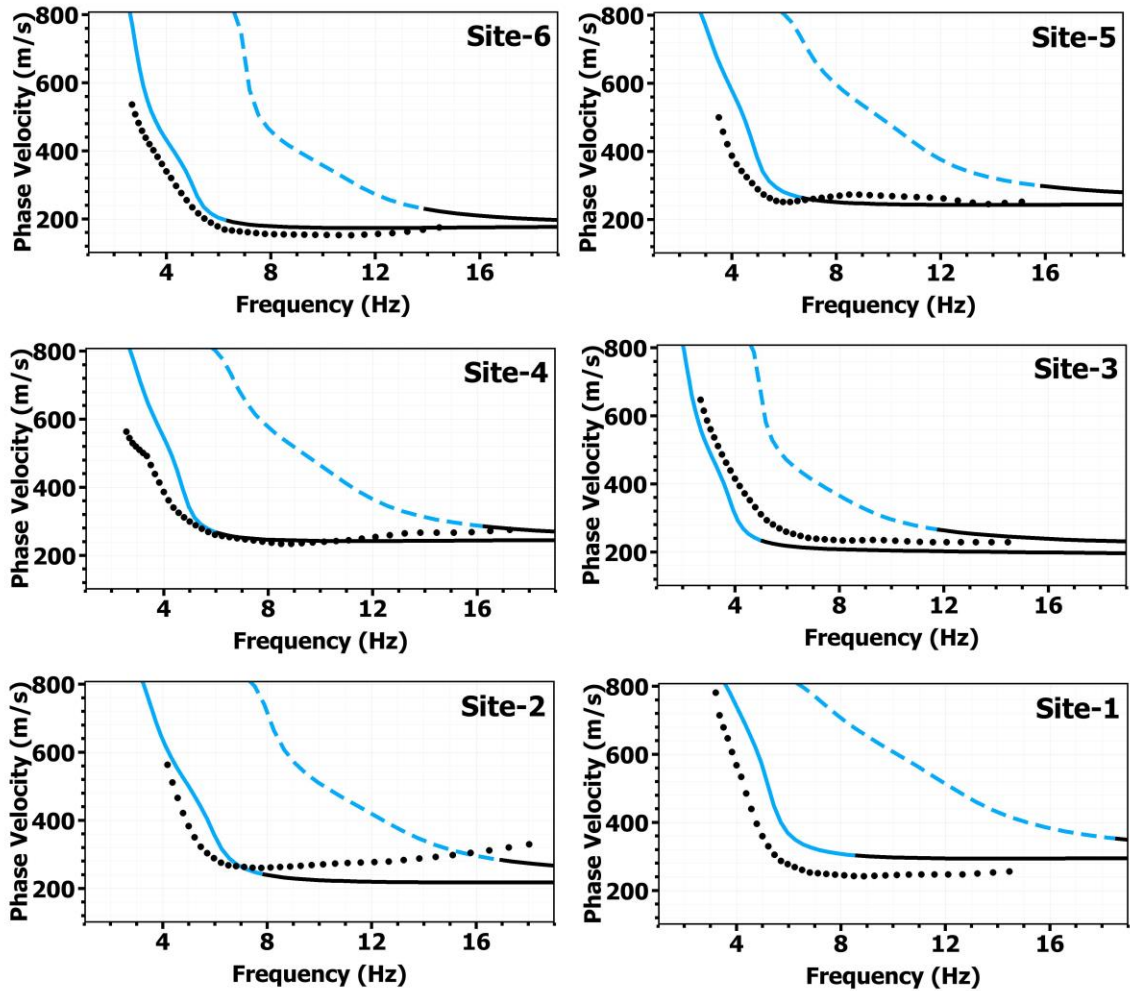


Figure 2.10: Comparison of invasive and non-invasive Vs profiles.

In Figure 2.11 the measured dispersion curves are compared with theoretical dispersion curves calculated from invasive  $V_S$  measurements at each site. To generate the theoretical dispersion curves, the invasive measurements are used to develop 1D layered models.  $V_S$  and  $V_P$  values from downhole and crosshole  $V_S$  profiles were used at Sites-1, 3 and 6. Converted CPT to  $V_S$  values were used at the remaining sites with  $V_P$  set to  $2V_S$ . An elastic half-space  $V_S$  of 1000 m/s was used to develop the 1D invasive models. The higher-frequency portion of the theoretical dispersion curve is defined by the invasive measurements, whereas the lower-frequency portion is defined by the arbitrary 1000 m/s half-space  $V_S$ .

Figure 2.11 shows the measured dispersion data are underestimated compared to the invasive-methods dispersion estimates at Sites 1 and 6. At Sites-2, 4 and 5, the measured and predicted dispersion estimates overlap at narrow frequencies with good agreement obtained at Site-4 (5-11 Hz). It is readily apparent that the non-invasive dispersion measurements provide a measure of  $V_S$  at depths greater (lower frequencies) than the invasive testing.



**Figure 2.11: Measured dispersion from microtremor array data (black dots) compared to fundamental (solid line) and first higher mode (dashed line) theoretical dispersion estimates based on invasive 1D models. Black lines represent dispersion estimates from invasive data and blue lines represents continuation into a 1000 m/s half-space  $V_s$ .**

## 2.11 Inter-method variability of $V_S$

We assess the variability between non-invasive and invasive  $V_S$  profiling methods based on the average relative difference and the RMSE in  $V_S$  between the average invasive  $V_S$  profile and the lowest misfit inverted model down to the depth of significant impedance at each site (Table 2.3). In general, excellent ( $< 10\%$ ) to very good ( $< 20\%$ ) agreement in  $V_S$  is obtained between methods with a well-matched depth to a major impedance. The best agreement is obtained at Site-4, an average relative difference in  $V_S$  of 4% between the average invasive and inverted  $V_S$  profiles. An average relative difference  $> 10\%$  is determined at three sites where a depth to major impedance contrast from the inverted  $V_S$  profiles are underestimated compared to the average invasive profiles (Figure 2.10). For comparison, Molnar et al. (2015) performed blind comparison of non-invasive microtremor and invasive  $V_S$  profiles data at 11 strong-motion stations in central and southern Chile, and obtained an average relative difference in  $V_S$  between both methods to be  $\sim 10\%$  for soil layers and  $\sim 30\%$  for bedrock. Using MASW, Xia et al. (2000) obtained  $V_S$  profiles from the inversion of Rayleigh wave dispersion data and compared them to  $V_S$  profiles from seven boreholes in the unconsolidated sediments of the Fraser River delta in Vancouver, B.C, Canada. They obtained an average relative difference in  $V_S$  to 30 m depth of 8 to 26% with an overall difference of 15% between both methods. These differences between non-invasive and invasive methodologies reported in literature are similar to the differences obtained in this study.

**Table 2.3 Assessment of the difference in  $V_S$  between mean invasive and inverted  $V_S$  profiles.**

<b>Location</b>	<b>Average relative difference (m/s)</b>	<b>Average relative difference (%)</b>	<b>RMSE (m/s)</b>
Site-6	39	18	42
Site-5	24	8	30
Site-4	12	4	20
Site-3	26	11	29
Site-2	18	6	21
Site-1	25	7	36

## 2.12 $V_{S30}$ -based earthquake site classification

The purpose of  $V_S$  profiling is to determine the time-averaged  $V_{S30}$  for earthquake site classification. We assess variability in  $V_{S30}$  between our non-invasive  $V_S$  profiles and the invasive  $V_S$  measurements to comment on how reliable non-invasive methods are for earthquake site classification.

The mean invasive  $V_S$  profile (Figure 2.10) is calculated by averaging the discrete crosshole measurements with the converted SPT and CPT  $V_S$  profiles. Average invasive  $V_S$  values are calculated within selected depth intervals based on known stratigraphy.  $V_{S30}$  is calculated using the following relationship;

$$V_{S30} = \frac{30}{\sum(\frac{h1}{V_{S1}} + \frac{h2}{V_{S2}} + \dots + \frac{hn}{V_{Sn}})} \quad (2.7)$$

where  $V_S$  is the shear wave velocity of each layer with thickness  $h$ .  $V_{S30}$  is calculated for both invasive and non-invasive methodologies and the corresponding site class is assigned according to CHBDC as shown in Table 2.4. Overall all sites are characterized as stiff soil (class D) conditions with stiffness generally increasing towards the south-east. The inverted  $V_S$  model systematically predicts a slightly stiffer  $V_{S30}$  value than the average invasive  $V_S$  profile for all sites except Site-6 where  $V_S$  estimates from the inverted  $V_S$  model are underestimated (Figure 2.10) compared to invasive  $V_S$  profiles. This prediction of a slightly stiffer  $V_{S30}$  value is expected since our inversion models typically ‘missed’ resolving lower  $V_S$  in the mid-depth range, which is determined by the invasive methods. The range in over prediction of  $V_{S30}$  by our non-invasive inversions is 6-19 m/s or 2-8% greater than the invasive methods. Interestingly, the  $V_{S30}$  estimate based directly on dispersion data (prior to inversion) is in very close agreement to  $V_{S30}$  determined from the average invasive  $V_S$  profile on average for the six sites (within 2 m/s), but can be significantly different for specific sites (5 m/s standard deviation). Variability in  $V_{S30}$  calculated between the converted CPT and the cross- or down-hole  $V_S$  profiles is much larger, between 11 and 55 m/s (5 to 17.5%). Better resolution of velocity changes by these invasive methods leads to greater variability in the  $V_{S30}$  estimate.

**Table 2.4 Site classification for both invasive and non-invasive methodologies.**

	Inverted Vs model		Converted CPT to Vs		Borehole Vs profile		Average Invasive Vs profile		Dispersion ( $V_{R40}$ ) data (Bilson Darko et al. 2018)	
Location	$V_{S30}$ (std.dev) <sup>1</sup>	Class	$V_{S30}$	Class	$V_{S30}$	Class	$V_{S30}$ (std.dev)	Class	$V_{S30}$	Class
Site-6	286 (45)	D	297	D	295	D	290 (52)	D	212	D
Site-5	268 (55)	D	254	D	N/A		249 (59)	D	250	D
Site-4	266 (41)	D	252	D	N/A		253 (44)	D	254	D
Site-3	247 (11)	D	237	D	226	D	229 (28)	D	255	D
Site-2	271 (27)	D	258	D	N/A		252 (39)	D	260	D
Site-1	273 (18)	D	260	D	315	D	267 (26)	D	268	D

\* $V_{R40}$  is the phase velocity of the fundamental mode Rayleigh wave at 40 m wavelength.

<sup>1</sup>Std. dev. determined from 1001 models.

## 2.13 Statistical correlation of $V_S$ and cone tip resistance

The parameters obtained from CPT, SPT and shear wave velocity testing are dependent on multiple factors such as age, geologic origin, mineralogy, grain size and compressibility. A number of methods have been developed to assess the *in situ* properties of soils from  $V_S$  (Hardin and Richart 1963; Robertson et al. 1995) and  $q_c$  (Jamiaolkowski et al. 1985, 2001; Baldi et al. 1986; Tanizawa et al. 1990). It is important to note that  $q_c$  and  $V_S$  represent soil responses at opposite ends of the highly non-linear stress-strain spectrum. That is,  $q_c$  obtained from CPT show the behavior of soil at large strain and  $V_S$  reflects the behavior at small strain. However, Mayne and Rix (1993) concluded that since penetration resistance and shear modulus are dependent on similar physical properties such as grain size/shape, mineralogy, confining stress, void ratio and compressibility, they can be assumed to be correlated. Fear and Robertson (1995) found that  $q_c$  and  $V_S$  are largely dependent on vertical effective stress ( $\sigma'_v$ ) and should be normalized to adequately represent the natural soil properties.

The equations used here to correct  $q_c$  for effective stress, discussed by Olsen (1994) are

$$q_{c1} = q_c \cdot \left( \frac{p_a}{\sigma'_v} \right)^n \quad (2.8)$$

where  $q_c$  is raw cone tip resistance (MPa);  $q_{c1}$  is normalized  $q_c$  (MPa);  $P_a$  is atmospheric pressure (100kPa);  $\sigma'_v$  is vertical effective overburden stress (kPa); and  $n$  is a normalization exponent. A normalized dimensionless  $q_c$  has also been proposed by Robertson and Wride (1998) and is given by

$$q_{c1N} = \left( \frac{q_c - \sigma_v}{P_a} \right) \cdot \left( \frac{P_a}{\sigma'_v} \right)^n \quad (2.9)$$

where  $q_{c1N}$  is a normalized dimensionless  $q_c$ ,  $\sigma_v$  is vertical stress and  $\sigma'_v$  is vertical effective stress. Robertson (2009) suggests that the normalization exponent ranges from 0.5 to 0.9 for most coarse-grained soils and is approximately 1.0 at vertical effective stress greater than 1 MPa. Typically, a value of 0.5 is used in practice for clean sand (Robertson and Wride 1998).

Robertson et al. (1992) proposed a relation for normalizing  $V_s$  of normally consolidated unaged sand given by:

$$V_{s1} = V_s \cdot \left( \frac{P_a}{\sigma'_v} \right)^{0.25} \quad (2.10)$$

where  $V_{s1}$  is normalized shear-wave velocity (m/s).

Many researchers have investigated the effects of other physical quantities on the relationship between  $q_c$  and  $V_s$  such as particle size distribution (Karray et al. 2011) and aging (Piratheepan and Andrus 2002; Correia et al. 2004). Table 2.5 summarizes some of the empirical relations proposed by different researchers in literature.

**Table 2.5: Some correlations between  $V_s$  and  $q_c$  in literature.**

Authors	Proposed correlation	Soil type	Notes
Rix and Stokoe (1991)	$\left(\frac{G_0}{q_c}\right)_{ave} = 1634 \left(\frac{q_c}{\sqrt{\sigma'_{v0}}}\right)^{-0.75}$	Uncemented sand	quartz $q_c$ in kPa
Robertson et al (1992)	$V_{s1} = 102(q_{c1})^{0.23}$	Clean and quartz sands	$V_{s1}$ in m/s and $q_{c1}$ in kPa
Fear and Robertson (1995)	$V_{s1} = 135(q_{c1})^{0.23}$	Compressible sand	tailings $V_{s1}$ in m/s and $q_{c1}$ in kPa
Wride et al. (2000)	$V_{s1} = Y(q_{c1})^{0.25}$ , $95.6 < Y < 110.8$	Quartz with feldspar	Canadian liquefaction experiment $0.16 < D_{50} < 0.25$
Piratheepan and Andrus (2002)	$V_s = 102(q_c)^{0.199} f_s^{0.003} ASF$ $V_{s1} = 102(q_{c1N})^{0.178} ASF$	For sands	Tested sites in Canada, Japan and California. $V_s$ in m/s and $q_c$ and $f_s$ in kPa
Karray et al. (2011)	$V_{s1} = 149(q_{c1})^{0.205}$ $V_{s1} = 125.5(q_{c1})^{0.23} D_{50}^{0.115}$	Quartz sand with small amount of feldspar	$V_{s1}$ in m/s and $q_{c1}$ in MPa. $D_{50}$ in mm $0.2 < D_{50} < 10$
Tonni and Simonini (2013)	$V_s = 104.1 (q_t)$	Silt and silt mixtures	$q_t$ in MPa

**Note:**  $G_0$  is shear modulus; ASF is age factor, Y is a constant determined from the experimental data;  $D_{50}$  is particle size

### 2.13.1 Proposed empirical correlation for $V_{s1}$ and $q_{c1}$

CPT and  $V_s$  data were carefully selected to develop a corrected  $q_c$  to  $V_s$  relation for the Windsor sites. Data from the first 4 m of soil were excluded from the analysis since they are measures of fill material. Additionally, obvious irregularities in  $q_c$  values which may be associated with contacts with coarse material or thin interbedded layers of different soils were considered outliers and were excluded from the analysis. A total of 91 data pairs of  $q_c$  and  $V_s$  values from five borehole locations (three inverted  $V_s$  profiles from AVA method, one downhole  $V_s$  profile and one crosshole  $V_s$  profile) were analyzed to develop a correlation between  $q_c$  and  $V_s$ . The distance between compared  $q_c$  and  $V_s$



profiles is within 300 m. Site-1 was excluded from the analysis due to the farther distance between  $q_c$  and  $V_s$  profiles. Generally, the Windsor soils are mainly composed of normally consolidated silt and silt mixtures interbedded with sand and clay. The average  $q_c$  values over particular depths are paired with corresponding  $V_s$  values within the same interval. Since penetration resistance and shear wave velocity are dependent on effective stress, analysis based on stress-normalized values at an effective stress of 100 kPa was adopted.  $q_{c1}$  and  $V_{s1}$  were obtained using Eq. (2.8) and (2.10) respectively. For  $q_{c1}$ , a normalization exponent of 0.5 was used. The sparsity of the data did not allow for segregation into different soil types. For this reason, a general relationship applicable to all soil types encountered in the area has been developed here. With respect to all of the available data for the Windsor sites, the general regression trend is determined to be

$$V_{s1} = 223.05(q_{c1})^{0.462} \quad (2.11)$$

where  $V_{s1}$  is in m/s and  $q_{c1}$  is in MPa.

The correlation between  $V_{s1}$  and  $q_{c1}$  is plotted in Figure 2.12 in comparison to other relations in literature. Despite the obvious scatter, it is evident that  $V_{s1}$  increases with increasing  $q_{c1}$ , as expected. The analysis provides a moderate coefficient of determination ( $R^2$ ) of 0.64. It is important to note that, the relationship between  $V_{s1}$  and  $q_{c1}$  is also influenced by age and particle size distribution and thus statistical improvement can be achieved when these factors are taken into account. Other correlations in literature brackets the proposed relation suggesting that, in the absence of direct measurement, it can be used to satisfactorily predict  $V_s$  from  $q_c$  measurements for sediments in Windsor, Ontario and surrounding areas.

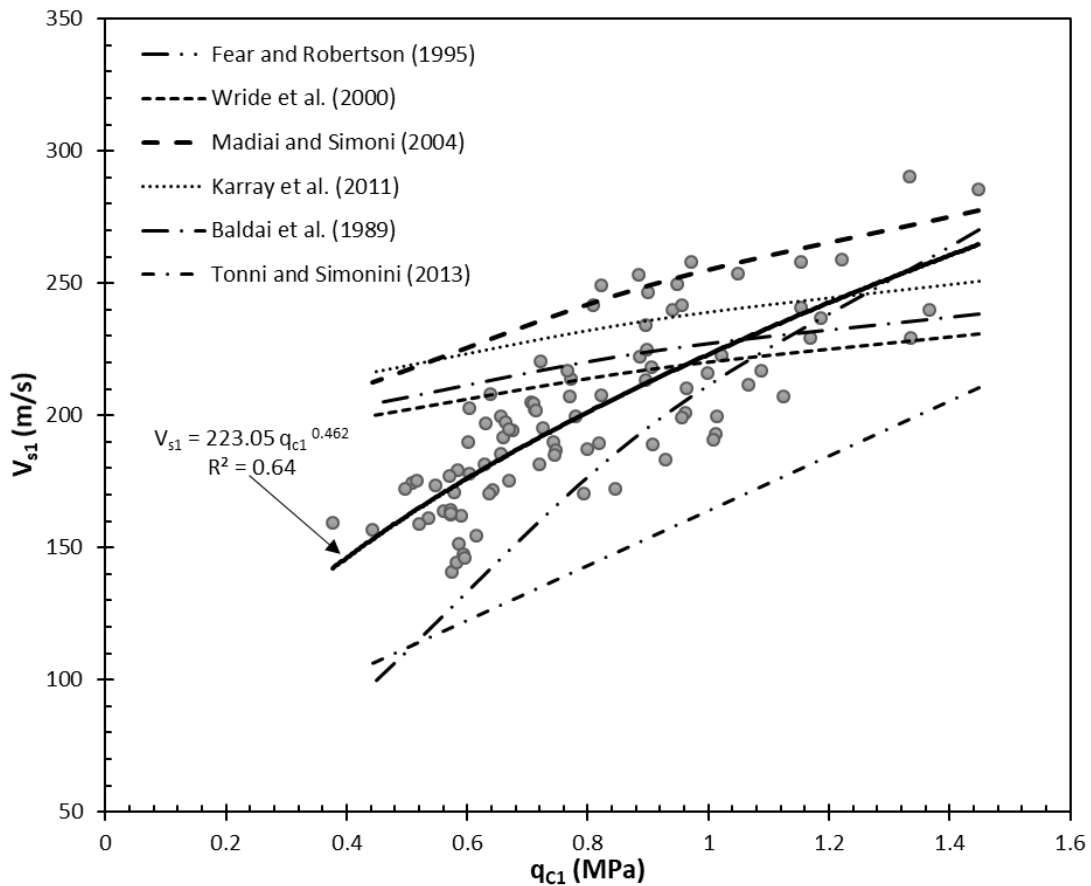


**Figure 2.12: Correlation between  $V_{s1}$  and  $q_{c1}$ .**

## 2.14 Discussion and conclusions

In this study, non-invasive surface wave and microtremor recordings were collected at six bridge sites in Windsor, Ontario co-located with previous geotechnical borehole information. One-dimensional  $V_S$  profiles were successfully retrieved from the joint inversion of MHVSR and dispersion estimates at each site without prior knowledge of the invasive data, i.e., a blind-test comparison. We compare our non-invasive  $V_S$  profiles to the invasive  $V_S$  profiling and also compare subsequent earthquake site classification based on  $V_{S30}$ .

The near-surface sedimentary structures in our non-invasive inverted models are adequately resolved and we obtain excellent agreement with velocities estimated by invasive methods, with an overall average relative difference in  $V_s$  of 39 m/s (within 18%) for all six sites. Our inverted  $V_s$  profiles are characterized by loss of resolution with depth, with higher degree of uncertainty in the half-space velocities. This observation is consistent with the overall non-uniqueness of surface wave data inversion (Garofalo et al. 2016a, b; Molnar et al. 2015). Although the invasive methods are characterized by higher depth resolution and can detect discrete  $V_s$  variations with depth, we obtained comparable  $V_s$  profiles between methodologies with good agreement in the depth to a significant impedance. In addition, our non-invasive  $V_s$  profiling is able to penetrate deeper, albeit with low resolution, compared to the invasive methods.

Overall, bridge sites tested in Windsor, Ontario, were found to be mostly characterized with sediments up to ~30 m thick overlying seismic bedrock ( $V_s \geq 1000$  m/s). Excellent agreement of  $V_{s30}$  estimates is obtained between both invasive and non-invasive methods from which these sediments are consistently categorized as site class D (stiff soil;  $V_s$  of 180-360 m/s) according to the 2015 CHBDC, regardless of the  $V_s$  profiling method. The results of this study highlights the efficiency of the rapid and cost-effective non-invasive methods which can be used in the absence of, or in conjunction with invasive  $V_s$  profiling techniques to obtain reliable  $V_s$  estimates for seismic site classification in Windsor, Ontario. Non-invasive methods also provide parameters ( $f_{peak}$  and  $V_s$  profiles) necessary for site response analysis and earthquake hazard evaluation.

A correlation between  $V_{s1}$  and  $q_{c1}$  (Eq. 2.11) for normally consolidated sediments has been proposed from the statistical regression analysis of 91 data pairs from the six Windsor bridge sites. The proposed correlation compares fairly with other relations in literature (Figure 2.12). However, the difference observed between existing relations in literature and the proposed relation can be attributed to site specific conditions and therefore the proposed relation should be used with caution at other geological settings.

## 2.15 Data and resources

All invasive data from geotechnical reports were obtained from the publicly available MTO online database (<http://www.mto.gov.on.ca/FoundationLibrary/index.shtml>).

## 2.16 Acknowledgements

Funding provided by the MTO Highway Infrastructure and Innovation Fund (HIIF) is highly appreciated. Thank you to Sebastian Braganza (former UWO MSc student) for field assistance and Hema Sharma (UWO PhD student) for collaboration of the non-invasive measurements.

## 2.17 References

- Aki, K. (1957). Space and time spectra of stationary stochastic waves, with special reference to microtremors. *Bulletin of the Earthquake Research Institute, University of Toronto*, 35, 415–456.
- Athanasopoulos, G. A. (1970). Empirical correlations  $V_s$ - $N_{SPT}$  for soils of Greece: A comparative study of reliability. *WIT Transactions on The Built Environment*, 15.
- Baldi, G., Bellotti, R., Ghionna, V., Jamiolkowski, M., and Pasqualini, E. (1986). Interpretation of CPT's and CPTU's. 2: Drained penetration in sands. *Proc., 4th Int. Geotechnical Seminar Field Instrumentation and In Situ Measurements*, Nanyang Technological Institute, Singapore, 143–156.
- Bettig B., P.-Y. Bard, F. Scherbaum, J. Riepl, and F. Cotton (2001). Analysis of dense array noise measurements using the modified spatial auto-correlation method (SPAC). Application to the Grenoble area, *Bolletino di Geofisica Teorica ed Applicata*. 42, 281-304.
- Boore, D. M. (2006). Determining subsurface shear-wave velocities: a review. *In 3rd International Symposium on the effects of surface geology on seismic motion*, Grenoble, France, 30, 67-85.

- Borcherdt, R. D. (1994). Estimates of site-dependent response spectra for design (methodology and justification). *Earthquake spectra*, 10(4), 617-653.
- Brown, L. T., J. G. Diehl, and R. L. Nigbor (2000). A simplified procedure to measure average shear-wave velocity to a depth of 30 meters ( $V_{S30}$ ). *Proceedings of the 12th World Conference on Earthquake Engineering*, Auckland, New Zealand, February 2000.
- Butler, D. K., and Curro Jr, J. R. (1981). Crosshole seismic testing—Procedures and pitfalls. *Geophysics*, 46(1), 23-29.
- Capon, J., (1969). High-resolution frequency-wavenumber spectral analysis. *Proc. IEEE.*, 57, 1408-1419.
- Correia, A. G., Fonseca, A. V. D., and Gambin, M. (2004). Routine and advanced analysis of mechanical in situ tests: Results on saprolitic soils from granites more or less mixed in Portugal. *Proceedings of the Second International Conference on Site Characterization*, ISC-2 Porto, Portugal, 19-22 September 2004, 75-95.
- Crow, H. L., Hunter, J. A., Olson, L. C., Pugin, A. J. M., and Russell, H. A. (2017). Borehole geophysical log signatures and stratigraphic assessment in a glacial basin, southern Ontario. *Canadian Journal of Earth Sciences*, 999, 1-17.
- CSA Group (2014). S6-14 Canadian Highway Bridge Design Code, Section 4 – Seismic design, Mississauga, Ontario, 171-226.
- Di Giulio, G., Savvaidis, A., Ohrnberger, M., Wathelet, M., Cornou, C., Knapmeyer-Endrun, B., and Bard, P. Y. (2012). Exploring the model space and ranking a best class of models in surface-wave dispersion inversion: Application at European strong-motion sites. *Geophysics*, 77(3), B147-B166.
- Dikmen, Ü. (2009). Statistical correlations of shear wave velocity and penetration resistance for soils. *Journal of Geophysics and Engineering*, 6(1), 61.

- Fear, C. E., and Robertson, P. K. (1995). Estimating the undrained strength of sand: a theoretical framework. *Canadian Geotechnical Journal*, 32(5), 859-870.
- Garofalo, F., Foti, S., Hollender, F., Bard, P.Y., Cornou, C., Cox, B.R., Ohrnberger, M., Sicilia, D., Asten, M., Di Giulio, G. and Forbriger, T. (2016a). InterPACIFIC project: Comparison of invasive and non-invasive methods for seismic site characterization. Part I: Intra-comparison of surface wave methods. *Soil Dynamics and Earthquake Engineering*, 82, 222-240.
- Garofalo, F., Foti, S., Hollender, F., Bard, P.Y., Cornou, C., Cox, B.R., Ohrnberger, M., Sicilia, D., Asten, M., Di Giulio, G. and Forbriger, T. (2016b). InterPACIFIC project: Comparison of invasive and non-invasive methods for seismic site characterization. Part I: Inter-comparison of surface wave methods. *Soil Dynamics and Earthquake Engineering*, 82, 241-254
- Golder (2009). Windsor-Essex Parkway Geotechnical Data Report, 07-1130-207-0-R01, 40J6-27, 1-986
- Golder (2010). Windsor-Essex Parkway Geotechnical Data Report Addendum No. 2, In Situ Cross-Hole and Vertical Seismic Profile Testing, 07-1130-207-0 / 09-1132-0080-5000-R01, 40J6-27, 1-27
- Hardin, B. O., & Richart Jr, F. E. (1963). Elastic wave velocities in granular soils. *Journal of Soil Mechanics & Foundations Div*, 89, 3407.
- Hasancebi, N., and Ulusay, R. (2007). Empirical correlations between shear wave velocity and penetration resistance for ground shaking assessments. *Bulletin of Engineering Geology and the Environment*, 66(2), 203-213.
- Hobiger, M., Le Bihan, N., Cornou, C., and Bard, P. Y. (2012). Multicomponent signal processing for Rayleigh wave ellipticity estimation: application to seismic hazard assessment. *IEEE Signal Processing Magazine*, 29(3), 29-39.
- Hudec, P. P. (1998). Geology and geotechnical properties of glacial soils in Windsor. *Urban geology of Canadian cities, GAC Special Publication*, 42, 225-236.

- Humar, J. (2015). Background to some of the seismic design provisions of the 2015 National Building Code of Canada. *Can. J. Civil Eng.*, 42, 940-952.
- Hunter, J. A., and Crow, H. L. (2012). Shear wave velocity measurement guidelines for Canadian seismic site characterization in soil and rock. Geological Survey of Canada. Open File, 7078, 227 pgs.
- Hunter, J.A. and Atukorala, U. (2015). Chapter 1.0: Introduction; in Shear Wave Velocity Measurement Guidelines for Canadian Seismic Site Characterization in Soil and Rock, (ed.) J.A. Hunter and H.L. Crow; Geological Survey of Canada, Open File 7078, 8-17.
- Imai T (1975). The relation of mechanical properties of soils to P and S-wave velocities for ground in Japan. *Technical note OYO Corporation*, Tokyo, Japan.
- Jamiolkowski, M., Ladd, C.C., Germaine, J.T. and Lancellotta, R. (1985). New developments in field and laboratory testing of soils. Theme Lecture. *Proc. XI ICSMFE. San Francisco, August 12-16, 1985.* 1,57-153.
- Karray, M., Lefebvre, G., Ethier, Y., and Bigras, A. (2011). Influence of particle size on the correlation between shear wave velocity and cone tip resistance. *Canadian Geotechnical Journal*, 48(4), 599-615.
- Konno, K., and Ohmachi, T. (1998). Ground-motion characteristics estimated from spectral ratio between horizontal and vertical components of microtremor. *Bulletin of the Seismological Society of America*, 88(1), 228-241.
- Kramer, S. L. (1996). Geotechnical earthquake engineering. Prentice Hall, Upper Saddle River, NJ
- Lacoss, R. T., E. J. Kelly, and M. N. Toksöz (1969). Estimation of seismic noise structure using arrays. *Geophysics*, 29, 21-38.
- Lee, S. H. H. (1990). Regression models of shear wave velocities in Taipei basin. *Journal of the Chinese Institute of Engineers*, 13(5), 519-532.

- Madiai, C., and Simoni, G. (2004). Shear wave velocity-penetration resistance correlation for Holocene and Pleistocene soils of an area in central Italy. In *Geotechnical and Geophysical Site Characterization. Proceedings of the 2nd International Conference on Site Characterization. Porto, Portugal, September 19-22*
- Martin, A. J., and J. G. Diehl (2004). Practical experience using a simplified procedure to measure average shear-wave velocity to a depth of 30 meters ( $V_{S30}$ ). in *Proceedings, 13th World Conference on Earthquake Engineering, Vancouver, B.C., Canada, August 2004.*
- Mayne, P. W., and Rix, G. J. (1993). G max-qc relationships for clays. *Geotechnical Testing Journal*, 16(1), 54-60.
- Mayne, P. W., and Rix, G. J. (1995). Correlations between shear wave velocity and cone tip resistance in natural clays. *Soils and foundations*, 35(2), 107-110.
- Moehle, J. P., and Eberhard, M. O. (2000). Earthquake damage to bridges. Bridge engineering handbook, CRC Press, Boca Raton, FL. 1-34.
- Molnar, S., Cassidy, J. F., Castellaro, S., Cornou, C., Crow, H., Hunter, J. A., and Yong, A. (2018). Application of microtremor horizontal-to-vertical spectral ratio (MHVSR) analysis for site characterization: State of the art. *Surveys in Geophysics*, 39(4), 613-631.
- Molnar, S., Dosso, S. E., and Cassidy, J. F. (2010). Bayesian inversion of microtremor array dispersion data in southwestern British Columbia. *Geophysical Journal International*, 183(2), 923–940.
- Molnar, S., Ventura, C. E., Boroschek, R., and Archila, M. (2015). Site characterization at Chilean strong-motion stations: Comparison of downhole and microtremor shear-wave velocity methods. *Soil Dynamics and Earthquake Engineering*, 79, 22-35.
- Morris, T. F. (1994). Quaternary geology of Essex County Southwestern Ontario; Ontario Geological Survey, Open file report 5886, 130p.



- Nakamura, Y. (1989). A method for dynamic characteristics estimation of subsurface using microtremor on the ground surface. *Railway Technical Research Institute, Quarterly Reports*, 30(1), 25-33.
- National Research Council (NRC) (2015). National Building Code of Canada 2015, Volume 1, Division B, Part 4.
- Nogoshi, M., and Igarashi, T. (1971). On the amplitude characteristics of microtremor (Part2). *J. Seismol. Soc. Japan*, 24(1), 26–40.
- Ohta, T., Hara, A., Niwa, M., and Sakano, T. (1972). Elastic shear moduli as estimated from N-value. In *Proc. 7th Ann. Convention of Japan Society of Soil Mechanics and Foundation Engineering*, 265-268.
- Olsen, R. S. (1994). *Normalization and prediction of geotechnical properties using the cone penetrometer test (CPT)* (No. WES/TR/GL-94-29). Army engineer waterways experiment station vicksburg MS geotechnical lab.
- Park, C. B., Miller, R. D., and Xia, J. (1999). Multichannel analysis of surface waves. *Geophysics*, 64(3), 800-808.
- Piratheepan, P. (2002). Estimating shear-wave velocity from SPT and CPT data. Clemson University, MSc Thesis, 184.
- Rix, G. J., and Stokoe, K. H. (1991). Correlation of initial tangent modulus and cone penetration resistance. In *Proceedings of the International Symposium on calibration chamber testing (ISOCCTI)*, Elsevier, Potsdam, New York, 351-362.
- Robertson, P. K. (2009). Interpretation of cone penetration tests—A unified approach. *Canadian geotechnical journal*, 46(11), 1337-1355.
- Robertson, P. K., and Wride, C. E. (1998). Evaluating cyclic liquefaction potential using the cone penetration test. *Canadian Geotechnical Journal*, 35(3), 442-459.

- Robertson, P. K., Sasitharan, S., Cunning, J. C., and Seago, D. C. (1995). Shear-wave velocity to evaluate in-situ state of Ottawa sand. *Journal of Geotechnical Engineering*, 121(3), 262-273
- Robertson, P. K., Woeller, D. J., and Finn, W. D. L. (1992). Seismic cone penetration test for evaluating liquefaction potential under cyclic loading. *Canadian Geotechnical Journal*, 29(4), 686-695.
- Sahadewa, A., Zekkos, D., and Woods, R. D. (2012). Observations from the implementation of a combined active and passive surface wave based methodology. In Proc., *State of the Art and Practice in Geotechnical Engineering Conf.* (Geocongress 2012): 2786-2795.
- Sambridge, M., L.R., J., E.L., M., W.T., V., & E., T. (1999). Geophysical inversion with a neighbourhood algorithm-II. Appraising the ensemble. *Geophysical Journal International*, 138(3), 727–746. <http://doi.org/10.1046/j.1365-246x.1999.00900.x>
- Samui, P., and Sitharam, T. (2010). Correlation between SPT, CPT and MASW. *International Journal of Geotechnical Engineering*, 4(2), 279-288.
- Scherbaum, F., Hinzen, K.-G., & Ohrnberger, M. (2003). Determination of shallow shear wave velocity profiles in the Cologne, Germany area using ambient vibrations. *Geophysical Journal International*, 152(3), 597–612. <http://doi.org/10.1046/j.1365-246X.2003.01856.x>.
- Schmertmann, J. H. (1977). Guidelines for CPT performance and Desing. *Federal Higway Administration HDV*, 22.
- Sharma, H. S., Molnar, S., and Bilson Darko, A. (2018). Evaluating inversion techniques for soft sites in Windsor, Ontario, Canada. *Seismological Research Letters*, 89, 2B, 820.
- Stokoe, K. H., Nazarian, S., Rix, G. J., Sanchez-Salinero, I., Sheu, J.-C., and Mok, Y.-J. (1988). In situ seismic testing of hard-to-sample soils by surface wave method. In

*Geotechnical Special Publication. Recent advances in ground-motion evaluation*  
ASCE, 264-278.

- Sykora D. W and Stokoe K. H. I. I. (1983). Correlations of in-situ measurements in sands of shear wave velocity. *Soil Dyn Earthquake Eng* 20(1-4):125–136
- Tanizawa, F., Tatsuoka, F., Teachavorasinskun, S., Iwasaki, K. and Zhou, S. (1990). On correlation among cone resistance and shear modulus and angle of shear resistance of Toyoura sand. *Proc. of 25th Japan National Conf. On SMFE*, 141-144.
- Tonni, L., and Simonini, P. (2013). Shear wave velocity as function of cone penetration test measurements in sand and silt mixtures. *Engineering Geology*, 163, 55-67.
- Wathelet, M. (2005). Array recordings of ambient vibrations: surface-wave inversion. *PhD Thesis, Universit´e de Li`ege, Belgium*.
- Wathelet, M. (2008). An improved neighborhood algorithm: Parameter conditions and dynamic scaling. *Geophysical Research Letters*, 35(9), L09301. doi:10.1029/2008GL033256.
- Wride, C. E., Robertson, P. K., Biggar, K. W., Campanella, R. G., Hofmann, B. A., Hughes, J. M., ... and Woeller, D. J. (2000). Interpretation of in situ test results from the CANLEX sites. *Canadian Geotechnical Journal*, 37(3), 505-529.
- Xia, J., Miller, R. D., Park, C. B., Hunter, J. A., & Harris, J. B. (2000). Comparing shear-wave velocity profiles from MASW with borehole measurements in unconsolidated sediments, Fraser River Delta, BC, Canada. *Journal of Environmental & Engineering Geophysics*, 5(3), 1-13.

## Chapter 3

### 3 Shear-wave Velocity Profiling at Ontario Bridge Sites in Ottawa and Oshawa

#### 3.1 Introduction

*In situ* tests play a key role for determining subsurface soil properties in geotechnical engineering. These tests provide many engineering parameters necessary for foundation and structural design, liquefaction analysis, earthquake site response analysis, earthquake hazard evaluation and site classification. Generally, geotechnical engineers assess soil behavior by determining its strength and stiffness parameters which can be evaluated through different methods ranging from laboratory to field techniques. Laboratory testing requires discrete soil samples which is relatively expensive. Disturbance from sample extraction, transportation and preparation present a major challenge. Additionally, material properties obtained from these samples at one or few locations may not be an adequate representation of soil characteristics for the entire site. Cone penetration testing (CPT) and Standard penetration testing (SPT) are the most popular *in situ* penetration tests for exploring subsurface ground conditions. These field measurements have an advantage over laboratory techniques because the soil is tested in its natural state with minimal disturbance to the site environment.

Various shear wave velocity ( $V_s$ ) profiling techniques are used for earthquake site classification. The 2015 NBCC and CHBDC seismic guidelines allow site classification not only based on  $V_{S30}$  but also based on SPT blowcount ( $N_{60}$ ) and undrained shear strength ( $S_u$ ) of the upper 30 m (Table 1.1). The evaluation of undrained shear strength plays a significant role in liquefaction assessment necessary for the safe design of structures to withstand earthquake shaking. Undrained shear strength can be determined through laboratory shear tests on undisturbed samples or *in situ* field tests (e.g. field vane test). In field vane tests, the vane insertion tends to disturb the soil structure by changing its stress state and reducing strength. Eden and Law (1980) examined the  $S_u$  of clay soils determined from different test methods and concluded that,  $S_u$  is primarily influenced by the test method, the anisotropic condition in the clay deposit, the rate of stress application

and the associated disturbance involved. Thus, thorough investigation both in the field and laboratory is required to adequately assess the behavior of soil.

In this study we perform a similar non-invasive seismic testing program described in Chapter 2 at four bridge sites in Ottawa and Oshawa, Ontario with co-located SPT and CPT measurements to assess the difference between invasive, non-invasive and laboratory  $V_S$  profiling methodologies and associated site classification in the different geological setting of central southwestern Ontario. Both active- and passive-source seismic array techniques are used to retrieve  $V_S$  profiles at co-located invasive test sites. Laboratory  $S_u$  and bender element  $V_S$  measurements of a borehole clay sample from the Oshawa site are conducted. A comparison of earthquake site classification from our non-invasive techniques with invasive methods is presented here.

### 3.2 Location and geological setting

Three test sites are located in eastern Ottawa along Highway 417 in the Township of Gloucester (Figure 3.1). These sites were selected amongst 15 bridge sites along this section of the highway. Ottawa is ~300 km further northeast from Oshawa and lies in the highly active seismic zone of west Quebec (Adams and Halchuk 2003). The surficial geology of the of the Ottawa area is comprises of post-glacial sediments, glacial deposits and bedrock outcrops. The sediments are made up of thick loosely consolidated post-glacial deposits (fine sands, silty clays and silts) formed by the Champlain Sea. Most sediments in this region consists of Late Wisconsinan glaciomarine sediments and Holocene fluvial deposits (Gadd and Fulton 1987). The Late Pleistocene and postglacial fine-grained sediments occur as deep as 120 m. Glacial sediments underlying the post glacial deposits are thin with thickness ranging between 1-5m. The bedrock in this region is mostly composed of Pre-Cambrian granite gneiss or Paleozoic limestone, dolostone, sandstone or shale (Hunter and Motezedian 2006). The stratigraphy in the tested area is generally characterized by an occasional surficial layer of silty sand overlying clayey silt, over sand and gravel, over a thin glacial till which overlies a flat-lying shale bedrock of the Billings formation.

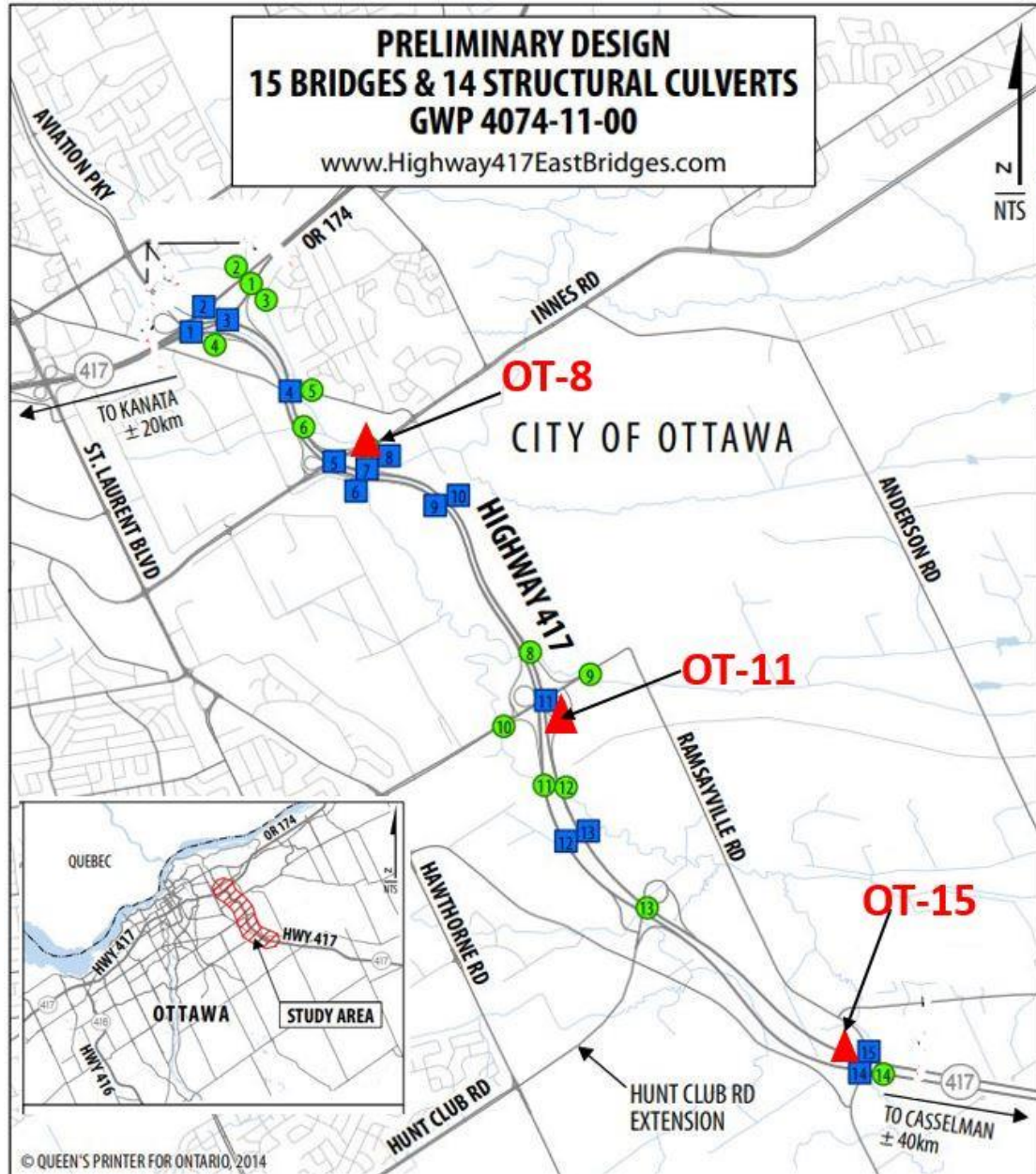


**Figure 3.1: Location of three test sites in Ottawa; blue squares represent bridges, green circles represent structural culverts and red triangles represent non-invasive test sites (modified from Thurber 2015).**

The fourth site is located along the proposed Highway 418 alignment within the municipality of Oshawa, Ontario (Figure 3.2) ~400 km northeast of Windsor. This region lies on the Iroquois Plain north of Lake Ontario. The Iroquois Plain is bounded to the north by the Oak Ridge Moraine. In the Oshawa region, Quaternary drift overlies

Ordovician Lindsay Formation limestones and Whitby Formation shales (Brennard 1998). Brennard (1998) describes a highly variable thickness of Quaternary sediments (0-114 m) with four tills, three glacio-lacustrine sequences and one subaerial fluvial unit occurring in this region. The bulk of surficial sediments is made of coarse-textured glacio-lacustrine deposits. The stratigraphy beneath our site location is made up of soft to very stiff clayey silt layer overlying a very soft silty clay layer which is underlain by Halton drumlinized till (exp 2016). The bedrock is comprised of grey to black shale.



**Figure 3.2: Location of test sites in Oshawa.**

### 3.3 Data collection

Passive-source ambient vibration array measurements were conducted using three-component Tromino® seismometers. Simultaneous vibration recordings were sampled at

128 Hz for ~15 minutes for arrays with sensors < 15 m apart and ~20 minutes for larger sized arrays. Active-source multi-channel analysis of surface waves (MASW; Park et al. 1999) array measurements were conducted using a Geode seismograph in continuous recording mode with a linear array of 12 vertical-component geophones. A 12 lb. sledgehammer was struck vertically on a metal plate at each end of the linear array to generate surface waves. The source offset distance was typically 5 m or 10 m for array spread lengths of  $\leq 11$  m and  $\geq 33$  m, respectively. Three hammer impacts were performed at each source offset location.

The Oshawa site (BS150) is located at Nash road and Hancock Roads in Carlington, Ontario. At the time of the non-invasive testing, active construction of the proposed Highway 418 was underway. A thick pad of artificial compact gravel fill, ~4 m above the natural ground surface, was present. Trominos were placed on this gravel ground surface at 120 m distance from the previous invasive SPT and CPT measurement locations. Each array was composed of 4 sensors in a cross configuration and a stationary 5th sensor at the centre (Figure 3.3 b); the radius of the array was varied from 5 to 10 and 15 m. The presence of the gravel fill surface prevented good sensor coupling of the active-source array geophones such that MASW testing was not accomplished. Instead, single station MHVSR recordings were conducted to assess the uniformity of the subsurface conditions at three sites northeast along the newly constructed highway (SS1, SS2 and SS3 shown in Figure 3.2). SS1 was co-located with the bridge site's CPT and SPT testing locations, while SS2 and SS3 were respectively 0.5 km and 1 km northeast of the bridge site.

In Ottawa, non-invasive testing was accomplished at three bridge sites (OT-8, OT-11 and OT-15) along the Trans-Canada Highway shown in Figure 3.1. Each passive seismic array was composed of three seismographs in an equilateral triangle configuration at four different radii (5, 10, 15, and 30 m). The triangular arrays were set up in open areas: in soil under relocated grass in fields at sites OT-15 and OT-11 and on the asphalt surface of a parking lot at site OT-8. Active-source (MASW) testing was also performed at all Ottawa sites except OT-15. Vertical component geophones were spaced 1 m then 3 m apart resulting in two linear array spread lengths of 11 m and 33 m, respectively.



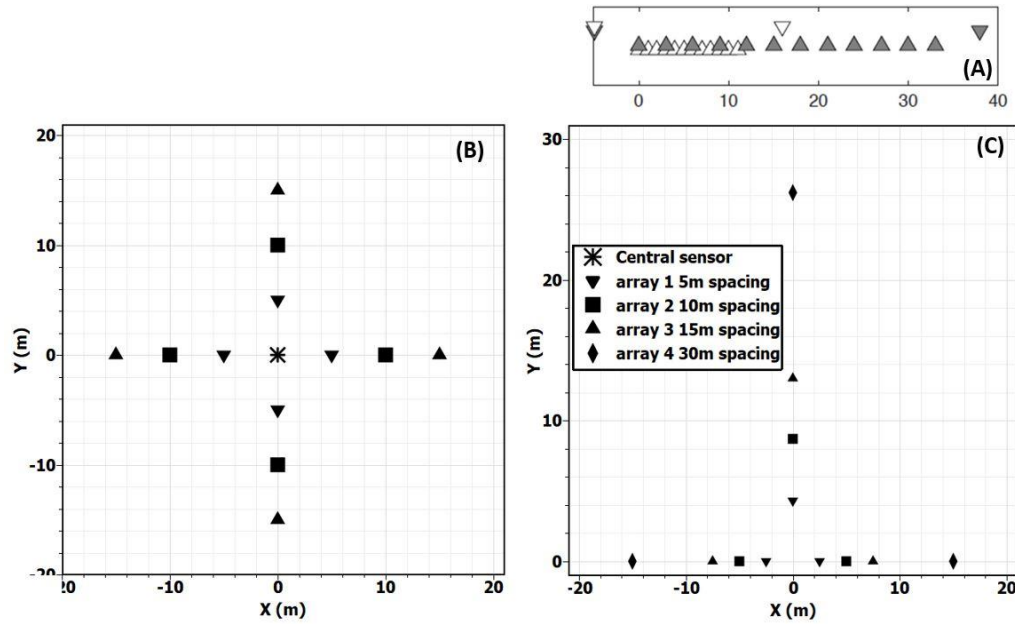


**Figure 3.3: (a) MASW array setup for 1 m (white symbols) and 3 m (grey symbols) spacings. Upward triangles represent geophone locations and downward triangles represent shot locations. (b) Three array apertures of the 5-sensor cross-shaped array geometry at the BS150. (c) Four apertures of the 3-sensor triangular array geometry at sites OT-8, 11 and 15.**

### 3.4 Data processing and analysis

For both dispersion and MHVSR processing, we used the Geopsy open source software (Wathelet, 2008; v. 2.9.1). When required, spurious noise signals resulting from personnel walking to and from sensors at the beginning and end of each array set up are removed from further analysis

#### 3.4.1 MHVSR

A time averaged MHVSR was calculated for each sensor's recording in an array then spatially averaged for each array (3 to 5 time averaged MHVSRs per array). Figure 3.4 shows the array-averaged MHVSRs for the Oshawa and Ottawa sites as well as single station time-averaged MHVSRs at three additional locations at the Oshawa site. Clearly defined sharp fundamental peaks with high amplification ( $>6$ ) are observed at all sites. In Ottawa, site OT-15 has a very low peak frequency (1 Hz) in comparison to OT-8 (peak  $\geq$

10 Hz). Hence site OT-15 is significantly deeper or softer than OT-8. The MHVSR at OT-11 identifies two impedance contrasts with peaks at 0.7 and 11 Hz. All MHVSRs in Oshawa exhibit a  $\sim 3$  Hz fundamental peak indicating a consistent depth to the significant impedance contrast along the 1 km stretch. The fundamental peak at BS150 is broader due to possible mixing of a second peak, which appears at higher and higher frequency towards the north (SS1 to SS3) and indicates changing thickness of a near-surface impedance contrast. For Oshawa, the soil properties vary amongst the locations but the depth to seismic bedrock is consistent.

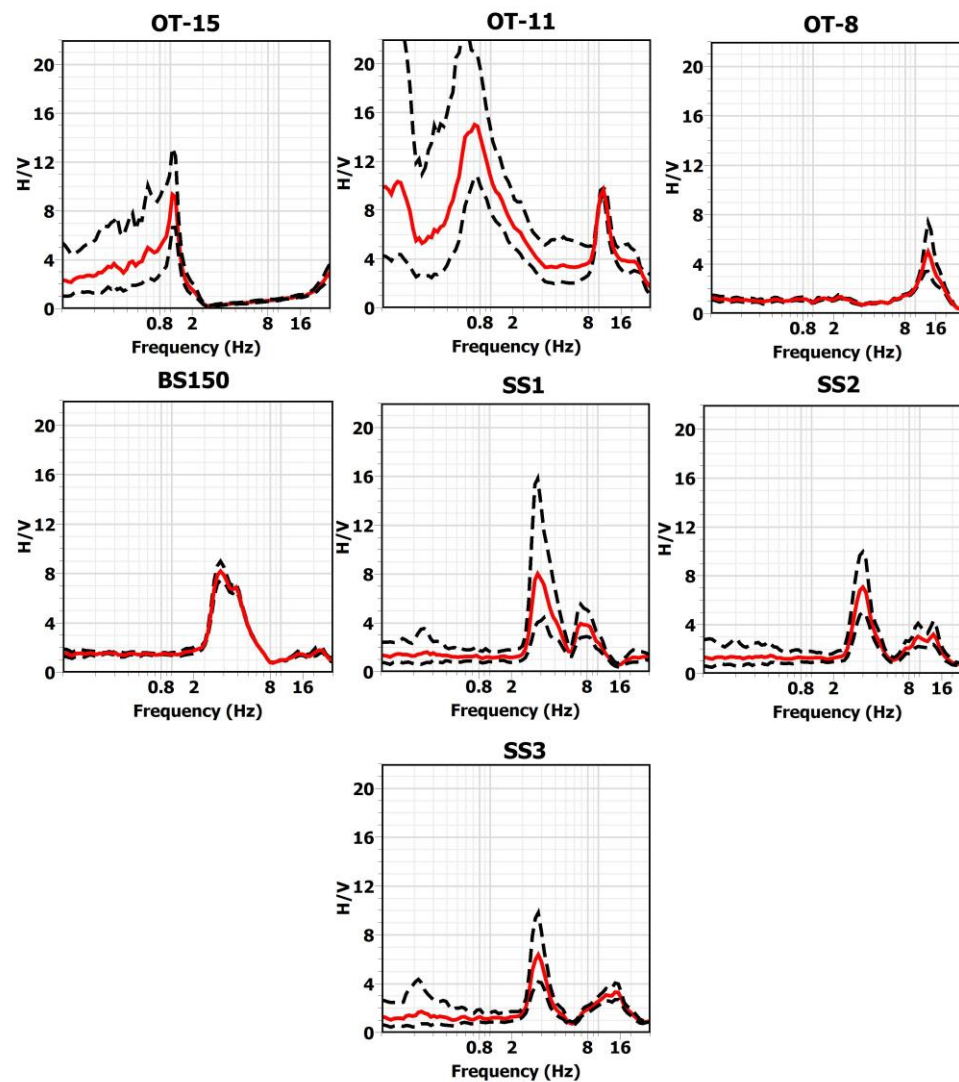


**Figure 3.4: Time-averaged MHVSR curves (red lines) representative of each site with one standard deviation (black dash lines).**

### 3.4.2 Dispersion curves

Dispersion estimates were extracted from the passive-source array recordings using the modified spatial auto-correlation (MSPAC; Bettig et al., 2001) technique, previously explained in Chapter 2 and briefly described here. A probability density function (PDF) of calculated phase velocities at select frequencies (histogram for all frequencies) is constructed to determine Rayleigh-wave dispersion estimates, i.e., the site's dispersion curve (Figure 3.5). A stacked histogram of dispersion estimates from all azimuthally averaged spatial autocorrelation ratios calculated at narrow distance intervals (rings) is generated and the fundamental mode Rayleigh wave dispersion curve is manually picked within the maximum resolution limit and the spatial aliasing limits of all arrays.

For the active-source MASW testing, the seismic recordings from each vertical component geophone are saved in 30 s duration SEG-Y files by the Geode seismograph in continuous recording mode. For this reason, individual SEG-Y files from each geophone are concatenated and all 12 concatenated geophone recordings are stored in a single mini-SEED as a simultaneous array recording. The array recordings are then imported into Geopsy database and cut into 1 s time windows containing waveforms of shots from hammer impact. To account for geometric spreading of surface waves, the waveform amplitudes were normalized using  $\frac{1}{\sqrt{\text{receiver distance}}}$ . The frequency wavenumber (FK) technique (Lacoss et al., 1969) was used to extract dispersion estimates from the active-source array recordings. Since FK processing perform best for unidirectional wave propagation, it is a preferred option for MASW data processing. The Fourier transform of the cross-correlation of the measurements provides a FK spectrum and its amplitude is associated with the power or coherence of the signal. For each frequency, the wavenumber coordinates of the peak of the FK spectrum ( $k_x, k_y$ ) determines the phase velocity ( $c$ ) of the dominant wave as well as its propagation direction ( $\emptyset$ ) as below:

$$c = \frac{2\pi f}{\sqrt{k_x^2 + k_y^2}} \quad (3.1)$$

$$\phi = \tan^{-1} \left( \frac{k_x}{k_y} \right) \quad (3.2)$$

A histogram of calculated phase velocities of the maximum power signal from all sensors at different frequencies is constructed to generate dispersion curves (Fig. 3.5). Fundamental mode dispersion estimates were manually picked from stacked histogram plots from each array set up.

Figure 3.5 shows that, phase velocities range between 100 to 900 m/s for sites in Ottawa and between 250 to 800 m/s for the Oshawa site. A rapid increase in phase velocities at frequencies below  $\sim 3$  Hz (approaching the  $\sim 1$  Hz peak frequency) is observed at OT-15 where the lowest phase velocities also occur. At OT-8 and OT-11, an increase in phase velocities occur at higher frequencies compared to OT-15. At the Oshawa site, a rapid increase in phase velocities is observed at  $\sim 9$  Hz, approaching the  $\sim 4$  Hz peak frequency of the site.

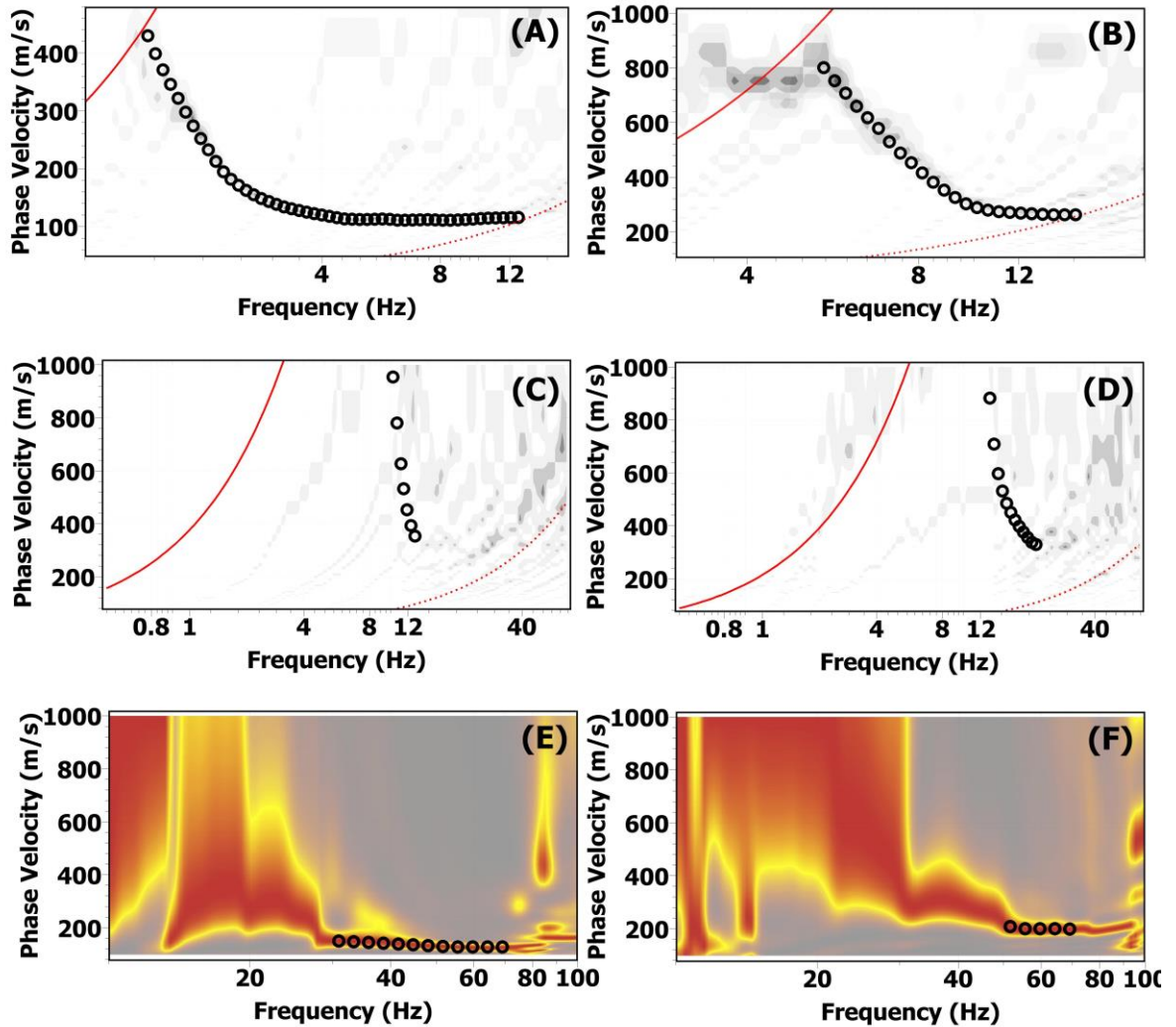


**Figure 3.5: Fundamental mode dispersion estimates (open circles). MSPAC dispersion estimates for (A) OT-15, (B) BS150, (C) OT-11 and (D) OT-8; background shading is MSPAC dispersion histogram; darker shades indicate higher count. FK dispersion estimates obtained from MASW processing for (E) OT-11 and (F) OT-8.**

### 3.5 Preliminary $V_{S30}$ assessment

Preliminary  $V_{S30}$  was estimated for each site from the experimentally determined dispersion curve based on relations between phase velocity and  $V_{S30}$  as described in Chapter 2. As shown in Figure 3.6, we determine  $V_{S30}$  for each site from the phase velocity value that intersects with the  $V_{R40}$  line. For sites in Ottawa, the data indicate  $V_{S30}$

values between 134 and 580 m/s corresponding to a CHBDC site Class E ( $< 180$  m/s) for OT-15 and site Class C (360-760 m/s) for both OT-8 and OT-11. A  $V_{S30}$  value of 353 m/s is obtained for BS150 corresponding to site Class D (180-360 m/s).

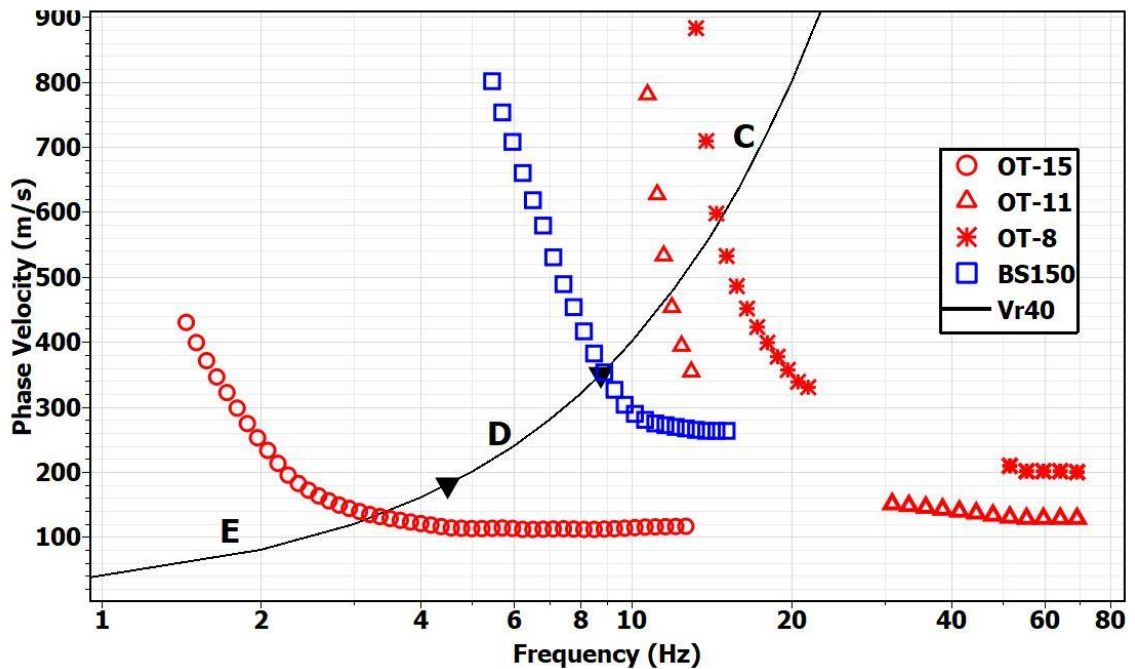


**Figure 3.6: Fundamental mode dispersion curves for each site. Black triangles indicate boundaries between site classes E, D, and C.**

### 3.6 Inversion results

Using the Dinver inversion tool, a joint inversion of the MHVSR and dispersion datasets is performed to retrieve  $V_S$  profiles at each site. A sole inversion of the individual datasets is first performed to assess their contribution to the model, then a joint inversion is performed to find minimum misfit models for both datasets. We start with a single uniform layer over a homogeneous half-space and progressively added layers to obtain an adequate fit to the complexity of our data. The final layers in the retrieved models ranged from 2 to 3 layers including a homogenous elastic half-space.

$V_S$  profiles are successfully retrieved by the joint inversion of MHVSR and dispersion estimates at all sites and are presented in Figure 3.7. The inverted  $V_S$  models in Ottawa are characterized by soft soils (120-180 m/s) with varying thickness (4-40 m) overlying

bedrock. At OT-15, the parameterization is unable to adequately fit the dispersion data at low frequency however, the near surface velocity structure is well retrieved by obtaining an excellent fit of the high frequency dispersion data as well as the right flank of the MHVSR peak. The high frequency dispersion data (from 50-70 Hz for OT-8 and from 28 to 45 Hz for OT-11) obtained from the MASW processing provide additional constraint of the near surface velocity structure at these shallow sites. For site BS150 in Oshawa, the parameterization fails to fit the broad peak in the MHVSR. A compromise is achieved where a good fit of the dispersion data and right-flank of the MHVSR is obtained.

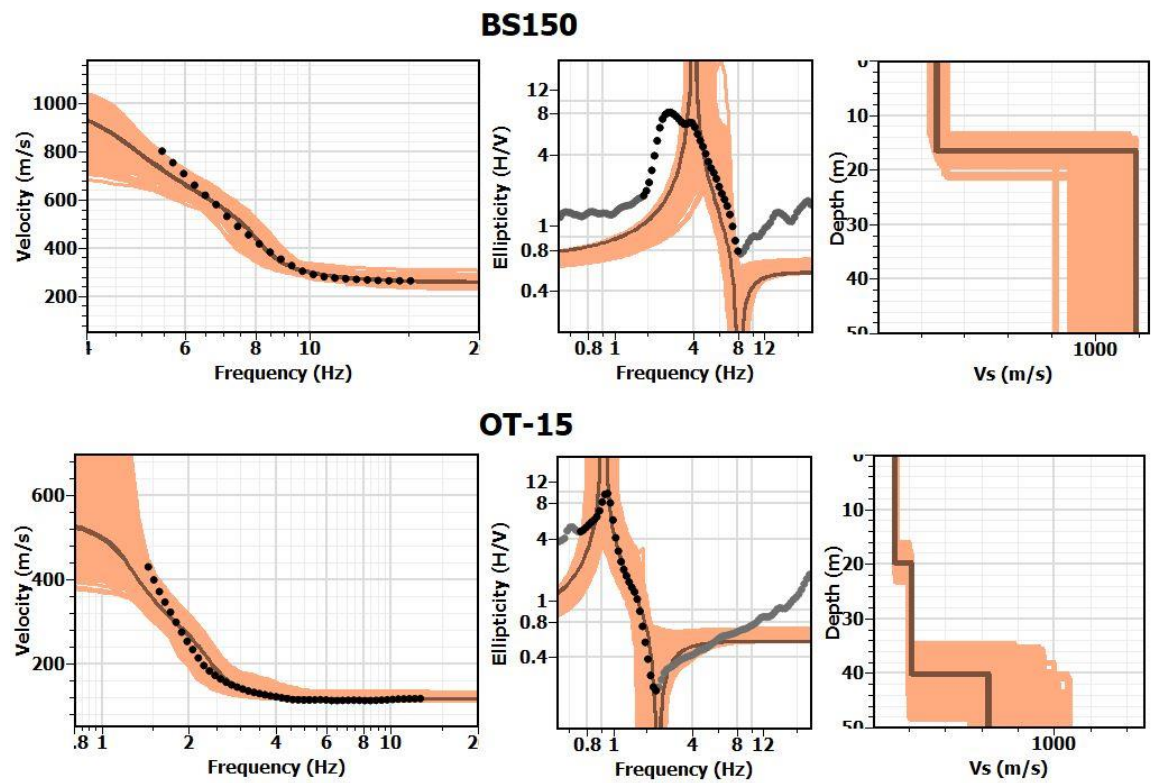


**Figure 3.7: Inversion results from bridge sites. Left panels show dispersion data (black dots), middle panels show MHVSR data (black line) and right panels show the retrieved  $V_s$  profiles for each site. The colored region represents the first 1,000 lowest misfit models and the solid brown line shows the minimum misfit model.**

**Grey dots represents portions of MHVSR not included in the inversion.**

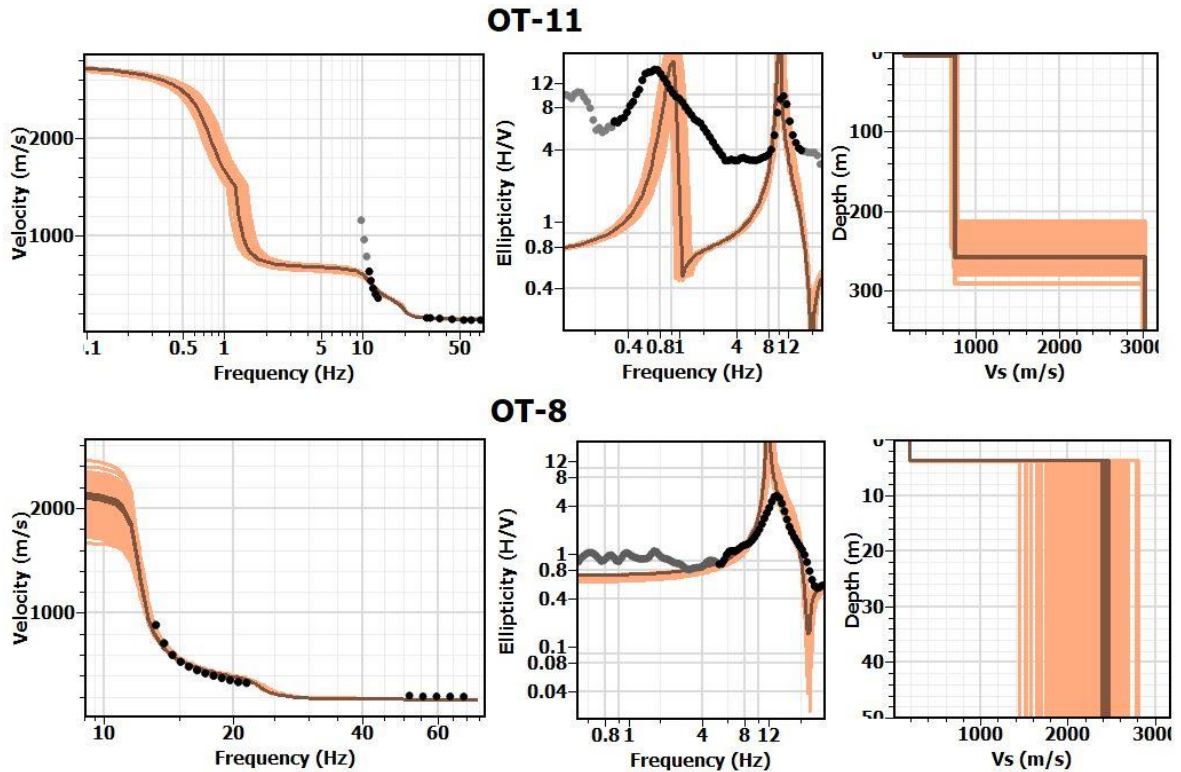


**Figure 3.7. (continued)**

## 3.7 Invasive methods

### 3.7.1 Ottawa

Three bridge sites were selected as part of foundation reviews carried out for existing infrastructure along Highway 417 in Ottawa, Ontario. No site investigations were carried at OT-8 and OT-11, however, a brief description of the subsurface conditions from previous geotechnical site testing conducted by the MTO Foundations Office (GEOCREC Report No. 31G5-190 dated May 1972) prior to construction were provided and are summarized here in Table 3.1. As part of the preliminary investigation, CPT and SCPT measurements were performed at OT-15. These invasive tests were performed in August 2015. Additional details are available in the geotechnical report (Thurber, 2015). The invasive testing is described briefly below.



The CPT was conducted using an integrated electronic piezocone penetrometer and data acquisition system. CPT was advanced to refusal which was encountered at a depth of 40 m below the ground surface. Measurements of corrected tip resistance, pore water pressure during pushing and sleeve-friction were obtained. Vs measurements were performed in conjunction with the piezocone penetration test (SCPT). Shear waves were generated by a hammer horizontally striking a beam at the ground surface and received by a 28 Hz geophone mounted behind the cone tip. The traces were recorded using an up-hole integrated digital oscilloscope which was part of the SCPT data acquisition system. Interval velocities were calculated by visually picking a common feature (e.g. the first characteristic peak or trough) on all of the recorded wave sets and taking the difference in ray path divided by the time difference between subsequent features.

**Table 3.1: Summary of subsurface geology at Ottawa sites (Thurber 2015).**

Site name	Subsurface conditions	Seismic profile & Liquefaction Susceptibility
OT-8	3.7 to 5.3 m of loose to very dense silty sand Shale bedrock	Soil Profile Type I. Site is not susceptible to liquefaction
OT-11	3.5 to 6.4 m of very stiff to firm silty clay 2.8 to 5.2 m of loose to very dense till Shale bedrock	Soil Profile Type I. Site is not susceptible to liquefaction
OT-15	1.5 to 2.7 m of clayey silt 30.8 to 38.6 m of very stiff to firm clay 11.1 to 13.6 m of loose to very dense till Shale bedrock	Base on SCPT testing, site is a Soil Profile Type III. Site is not susceptible to liquefaction

### 3.7.2 Oshawa

SPT and CPT measurements were performed at the Oshawa site for the proposed bridge site as part of the proposed Highway 407 East Phase 2 project. Soil samples were taken at various depths by the SPT method in accordance with ASTM D1586 standard. These invasive tests were performed from May to August 2015 and are briefly described below. Additional details are available in the geotechnical report (exp 2016).

The SPT consisted of freely dropping a 63.5 kg hammer through a vertical distance of 0.76 m to drive a 51 mm split-spoon sampler into the ground. The number of blows of the hammer required to drive the sampler into the undisturbed ground by a vertical height of 0.30 m was recorded as the SPT penetration resistance (N-value) of the soil. CPT was

advanced to refusal which was encountered at a depth of 7.5 m below the ground surface. Measurements of corrected tip resistance, pore water pressure during pushing and sleeve-friction were obtained.

### 3.8 Invasive $V_S$ profiles

CPT  $q_c$  and SPT N-values were converted to  $V_S$  using the approach discussed in Chapter 2. For each site, predicted  $V_S$  from various empirical relations in literature (Chapter 2, Table 2.2) are compared to measured  $V_S$  values from downhole and crosshole methods (Appendix E). For brevity, the root-mean-square-error (RMSE) is reported in Table 3.2 for site OT-15 and reported in Appendix E for site BS150. The relation providing the best agreement (smallest RMSE) is subsequently used to convert  $q_c$  to  $V_S$ . At the OT-15 site in Ottawa, the following correlation proposed by Mayne and Rix (1995) for intact clays was used ( $q_c$  in kPa):

$$V_S = 1.75q_c^{0.627} \quad (3.3)$$

For site BS150 in Oshawa where no invasive  $V_S$  measurements are available,  $V_S$  values from the inverted  $V_S$  profile are used to check the accuracy of relations for converting  $q_c$  to  $V_S$ . Eq. (2.6) proposed by Madiari and Simoni (2004) for Pleistocene sediments was used ( $q_c$  in MPa):  $V_S = 230q_c^{0.25}$

**Table 3.2: RMSE obtained for each correlation used at the Ottawa site (OT-15).**

Reference	Correlation	RMSE (m/s)
Hegazy and Mayne (1995)	$V_S = 12.02q_c^{0.319}f_s^{-0.0466}$	69
Baldai et al. (1989)	$V_S = 227q_c^{0.13}$	70
Mayne and Rix (1995)	$V_S = 1.75q_c^{0.627}$	19
Madiari and Simoni (2004)	$V_S = 230q_c^{0.25}$	78
Samui and Sitharam (2010)	$V_S = 1.93q_c^{0.58}$	48
Piratheepan (2002)	$V_S = 25.3q_c^{0.163}f_s^{0.029}z^{0.155}$	85
McGann et al. (2015)	$V_S = 18.4q_c^{0.144}f_s^{0.0832}z^{0.278}$	22
Perrett et al. (2016)	$V_S = 39q_t^{0.164}z^{0.137}$	27

Figure 3.8 presents  $V_S$  profiles from the converted SPT and CPT data, as well as the SCPT  $V_S$  measurements for all sites. Despite some variation, the converted and measured

$V_s$  profiles from the invasive techniques indicate comparable  $V_s$  values. An increasing trend of  $V_s$  with depth is observed at OT-15. At BS150, SPT and CPT data were obtained from two boreholes  $\sim 20$  m apart. A low velocity zone is identified by both converted SPT and CPT profiles with values comparable with  $V_s$  from our laboratory bender element testing (section 3.9.2). However, a  $\sim 100$  m/s variability in  $V_s$  estimates is obtained from both profiles. This can be attributed to the lack of direct  $V_s$  measurements to check the accuracy of converted CPT and SPT profiles which are also separated by 20 m (possible change in ground conditions).

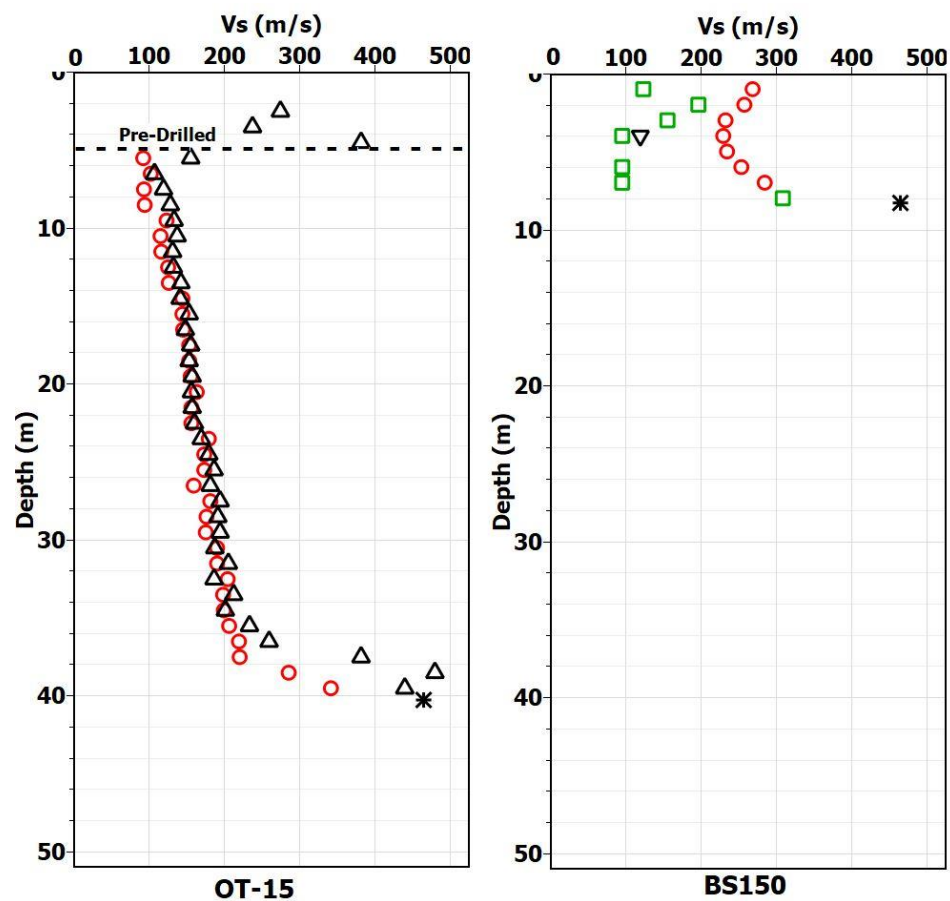


**Figure 3.8: Invasive  $V_s$  measurements at the tested borehole locations: converted CPT (circles), converted SPT (squares), SCPT  $V_s$  (upward triangle), bender element  $V_s$  measurement (downward triangle) and refusal depth (stars).**

## 3.9 Laboratory tests

In this study, laboratory tests are performed on silty clay sample obtained at a depth of 4 m below the ground surface at the Oshawa bridge site (BS150). A specific gravity ( $G_s$ ) of 2.65, void ratio of 0.76 and moisture content of 26% were determined for the sample.

### 3.9.1 Specimen preparation and consolidation

To prepare the Oshawa soil sample for laboratory measurement, the specimen was trimmed to the required size (50 mm in diameter and 25.4 mm tall) using a triaxial trim table with minimum sample disturbance to maintain the *in situ* fabric of the soil. The specimen was then confined in a latex membrane folded over stacked rigid stainless steel rings and mounted on the bottom platen of the direct simple shear equipment. The vertical loading ram which holds the top platen was lowered onto the clay specimen surface and the membrane was folded back on the loading ram. The membrane and stacked rings were held in place with an O-ring and two supporting retainers respectively. A small vertical seating stress of 5 kPa was applied to eliminate seating displacement errors. The specimen was then consolidated one-dimensionally to an effective vertical consolidation stresses of 60 kPa (which reflects the *in situ* stress condition) and 120 kPa.

### 3.9.2 Laboratory bender element $V_s$ measurements

Shear wave velocity of the prepared Oshawa soil sample was measured using a bender element test originally proposed by Shirley and Hampton (1978). This is a simple test which allows for rapid determination of  $V_s$  of soil specimens. A pair of piezoelectric bender elements mounted on circular cross-sectional platens are inserted at the top and base of the soil specimen. Voltage is applied to one element to generate a shear wave signal through the soil specimen. The element at the other end of the soil sample acts as a receiver to pick up the signal. The  $V_s$  is then calculated from the travel time of the signal through the specimen and the tip-to-tip distance between the bender elements. After the end of primary consolidation, shear wave signals (shots) were generated at a frequency of 40 kHz with an input voltage of 14 V. This high frequency signal was chosen to facilitate the development and propagation of shear waves through the specimen such that a

wavelength of at least half the distance between the bender elements was achieved. The signal to noise ratio was improved by stacking a minimum of 10 shots.

Figure 3.9 shows the input source and stacked receiver waveforms from the bender element test. The travel time of the shear wave signal through the specimen was calculated using the peak-to-peak method. The time interval between the peak of the source signal (time zero) and the arrival time of the first peak in the receiver waveform is the shear wave travel time. The peak-to-peak method generally provides an accurate measure of  $V_S$  (Brignoli et al., 1996, Viggiani and Atkinson 1995, Yamashita et al., 2009). The travel distance between the bender elements was calculated by subtracting the heights of the bender elements from the height of the specimen, i.e., the bender elements are slightly embedded in the sample.  $V_S$  of the soil specimen was determined by dividing the travel time by the distance. Signals generated at higher frequencies (50 and 60 kHz) resulted in similar  $V_S$  indicating robust measure of  $V_S$  of the soil specimen. Subsequently,  $V_S$  was determined to be 120 m/s.

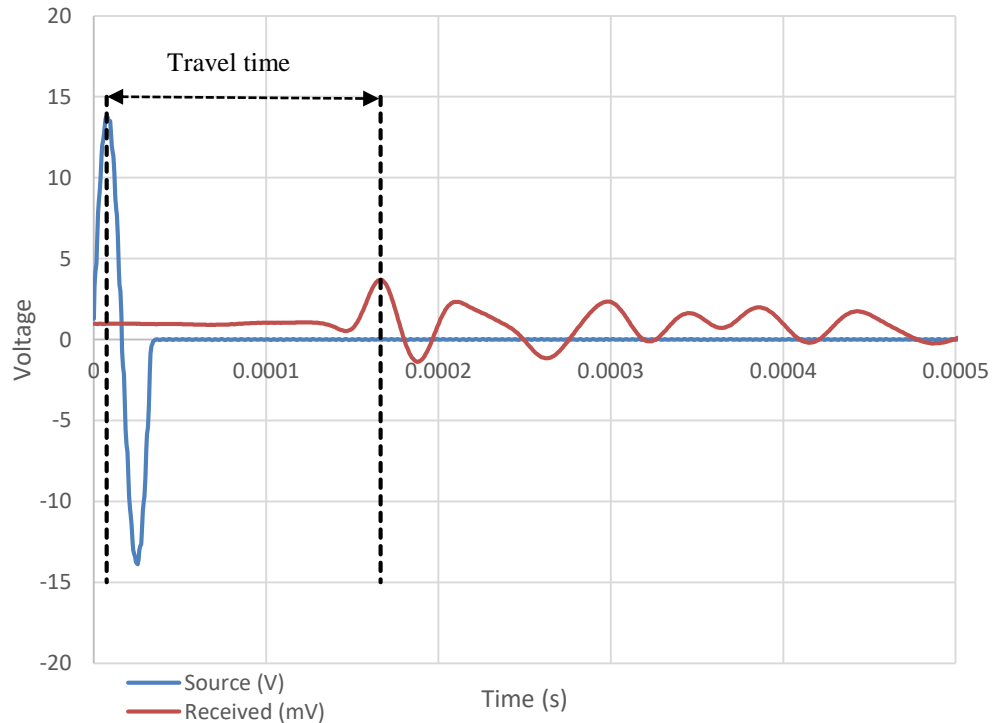


**Figure 3.9: Incipient and transmitted waveforms from the bender element test.**

### 3.9.3 Direct simple shear test

The specimen was sheared by displacing one platen tangentially relative to the other at a constant rate of displacement. An undrained condition was simulated by keeping the volume of the specimen constant during shearing. Figure 3.10 presents the stress paths from the constant volume direct simple shear (DSS) test. An undrained shear strength of approximately 24 kPa was obtained and the deviator stress became essentially constant at an axial strain of approximately 12%.

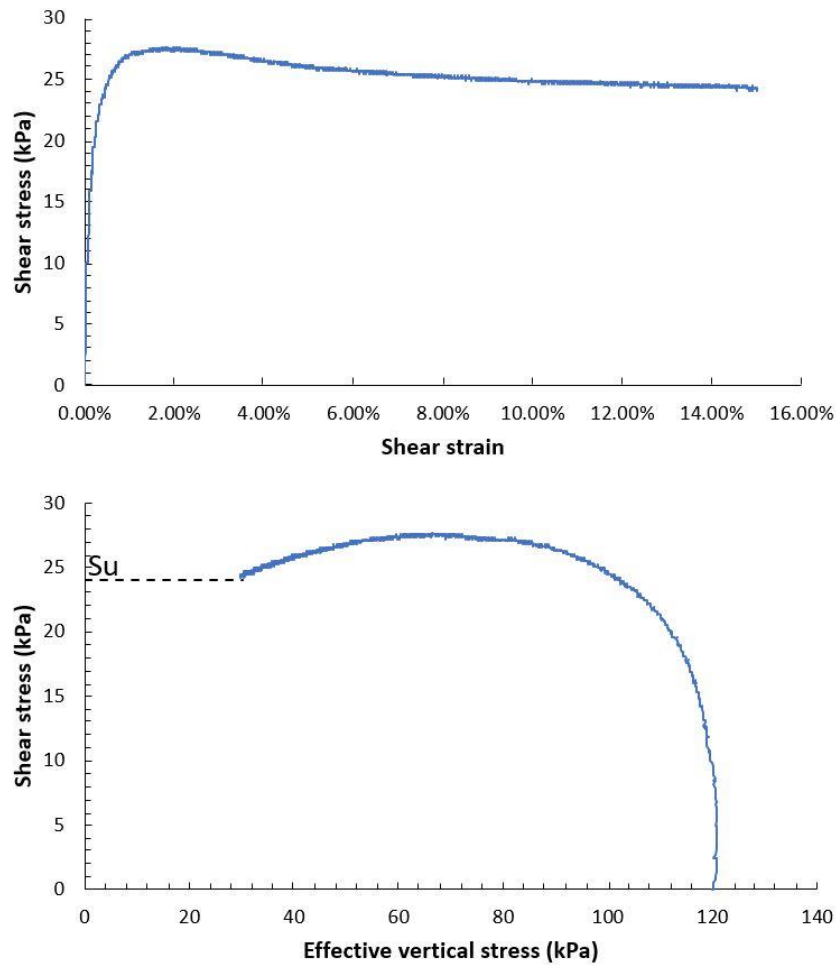


**Figure 3.10: Stress paths obtained from DSS test.**

### 3.10 Comparison of $V_s$ from different methodologies

A blind test comparison was conducted to objectively assess the difference between invasive and non-invasive  $V_s$  profiling methodologies similar to our Windsor study presented in Chapter 2. Figure 3.11 compares the minimum misfit  $V_s$  profile from inversion of the surface wave non-invasive data with co-located invasive  $V_s$  measurements and converted- $V_s$  estimates for each bridge site. At OT-15, the inverted model resolves 20 m of soft material ( $V_s \sim 122$  m/s) overlying a slightly higher velocity ( $V_s \sim 210$  m/s) layer. This is in good agreement with both SCPT and converted CPT  $V_s$  profiles which show a gradual increase in velocity with depth. At OT-15, the inverted  $V_s$  profile captures the general increase in  $V_s$  with depth to a significant impedance identified at 40 m which is in excellent agreement with the invasive measurements. The average relative difference in  $V_s$  for this soil layer is 27 m/s within the  $\sim 20\%$  difference between invasive and non-invasive  $V_s$  profiling methods (Garofalo et al. 2016). A 4 m layer ( $\sim 184$  m/s) overlying an elastic half-space is resolved by the inverted model at OT-8. This is consistent with the 3.7 to 5.3 m of loose to very dense silty sand overlying shale bedrock at the site (Table 3.1). Although slightly softer, the 4 m near surface material ( $V_s \sim 156$  m/s) determined by the inverted  $V_s$  profile at OT-11 is in good agreement with the expected 3.5 to 6.4 m of stiff to firm silty clay present at the site (Table 3.1). The inverted model is also able to resolve about 250 m of soft rock ( $V_s \sim 770$  m/s) overlying hard rock ( $V_s \sim 3000$  m/s) at this site.

The inverted  $V_s$  profile at site BS150 in Oshawa determines slightly higher  $V_s$  within the upper 10 m than the converted CPT and SPT measurements. The depth to a significant impedance is deeper than the SPT refusal depth recorded at 12 m. It is important to note that the first 4 m of the inverted profile is considered as fill material. Additionally, the inverted  $V_s$  model is unable to resolve the thin soft layer (7-11 m depth) identified by both converted SPT and CPT profiles. This results in an average relative difference in  $V_s$  of the soil layers of 73 m/s between invasive and non-invasive  $V_s$  profiles. The greater variability in  $V_s$  models can be attributed to the changing near surface ground conditions present at the site between invasive (pre-construction) and non-invasive (during bridge construction) testing. The  $V_s$  of the soft (120 m/s) silty clay sample obtained from the

bender element test is comparable to converted SPT  $V_s$  values at the same depth. The bender element test is therefore specific to the soft silty clay layer present at 4 m depth below the reference ground surface as described in earlier sections.

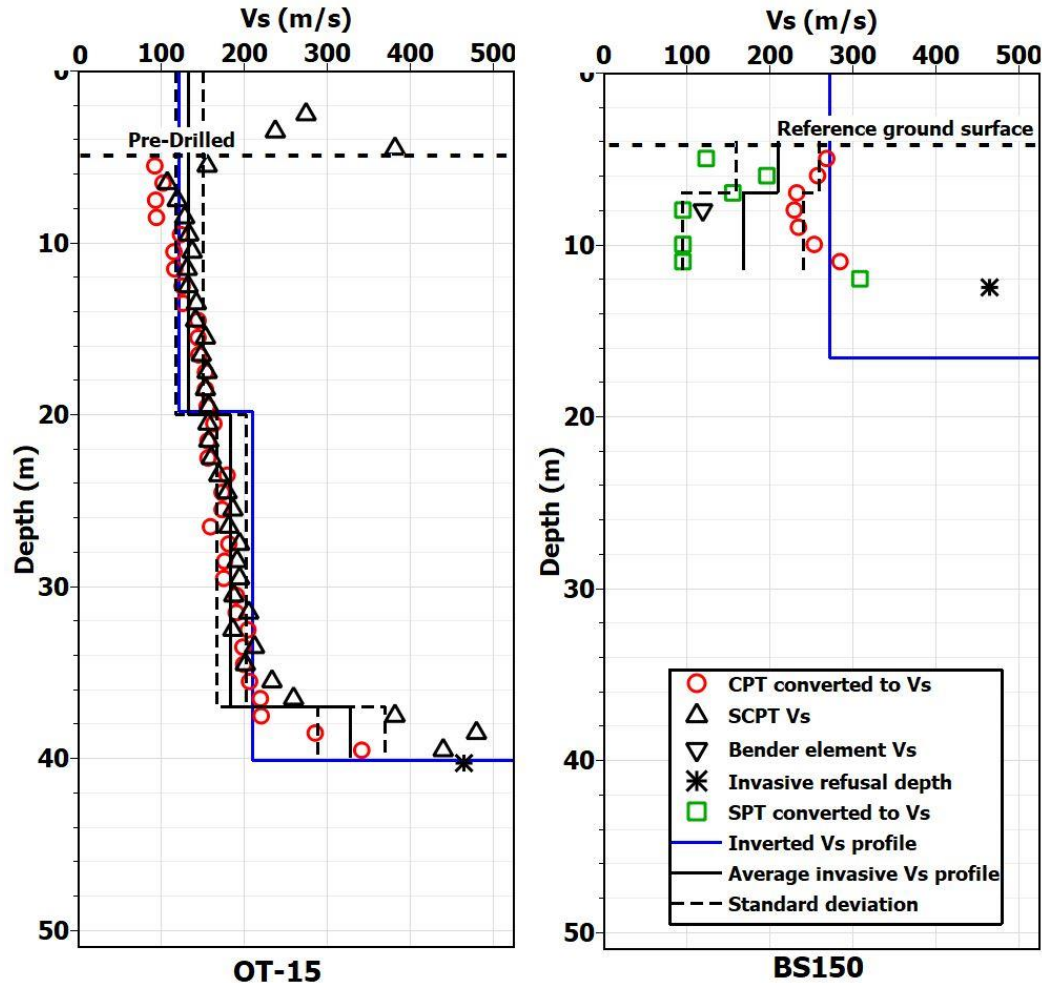


Figure 3.11: Comparison of invasive and non-invasive  $V_s$  profiles.

### 3.11 $V_{s30}$ -based earthquake site classification

The mean invasive  $V_s$  profile (Figure 3.11) is calculated by averaging the converted CPT profiles with the discrete SCPT measurements and/or converted SPT profiles. Average invasive  $V_s$  values are calculated within selected depth intervals based on stratigraphy. The average invasive  $V_s$  profiles at OT-8 and OT-11 are calculated using the subsurface description from Table 3.1 and shown in Figure 3.12. An average  $V_s$  of 150 m/s (average  $V_s$  of Champlain Sea sediments in Ottawa; Motazedian and Hunter 2008) is assigned to



all sediments described. Additionally, average interval velocities of 500 m/s and 2166 m/s are used respectively for glacial till and bedrock in Ottawa following the works of Hunter et al. 2007 and Motazedian et al. 2011.  $V_{S30}$  is calculated using Eqn. (2.7). At site BS150 where the invasive data does not extend to 30 m depth, a  $V_S$  value of 465 m/s is assigned after the depth at which the sediments end (past refusal depth) which is the average  $V_S$  of surficial tills in southern Ontario (Crow et al. 2017). These values are used to compute  $V_{S30}$  at sites where glacial till and/or bedrock occur within the upper 30 m.  $V_{S30}$  is calculated for both invasive and non-invasive  $V_S$  profiles and the corresponding site class is assigned according to CHBDC in Table 3.3.

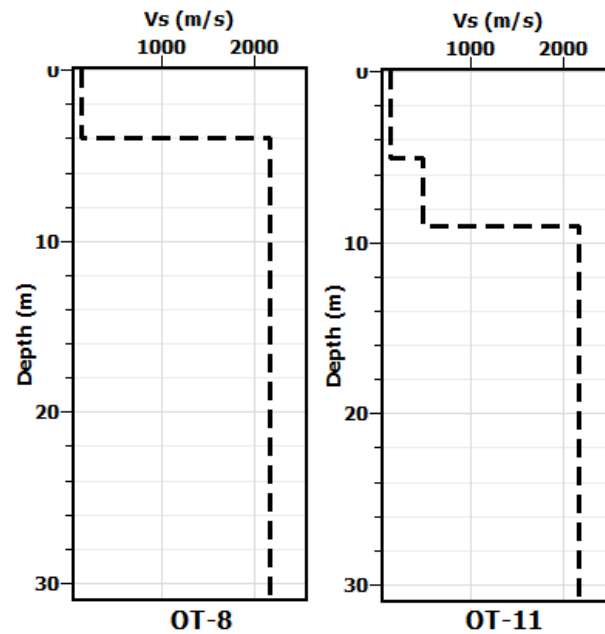


**Figure 3.12: Average invasive  $V_S$  profiles for  $V_{S30}$  estimation at sites OT-8 and OT-11 calculated using the subsurface description from Table 3.1.**

The ground surface conditions in Ottawa vary between rock, till, and thick to thin layers of soft sediments (Table 3.1). This resulted in different CHBDC site classes between individual sites. However, the site classes obtained from this study are in good agreement with site classes from the  $V_{S30}$  map of Ottawa developed by Motazedian et al. (2011). At site BS150 in Oshawa, both average invasive and inverted  $V_S$  profiles determine similar  $V_{S30}$  values. The  $V_{S30}$  estimate from the dispersion data which intersected the  $V_{R40}$  line at

the boundary between site class C and D (Figure 3.6) is slightly underestimated compared to invasive and inverted  $V_s$  profiles and classified accordingly as C/D.

**Table 3.3: Site classification for both invasive and non-invasive methodologies.**

Location	Inverted $V_s$ model		Converted CPT to $V_s$		SCPT $V_s$ profile		Average Invasive $V_s$ profile		Dispersion ( $V_{R40}$ ) data		Motazedian et al (2011)	
	$V_{S30}$ (std.dev) <sup>1</sup>	Class	$V_{S30}$	Class	$V_{S30}$	Class	$V_{S30}$ (std.dev)	Class	$V_{S30}$	Class	$V_{S30}$	Class
OT-8	908 (112)	B	N/A		N/A		776 (85)	B	583	C	898	B
OT-11	496 (62)	C	N/A		N/A		587 (61)	C	478	C	557	C
OT-15	158 (43)	E	159	E	160	E	160 (24)	E	133	E	144	E
BS150	420 (52)	C	415	C	N/A		404 (64)	C	353	C/D	N/A	N/A

<sup>1</sup>Std. dev. determined from 1001 models.

### 3.12 $S_u$ -based site classification

At site BS150 in Oshawa,  $S_u$  values from the geotechnical report (exp 2016) and from our laboratory test are used to classify the site based on undrained shear strength properties of the upper 30 m according to CHBDC. Since glacial till occurs within the upper 30 m, a value of 660 kPa which is the  $S_u$  of dense glacial till in Wesleyville, Ontario (Radhakrishna and Klym 1974) ~27 km from our test location is used. This value is assigned after the depth at which the sediments end (past refusal depth). Details of  $S_u$  values for individual soil units are given in Table 3.4. Consequently, a weighted average  $S_u$  value of 117 kPa corresponding to site class C ( $S_u > 100$  kPa) is determined for site BS150 which is consistent with the  $V_{S30}$ -based site class reported in Table 3.3.

**Table 3.4: Soil parameters for  $S_u$ -based site classification.**

Height (m)	Soil layer	$S_u$ (kPa)
3	Clayey silt soft to firm	55
4	Silty clay very soft	24
21	Silty sand (Till) compact to very dense	660

### 3.13 Conclusions

In this study, AVA and MASW recordings were collected at four bridge sites in Oshawa and Ottawa, Ontario, co-located with previous invasive measurements. Joint inversion of dispersion and MHVSR data-sets was performed to obtain 1D velocity depth profiles. A laboratory based bender element test was performed to obtain  $V_S$  for a shallow silty clay sample from the Oshawa site. Subsequently, a blind test comparison was conducted to objectively assess the difference between invasive, non-invasive and laboratory  $V_S$  profiling techniques. Individual  $V_{S30}$ -based site classes were examined and consistent earthquake site classification was obtained between methodologies.

We find that the inclusion of dispersion data from MASW analysis in surface wave inversion provides additional constraints on the near surface velocity structure and can be useful at sites where the depth to significant impedance is shallow. Despite the inability of the inversion to resolve thin layers, comparable  $V_S$  estimates are obtained between methodologies. CHBDC site classes B, C and E are obtained for the Ottawa sites and compare well with existing  $V_{S30}$  map of Ottawa developed mainly from invasive testing. Site class C is obtained for the Oshawa site with consistent agreement between  $V_S$  profiling methods. Additionally, the use of dispersion data for determining site class generally resulted in lower  $V_{S30}$  compared to other methods with significant underestimation observed at shallow sites. Although sample disturbance and boundary conditions involved in bender element testing affects the resulting  $V_S$ , a robust measure

of  $V_s$  is obtained and is in agreement with, and therefore representative of, the *in situ* condition.

### 3.14 Data and resources

All invasive data from geotechnical reports were obtained from the publicly available MTO online database (<http://www.mto.gov.on.ca/FoundationLibrary/index.shtml>).

### 3.15 Acknowledgements

Funding provided by the MTO Highway Infrastructure and Innovation Fund (HIIF) is highly appreciated. Thank you to Melanie Postman (UWO BSc student) and Samantha Palmer (UWO PhD student) for field assistance.

### 3.16 References

- Bettig B., P.-Y. Bard, F. Scherbaum, J. Riepl, and F. Cotton (2001). Analysis of dense array noise measurements using the modified spatial auto-correlation method (SPAC). Application to the Grenoble area, *Bolletino di Geofisica Teorica ed Applicata*. 42, 281-304.
- Brennand, T. A. (1998). Urban geology note: Oshawa, Ontario. *Urban Geology of Canadian Cities*. Edited by PF Karrow and OL White. Geological Association of Canada, *Special Paper*, 42, 353-364.
- Brignoli, E. G. M., Gotti, M., and Stokoe, K. H. (1996). Measurement of shear waves in laboratory specimens by means of piezoelectric transducers. *Geotechnical Testing Journal, ASTM*, 19(4), 384 - 397.
- Capon, J., (1969). High-resolution frequency-wavenumber spectral analysis. *Proc. IEEE.*, 57, 1408-1419.

- Crow, H. L., Hunter, J. A., Olson, L. C., Pugin, A. J. M., and Russell, H. A. (2017). Borehole geophysical log signatures and stratigraphic assessment in a glacial basin, southern Ontario. *Canadian Journal of Earth Sciences*, 999, 1-17.
- Eden, W. J., and Law, K. T. (1980). Comparison of undrained shear strength results obtained by different test methods in soft clays. *Canadian Geotechnical Journal*, 17(3), 369-381
- exp (2016). Highway 407 East Phase 2, Geotechnical Design Report for Structure E-21, Draft R3, exp report R3-90-D1B-GT-E21, 30M15-285, 1-125 pgs.
- Gadd, N. R., and Fulton, R. J. (1987). Geological setting and Quaternary deposits of the Ottawa Region. *Quaternary geology of the Ottawa Region, Ontario and Quebec. Edited by RJ Fulton. Geological Survey of Canada*, 86-23.
- Hunter, J. A., Burns, R. A., Good, R. L., Aylsworth, J. M., Pullan, S. E., Perret, D., and Douma, M. (2007). Borehole shear wave velocity measurements of Champlain Sea sediments in the Ottawa-Montreal region. *Geological Survey of Canada, Open File Report*, 5345.
- Lacoss, R. T., E. J. Kelly, and M. N. Toksöz (1969). Estimation of seismic noise structure using arrays. *Geophysics*, 29, 21-38.
- Madiai, C., and Simoni, G. (2004). Shear wave velocity-penetration resistance correlation for Holocene and Pleistocene soils of an area in central Italy. In *Geotechnical and Geophysical Site Characterization. Proceedings of the 2nd International Conference on Site Characterization. Porto, Portugal, September 19-22*.
- Mayne, P. W., and Rix, G. J. (1995). Correlations between shear wave velocity and cone tip resistance in natural clays. *Soils and foundations*, 35(2), 107-110.
- Motazedian, D., and Hunter, J. (2008). Development of an NEHRP map for the Orleans suburb of Ottawa, Ontario. *Canadian Geotechnical Journal*, 45(8), 1180-1188.

- Motazedian, D., Hunter, J. A., Pugin, A., and Crow, H. (2011). Development of a  $V_{s30}$  (NEHRP) map for the city of Ottawa, Ontario, Canada. *Canadian Geotechnical Journal*, 48(3), 458-472.
- Park, C. B., Miller, R. D., and Xia, J. (1999). Multichannel analysis of surface waves. *Geophysics*, 64(3), 800-808.
- Radhakrishna, H. S., and Klym, T. W. (1974). Geotechnical properties of a very dense glacial till. *Canadian Geotechnical Journal*, 11(3), 396-408.
- Shirley, D. J., and Hampton, L. D. (1978). Shear-wave measurements in laboratory sediments. *The Journal of the Acoustical Society of America*, 63(2), 607-613.
- Thurber (2015). Preliminary Foundation Design Highway 417 – 15 bridges, City of Ottawa, Ontario, Vol 1, Thurber report 4074–11–00, 31G5-263, 316 pgs.
- Viggiani, G., and Atkinson, J. H. (1995). Interpretation of bender element tests. *Geotechnique*, 45(1), 149 - 154.
- Wathelet, M. (2008). An improved neighborhood algorithm: Parameter conditions and dynamic scaling. *Geophysical Research Letters*, 35(9), L09301. doi:10.1029/2008GL033256
- Yamashita, S., Kawaguchi, T., Nakata, Y., Mikami, T., Fujiwara, T., and Shibuya, S. (2009). Interpretation of International Parallel Test on the Measurement of G(Max) Using Bender Elements. *Soils and Foundations*, 49(4), 31-650.

## Chapter 4

### 4 Conclusions and recommendations

With the adoption of  $V_{S30}$  as the earthquake site classification criterion in the 2015 bridge design code (CSA Group 2014), the MTO seeks a wider range of applicable geophysical techniques towards optimizing a robust site classification procedure(s) for Ontario bridge sites. The primary objective of this thesis is to perform a true blind test comparison at Ontario bridge sites to assess the reliability of non-invasive techniques in comparison to invasive methods for earthquake site classification.

In Chapter 2 we successfully extracted dispersion data from ambient vibration array recordings at six bridge sites across Windsor, Ontario. We used the dispersion curves to estimate  $V_{S30}$  and find that all sites are categorized as site class D (stiff soil) according to CHBDC. A limitation of this method is the potential errors that may arise from the subjective task of manually picking the dispersion curves. However, this non-invasive method offers a rapid and cost-effective way to measure  $V_{S30}$ , and can also be used for large-scale site classification projects. Joint inversion of the MHVSR and dispersion curves is performed to obtain detailed subsurface  $V_S$  profiles at each site. These  $V_S$  depth profiles are compared to the available geotechnical borehole information for which an average relative difference of 27 m/s (9%) is obtained. Additionally, excellent agreement of  $V_{S30}$  estimates is obtained between both invasive and non-invasive methods from which these sediments are consistently categorized as site class D (stiff soil). The inverted  $V_S$  profiles obtained from the surface wave data are used together with the non-invasive data to develop a relation between  $V_{S1}$  and  $q_{c1}$ . The proposed relation compares well with other relations in literature and produces a good agreement between measured and predicted  $V_S$ . Although it is preferable to measure  $V_S$  directly in the field, this relation provides a satisfactory alternative when it is not economically feasible to perform  $V_S$  measurements at all locations in Windsor, Ontario and surrounding areas. In Chapter 3 we show that the inclusion of MASW dispersion data provides additional constraints in the retrieval of near surface velocity structure. Comparable  $V_S$  is obtained between methodologies despite the inability of the inverted  $V_S$  profiles to resolve thin layers. We

are also able to retrieve parameters,  $f_{peak}$  and  $V_S$  profiles, necessary for site response analysis and earthquake hazard evaluation. Overall, we highlight the efficiency of the rapid and cost-effective non-invasive method which can be used in the absence of, or in conjunction with invasive  $V_S$  profiling techniques to obtain reliable  $V_S$  estimates for site classification at our tested Ontario bridge sites.

## 4.1 Robust earthquake site classification procedure

The results of this study highlights the efficiency of the rapid and cost-effective non-invasive methods to obtain reliable  $V_S$  estimates for seismic site classification. We acknowledge the non-uniqueness of the solution of the inverse problem to obtain  $V_S$  profiles and the inability of our non-invasive profiles to detect discrete  $V_S$  variations within soil layers with depth. However, since  $V_{S30}$  is an average parameter, discrete changes in  $V_S$  with depth has minimal effect on estimating  $V_{S30}$  as demonstrated by the observed consistency in our  $V_{S30}$  estimates obtained between both invasive and non-invasive methods. Thus, we recommend the use of non-invasive seismic testing as the first choice for earthquake site classification based on  $V_{S30}$ , with invasive testing being a complementary alternative when required. Based on the findings related to the tested materials and sites in this study, a recommended general procedure for earthquake site classification is described below and summarized in the flow chart in Figure 4.1. Since the primary interest of this procedure is to obtain  $V_{S30}$ , recommendations are made here based on a maximum investigation depth of 30 m below the ground surface.

1. Always as a first step, we recommend the use of MHVSR as a reconnaissance tool to explore the subsurface ground conditions around the site of interest, e.g., a future bridge site or stretch of highway. The number of MHVSR measurements to be collected is dependent on the scale of project. Collecting a minimum of five MHVSR measurements at a site is beneficial to assess its lateral homogeneity and 1D subsurface conditions. Where available, the use of geological information (e.g. surficial geology, drift thickness maps) in conjunction with MHVSRs will facilitate the understanding of ground conditions based on sediment thickness and potential stiffness. If geology is known from drilling or average stiffness of the



same geology, then the MHVSRs can be directly inverted for  $V_s$  profiles and  $V_{S30}$  determination.

2. As a second step, we recommend inspection of the MHVSR morphology (shape, height, etc.) as the basis for choosing the appropriate testing method for site characterization. If the MHVSRs show consistent single high amplitude and/or low frequency ( $< 5$  Hz) peaks indicative of deep impedance contrast(s), we recommend AVA testing method due to its ability to sample a wide frequency band and provide a greater depth of investigation. MASW should be used as a complementary method to extend the dispersion curve to higher frequencies, if needed. Conversely, if the MHVSRs exhibit low-amplitude high-frequency ( $> 5$  Hz) peaks implying shallow impedance contrast(s), both AVA and MASW testing are recommended. MASW has the ability to provide high frequency data necessary for characterizing shallow sediments.
  - The choice of AVA array geometry is strongly dependent on the number of available sensors, the depth of interest and the available layout space. For AVA, a minimum of 3 sensors in a common base triangular configuration equidistantly spaced at 5, 10, 15 and 30 m (see Section 2.4) is recommended. Denser array configurations (e.g. circular and nested triangle) can be used where availability of sensors and space permit. For MASW, a linear array of a minimum of 12 geophones spaced at 1 m and 3 m with source offsets at 5 m and 10 m respectively and a minimum of three hammer impacts at each source offset location is recommended.
  - We recommend the use of MSPAC and F-K processing techniques to extract dispersion estimates from AVA and MASW recordings, respectively. The ability of MSPAC to account for non-symmetric arrays and effectiveness with a small number of sensors makes it ideal for processing AVA data. Since F-K processing perform best for unidirectional wave propagation, it is a preferred option for MASW data processing.
- a) For lower-consequence sites (e.g., between bridge sites),  $V_{S30}$  can be estimated directly from phase velocity values that intersect with the  $V_{R40}$  line

(see Section 2.6). A limitation of this method is the potential errors that may arise from the subjective task of manually picking the dispersion curves. Associated CHBDC site class can then be assigned.

- b) For higher-consequence sites (e.g., a bridge site), joint inversion will be performed using dispersion estimates extracted from AVA and/or MASW recordings with an MHVSR representative of the site to retrieve  $V_S$  profile(s) and consequently  $V_{S30}$  of the site. Joint inversion provides a robust  $V_S$  profile with depth and is recommended above sole inversion of dispersion or MHVSR curves. Combined MHVSR and dispersion inversion is the preferred non-invasive testing approach to retrieve subsurface  $V_S$  profiles for  $V_{S30}$  estimation and site classification.
3. In instances where the MHVSR curves vary considerably within the vicinity of the site and suggest a significant deviation from the 1D assumption necessary for surface wave analysis, then invasive testing which samples smaller subsurface volumes will be required. We recommend at least one SCPT and two other CPT tests (total of 3 CPT tests) are performed across the site, with invasive testing locations directed by the MHVSR reconnaissance. SCPT is a required option to obtain a  $V_S$  profile for  $V_{S30}$  and site class determination. Variation in  $V_{S30}$  between the SCPT and CPT test locations can be determined from converting tip resistance to  $V_S$  to obtain  $V_{S30}$  (see section 2.13). When sediments are too stiff for CPT penetration, SPT testing shall be performed instead and  $N_{60}$  used for site classification.
4. The recommended “method of last resort” due to highest costs is invasive drilling combined with downhole or cross-hole  $V_S$  measurements to 30 m depth. MHVSR reconnaissance will determine locations and number of drillholes required to capture the site variability. For high consequence or multi-million dollar projects, down- and cross-hole  $V_S$  profiling may replace and/or complement SCPT and CPT testing (option 3).

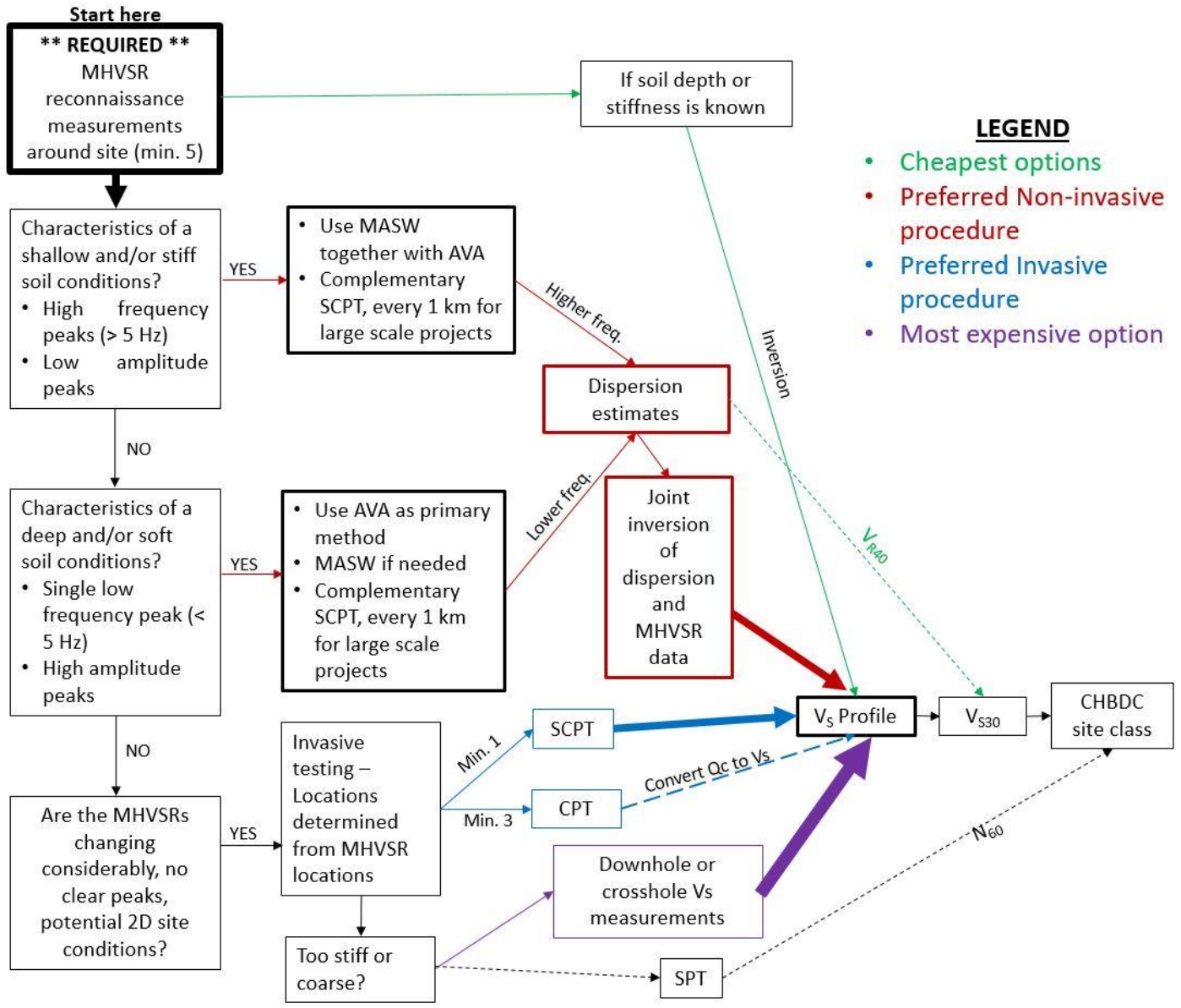


**Figure 4.1: Flow chart summarizing proposed robust earthquake site classification procedure. Dashed line indicates  $V_s$  proxy method, solid line indicates  $V_s$  method; the thicker the solid lines, the more preferred the method.**

## 4.2 Future Work

This research evaluates the application of non-invasive surface wave analyses to obtain reliable  $V_S$  profiles at 10 bridge sites in southern Ontario. A major shortcoming in our final results is the lack of quantification of uncertainty in  $V_S$  profiles which result from subjective picking of dispersion estimates and MHVSR peaks and/or non-uniqueness of the solution. This could be quantified in future studies by inclusion of dispersion and MHVSR data errors and/or the use of more advanced inversion algorithms. Additionally, the final inversion results could be improved by including Love-wave dispersion estimates from the horizontal component recordings (not included here). Multiple soil samples at different depths and from multiple sites would be beneficial to develop laboratory based  $V_S$  and  $S_u$  profiles for direct comparison with *in situ* techniques. Lastly, future data collection at many more bridge sites in Ontario will provide additional analysis/development of  $q_c$  to  $V_S$  relations for different sediment types across the region.

## 4.3 References

CSA Group (2014). S6-14 Canadian Highway Bridge Design Code, Section 4 – Seismic design, Mississauga, Ontario, 171-226

## Appendices

### Appendix A. HRFK and MSPAC dispersion comparison

This appendix provides an example of HRFK dispersion estimates retrieved for each array setup at Site-6 in Windsor, Ontario. Dispersion estimates are extracted using both HRFK and MSPAC methods for quality control. Consistent dispersion estimates are obtained from both methods as shown in Figure A 1 below.

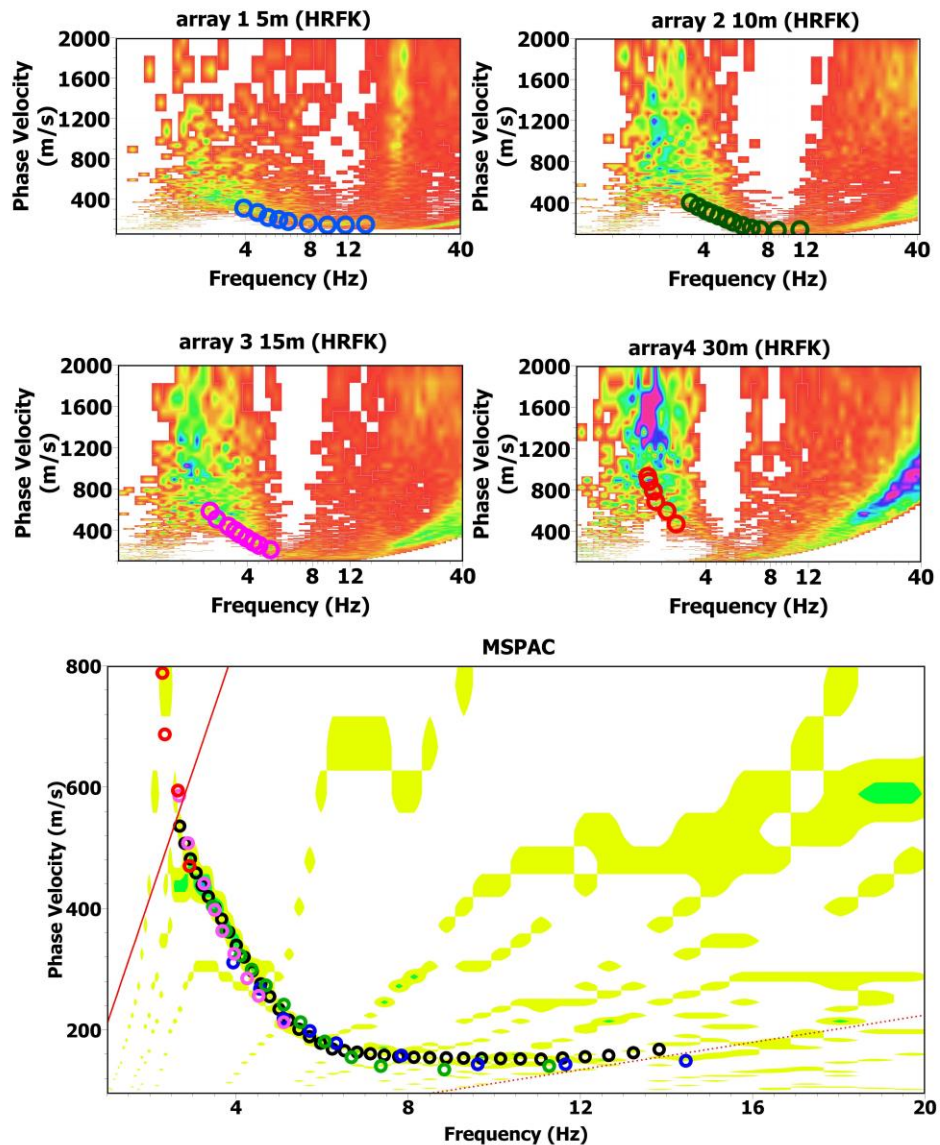


**Figure A 1:** Colored region in upper panels represents HRFK histogram counts for Site-6; blue, green, purple and red open circles are HRFK dispersion estimates from

**5, 10, 15 and 30 m array spacings. Bottom panel compares these HRFK dispersion estimates with the MSPAC dispersion histogram and MSPAC dispersion estimates (black open circles).**

## Appendix B. Alternate inversion attempts considering higher modes

Figures B1 and B2 present alternate inversion results and comparison with invasive data for Sites-2 and 4 in Windsor, Ontario. At both sites, apparent experimental dispersion estimates are obtained possibly due to site complexities or lack of spatial resolution in the data acquisition (Foti et al 2018). For this reason, the modes of propagation are not distinctively separated at both sites. Rather, a progressive shift towards higher modes which is indicative of a higher velocity layer near surface is observed. An attempt is made here to simultaneously invert the fundamental and first higher modes to retrieve subsurface  $V_s$  depth profiles.

At Site-4 dispersion estimates are jointly inverted with MHVSR. The fundamental mode dispersion data is dominant over the low frequency range (2.4-11 Hz). The first higher mode is assigned to dispersion estimates from 13-17 Hz and the estimates within the narrow frequency band representing a continuous shift to higher mode (11-14 Hz) are excluded from the inversion (Figure B 1; A). Inversion is performed for a single uniform layer over elastic half-space. The inversion overestimates and underestimates the phase velocities at low and high frequencies respectively. Adequate fitness of MHVSR fundamental peak frequency and higher mode dispersion estimates are obtained. In this interpretation, the inverted  $V_s$  profile underestimates the depth to significant impedance which was resolved at ~28 m. Similarly,  $V_s$  values from the inverted profile are consistently underestimated except at 14 and 15 m (Figure B 1; D). However, a good agreement is obtained between profiles with an average relative difference between inverted and average invasive profile of 20 m/s (6.5%).  $V_{s30}$  obtained from the inverted model is 246 m/s corresponding to site class D.

At Site-2 the fundamental mode extends up to ~8 Hz. Dispersion estimates within the transition zone between modes (~8-12 Hz) are excluded from the inversion and estimates

from 12-18 Hz assigned as the first higher mode. A good fit between theoretical and measured fundamental mode dispersion estimates is obtained however the fit is less ideal for the first higher mode estimates (Figure B 2; A). The inversion resolves a thin (2.5 m) stiff layer (390 m/s) overlying a 252 m/s layer up to a depth of 26 m.  $V_s$  of the stiff layer is overestimated compared to the near surface  $V_s$  values measured by the invasive profiles. The depth to a significant impedance is underestimated (~26 m) by the inverted model compared to the converted SPT profile which is slightly deeper (Figure B 2; C). Overall a good agreement is obtained between methodologies with an average relative difference in  $V_s$  of 34 m/s (11.5%). Due to the general overestimation in  $V_s$  by the inverted model, the  $V_{s30}$  obtained (290 m/s) is slightly higher than values obtained by invasive methods (Chapter 2, Table 2.3) at this site although they are consistently characterized as site class D.

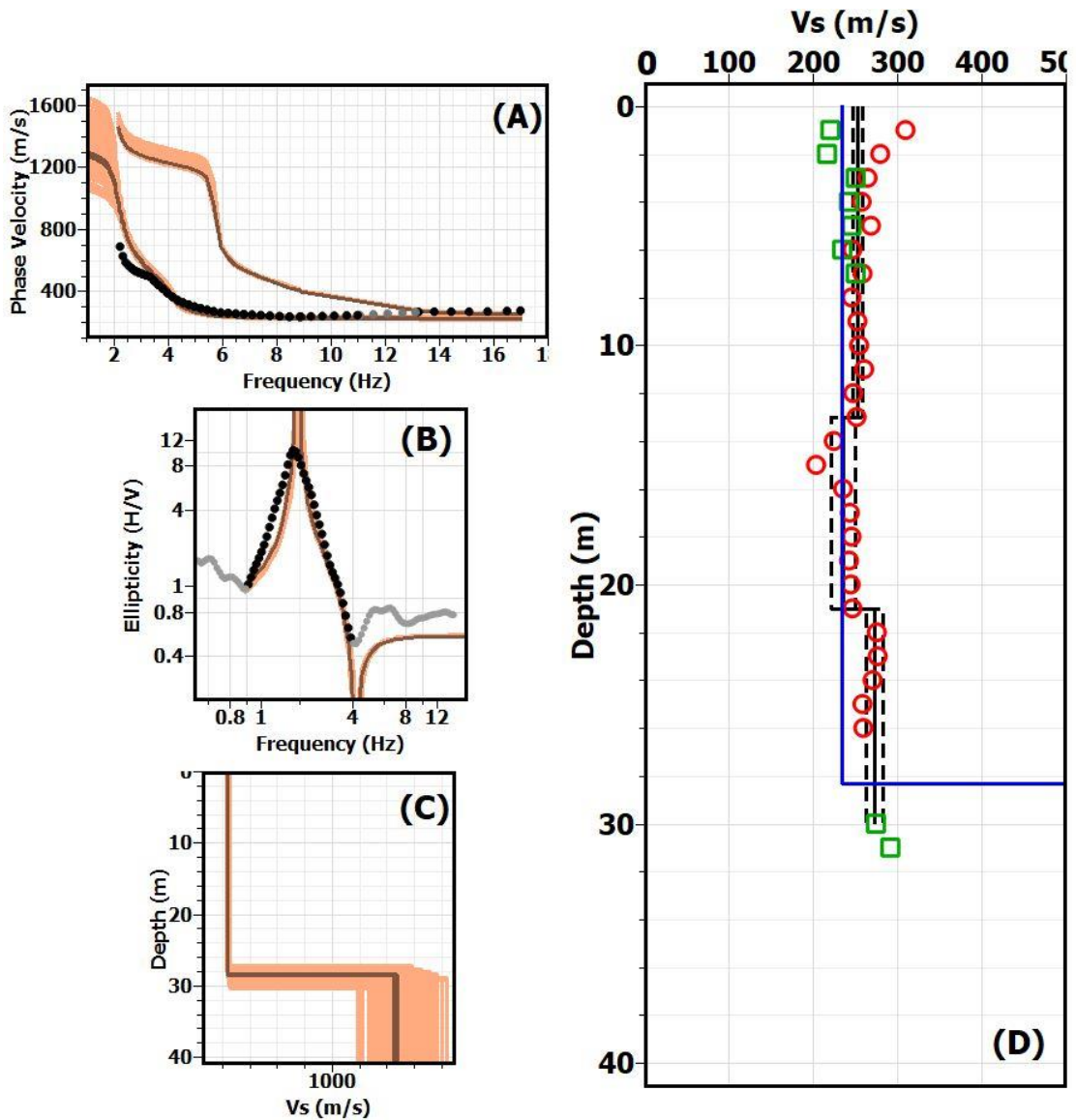


**Figure B 1: Inversion results and comparison with invasive data for Site-4. (A)** shows the dispersion data (black dots), **(B)** shows the MHVSR data (black dots) and **(C)** shows the retrieved  $V_s$  profiles for each site. The colored region represents the first 1,000 lowest misfit models and the solid brown line shows the minimum misfit model. Grey dots represents portions of MHVSR and dispersion estimates not included in the inversion. **(D)** shows the comparison of non-invasive and invasive  $V_s$  profiles.



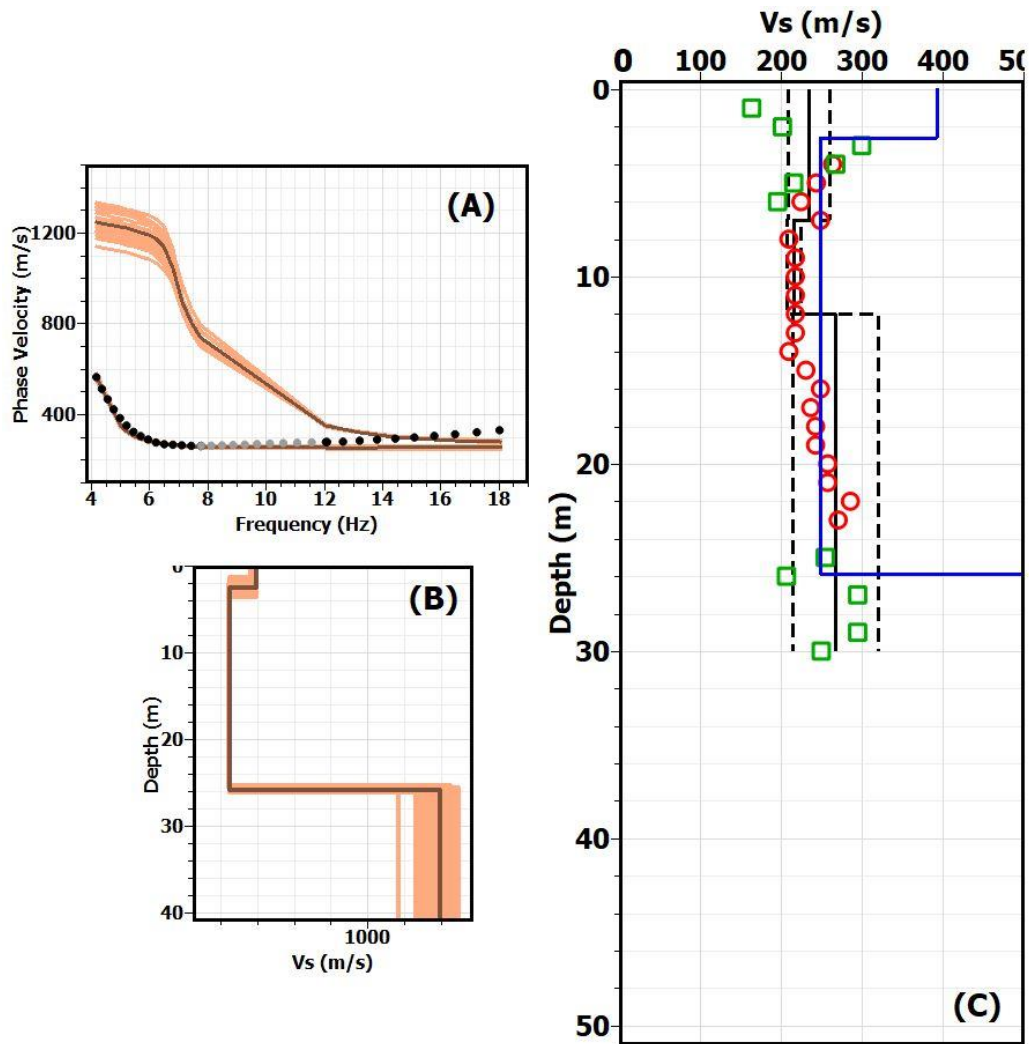


**Figure B 2: Inversion results and comparison with invasive data for Site-2. (A) shows the dispersion data (black dots) and (B) shows the retrieved  $V_s$  profiles for each site. The colored region represents the first 1,000 lowest misfit models and the solid brown line shows the minimum misfit model. Grey dots represents portions of MHVSR and dispersion estimates not included in the inversion. (C) shows the comparison of non-invasive and invasive  $V_s$  profiles.**

## Appendix C. CPT logs

Measurements of raw tip resistance and sleeve-friction were obtained at six locations along the Windsor-Essex Parkway during construction. CPT logs of  $q_c$  and  $f_s$ , near our non-invasive testing site locations are shown in Figure C 1 below.

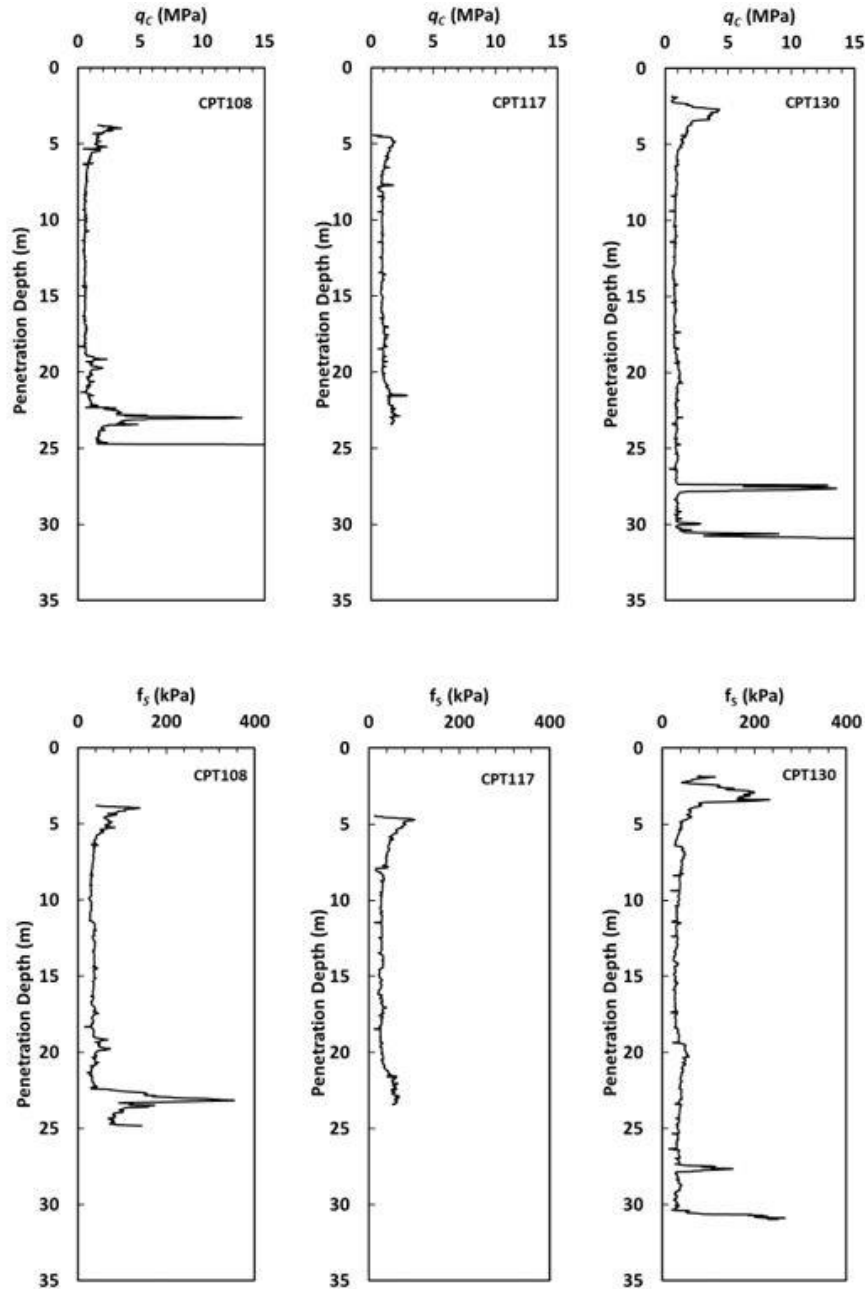


**Figure C 1. Measurements of raw tip resistance (top panel) and sleeve friction (bottom panel) from three CPT tests locations.**

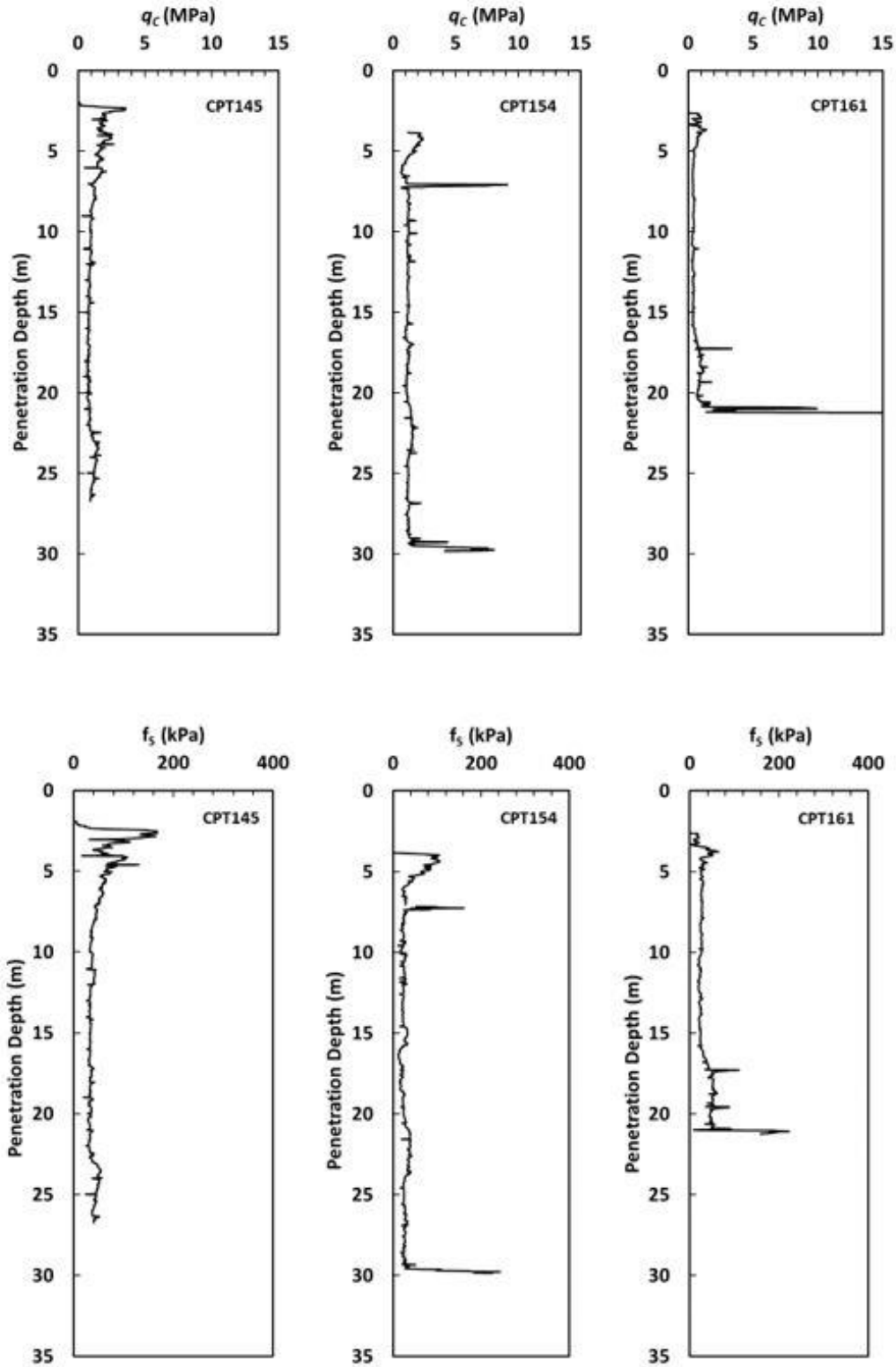
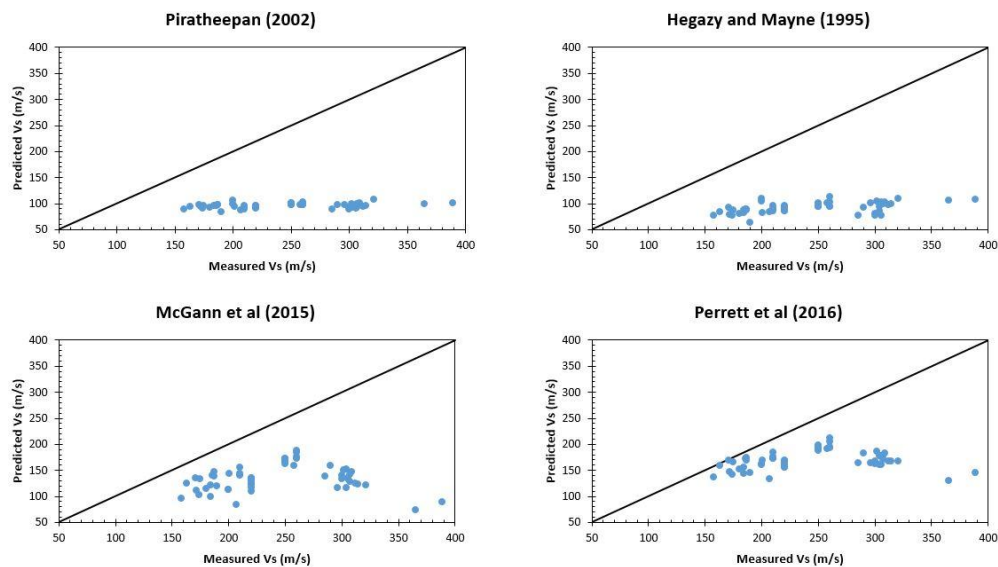


Figure C 1. Measurements of raw tip resistance (top panel) and sleeve friction (bottom panel) at an additional three CPT test locations.

## Appendix D. Other $q_c$ to $V_s$ relations.

Other  $q_c$  to  $V_s$  relations were examined for Windsor sites and shown in Figure D 1 with their corresponding RMSE reported in Table D 1. The relation that provided the least RMSE (grey highlighted text) and with values falling close to the 1:1 line was used for converting  $q_c$  to  $V_s$  at each site.



**Figure D 1: Comparison between  $V_s$  values predicted from empirical relations in literature and  $V_s$  values measured from crosshole and downhole surveys.**

**Table D 1: RMSE obtained for each correlation used at Windsor sites.**

Reference	Correlation	RMSE (m/s)
Hegazy and Mayne (1995)	$V_s = 12.02q_c^{0.319}f_s^{-0.0466}$	159
Baldai et al. (1989)	$V_s = 227q_c^{0.13}$	52
Mayne and Rix (1995)	$V_s = 1.75q_c^{0.627}$	116
Madiai and Simoni (2004)	$V_s = 230q_c^{0.25}$	49
Samui and Sitharam (2010)	$V_s = 1.93q_c^{0.58}$	142
Piratheepan (2002)	$V_s = 25.3q_c^{0.163}f_s^{0.029}z^{0.155}$	156
McGann et al. (2015)	$V_s = 18.4q_c^{0.144}f_s^{0.0832}z^{0.278}$	122
Perrett et al. (2016)	$V_s = 39q_t^{0.164}z^{0.137}$	90

## Appendix E. $q_c$ to $V_s$ relations for Ottawa and Oshawa sites.

$q_c$  to  $V_s$  relations were examined for Ottawa and Oshawa sites and shown in Figure E 1 their corresponding RMSE reported in Table E 1. The relation that provided the least RMSE (grey highlighted text) and with values falling close to the 1:1 line was used for converting  $q_c$  to  $V_s$  at each site.

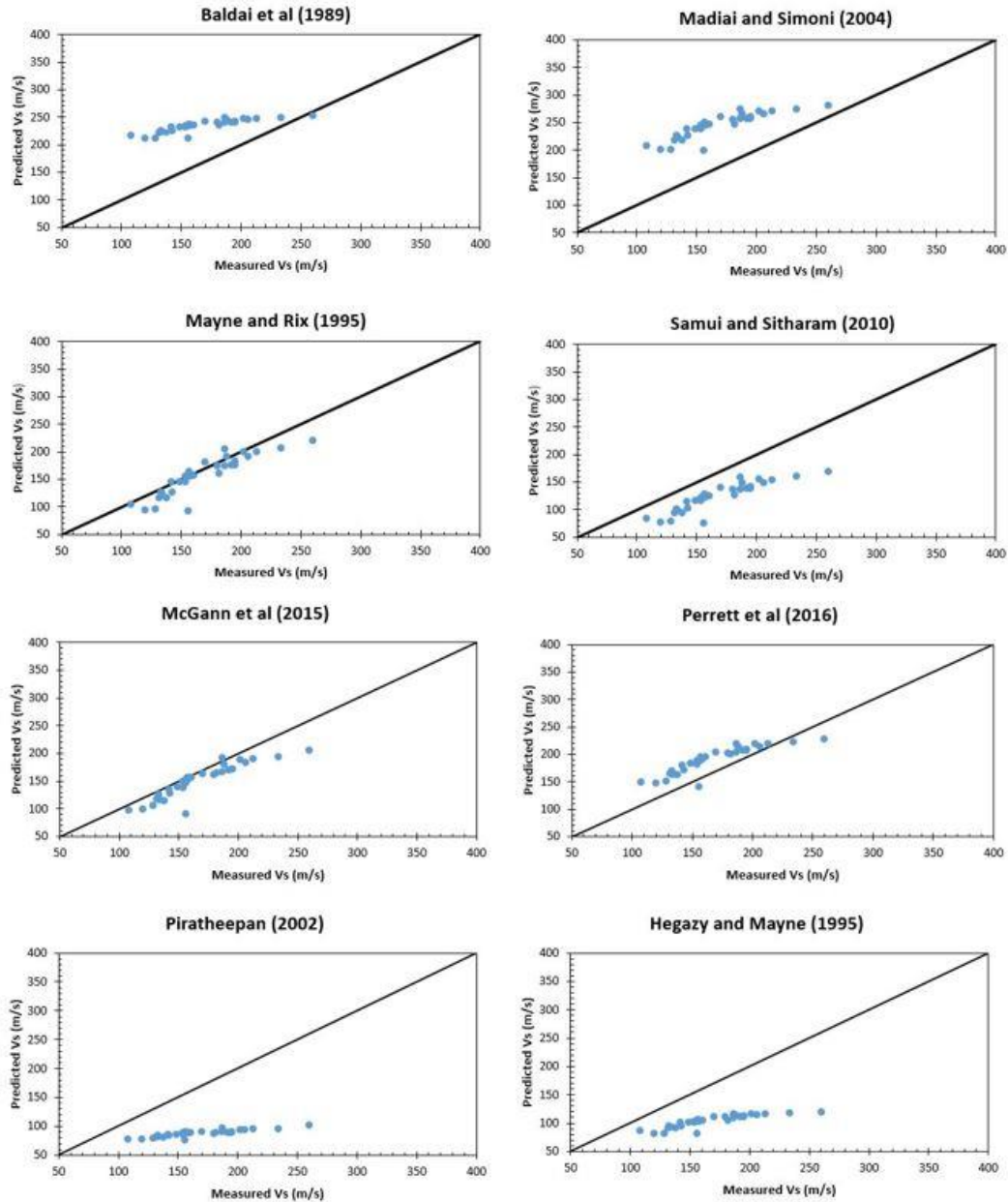


**Figure E 1: Comparison between  $V_s$  values predicted from empirical relations in literature and  $V_s$  values measured from SCPT for site OT-15.**

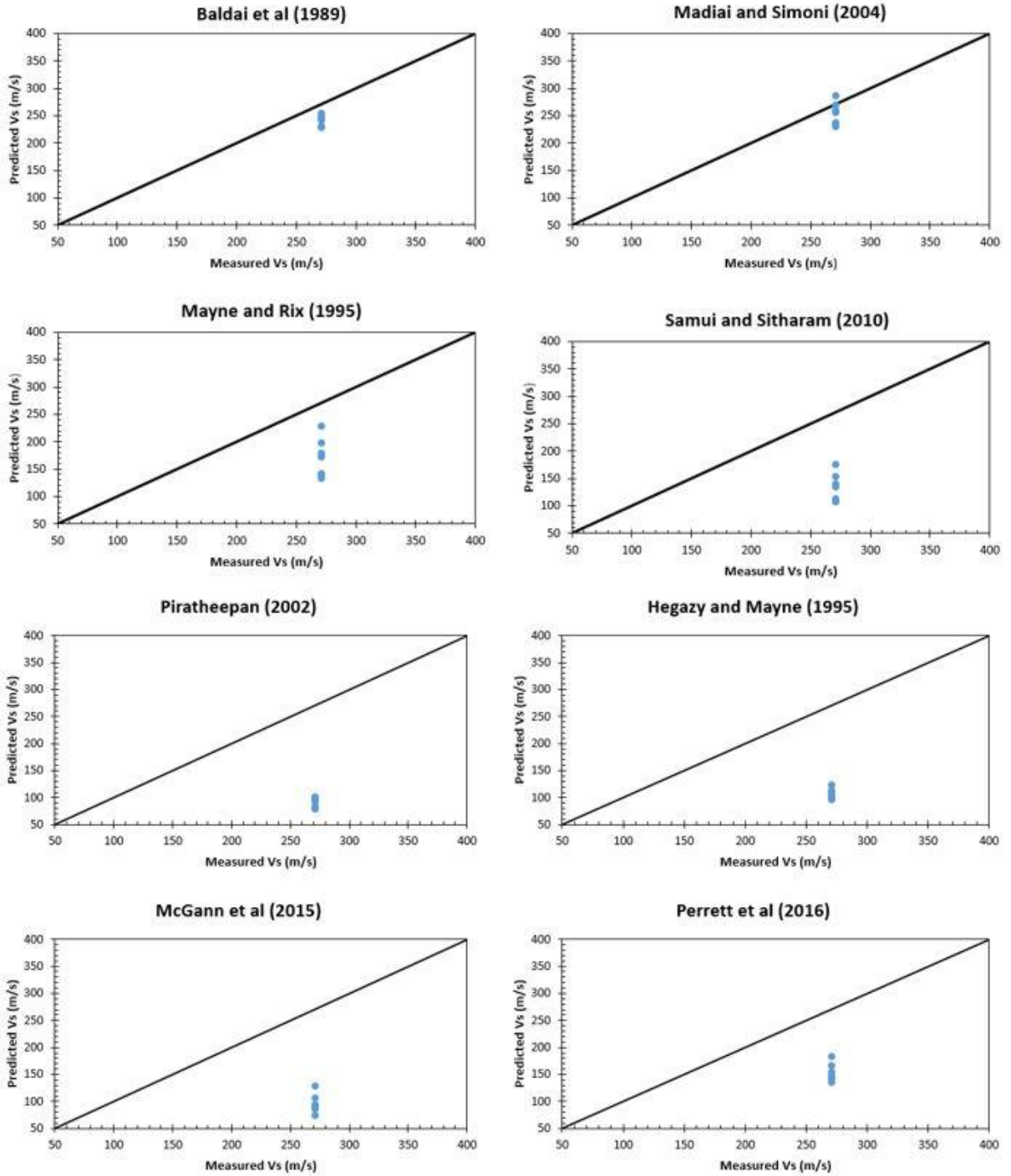


**Figure E 2: Comparison between Vs values predicted from empirical relations in literature and Vs values from inverted Vs model for site BS150.**

**Table E 1: RMSE obtained for each correlation used at the Oshawa site (BS150).**

Reference	Correlation	RMSE (m/s)
Hegazy and Mayne (1995)	$V_S = 12.02q_c^{0.319}f_s^{-0.0466}$	164
Baldai et al. (1989)	$V_S = 227q_c^{0.13}$	34
Mayne and Rix (1995)	$V_S = 1.75q_c^{0.627}$	106
Madiari and Simoni (2004)	$V_S = 230q_c^{0.25}$	27
Samui and Sitharam (2010)	$V_S = 1.93q_c^{0.58}$	140
Piratheepan (2002)	$V_S = 25.3q_c^{0.163}f_s^{0.029}z^{0.155}$	182
McGann et al. (2015)	$V_S = 18.4q_c^{0.144}f_s^{0.0832}z^{0.278}$	177
Perrett et al. (2016)	$V_S = 39q_t^{0.164}z^{0.137}$	120

## Curriculum Vitae

**Name:** Alex Bilson Darko

**Post-secondary Education and Degrees:** Kwame Nkrumah University of Science and Technology  
Kumasi, Ghana  
2009-2013 B.Sc.

University of Western Ontario  
London, Ontario, Canada  
2015-2018 M.Sc

**Honours and Awards:** American Geophysical Union Annual Travel Grant  
Dec. 2017

**Related Work Experience**

Graduate Research and Teaching Assistant  
The University of Western Ontario  
2016-2018

Co-leader, Seismic microzonation mapping project in Metro Vancouver, British Columbia  
July 2018

Co-instructor, Non-invasive seismic methods training  
The University of Western Onatrio  
May 2018

Geophysicist  
AngloGold Ashanti Iduapriem Mine, Ghana  
Dec 2014 – June 2015

Graduate Exploration Geophysicist  
AngloGold Ashanti Iduapriem Mine, Ghana  
Sep. 2013 - Sep 2014

Junior Geologist  
AngloGold Ashanti Iduapriem Mine, Ghana  
May 2012 – Aug 2012

**Publications:**  
Bilson Darko, A., Molnar, S., and Sadrekarimi, A. (2018) Robust Earthquake Site Characterization at Ontario Bridge Sites: *Geotechnical Earthquake Engineering and Soil Dynamics V, Austin, Texas, June 10-13 2018, doi: 10.1061/9780784481486.051*



Conference presentations with published abstract

Bilson Darko, A., Molnar, S., and Sadrekarimi, A. (2018) Robust Earthquake Site Characterization at Ontario Bridge Sites: *Geotechnical Earthquake Engineering and Soil Dynamics V, June 10-13 2018*. Poster

H. Sharma, S. Molnar, A. Bilson Darko (2018). Evaluating inversion techniques for sediment sites in Windsor, Ontario, Canada, SSA annual meeting, Miami, Florida, May 14-17 2018, Poster.

Bilson Darko, A., Molnar, S., and Sadrekarimi, A. (2017). Non-Invasive Seismic Methods for Earthquake Site Classification Applied to Ontario Bridge Sites. In *AGU Fall Meeting Abstracts*, New Orleans, Louisiana, December 11-15 2017, Poster.